Response to RAI 1.1:

a) Atomic numbers 3 through 83 were chosen to allow for various types of plated or sealed form sources to be used under the reactor license for radiation monitor check and calibration purposes. These sources shall be used only under the reactor license for reactor-related purposes.

b) The "50 grams of plutonium-beryllium sources" refers to the mass of plutonium in the matrix of beryllium.

Response RAI 9.1:

a) The document entitled "UMLRR Storage Rack Criticality Analysis Results" dated August 11, 2016 is submitted as Appendix A of this response in support of the UML response dated August 11, 2016 (ADAMS Accession No. ML16224A322) to NRC Generic Letter 2016-01, "Monitoring of Neutron-Absorbing Materials in Spent Fuel Pools," dated April 7, 2016 (ADAMS Accession No. ML16097A169). This document provides the additional detailed analyses as requested in RAI 9.1(a).

b) The storage racks are designed and fabricated to hold a maximum of 9 elements. Figure 9-4 is a simplified depiction showing the main components of the fuel storage rack. A future update to the SAR will include a more accurate depiction for figure 9-4 to eliminate any confusion of the fuel rack storage capacity.

c) A final draft version of the Technical Specifications is to be submitted at a later date as part of this relicensing effort and shall include a specification requiring fuel and other fissionable material be stored in a criticality-safe configuration.

d) A final draft version of the Technical Specifications shall include a specification requiring irradiated fuel and other irradiated fissionable material be stored such that adequate cooling will be ensured.

Response to RAI-11.2.a

The nearest residence is approximately 200 meters away from the reactor facility stack in the west-north-west direction as shown on Figure 1. The dose to a member of the public, due to the assumed continuous full-power operation Ar-41 airborne release was calculated using the following formula (see also response to RAI-13.5.e):

$$Dose = \frac{\chi}{Q} \times DCF_S \times A_E \times t$$

χ/Q = atmospheric dispersion factor
DCF_S = dose conversion factors for air submersion, FGR-12
A_E = rate of radionuclide release from source
T = exposure time

The χ/Q, atmospheric dispersion factor was calculated using the ARCON96 code (see also response to RAI-13.5.e) and assumes the person is continuously exposed and immersed in the Ar-41 cloud at the residence for the whole year. The dose estimate is obtained by using a weather pattern that is reflective of historical meteorological data calculating the 95% percentile doses up to 16 wind direction sectors as shown in Figure 4. The analysis also considered the effect of different Pasquille atmospheric stability classes. Table 1 shows the results of the dose analyses at the nearest permanent residence (Sector 14) in the west-north-west direction. The maximum exposure location (Sector 5) in the east direction that is accessible to the public is located 36 m from the release point, in the parking lot next to the reactor building.

The available meteorological data, while including wind speed and direction, do not provide any indication of the stability classes for each specific measurement point. In order to illustrate the effect of historical stability class influence on the dose calculation, a typical stability class frequency distribution may be considered from the Pilgrim nuclear plant located in Plymouth Massachusetts. Figure 2 shows the stability class distribution frequency that was derived from measured temperature data using a weather tower with instruments at 10 and 60 meters height[1]. An approximate effective dose value may be derived using the stability frequency distribution as a weight factor for each dose value as calculated by the above formula and ARCON96 for a specific stability class at a given distance. While site specific stability class frequency data is not available for the UMLRR, the stability class frequency averaged dose calculated using the Pilgrim distribution data illustrates the potential effect of varying stability class conditions.

Response to RAI-11.2.b

The effect of atmospheric stability classes are indicated in Table 1 with a number of ARCON96 calculations showing the dose values for stability classes A, D, and F at the location with the maximum exposure.

As in the previous response, a stability frequency averaged dose value may be derived using frequency data from the Pilgrim nuclear power plant site shown in last column of Table 1. The results indicate that even assuming an unrealistic stability condition throughout the year, the maximum TEDE would still be well below the 10CFR 20 limit with the additional conservative assumptions of continuous full power operation throughout the year and having the maximally exposed individual continuously located in the parking lot at the 36 m distance from the release point for the full year.

Response to RAI-11.2.c.i

SAR Figure 3-2 provides an incorrect height for the top of the reactor building dome above the core centerline. The correct height is 65ft based upon a review of engineering "as built" blueprints. The elevations in Figure 3-3 are provided presumably relative to the Coast and Geodetic elevation. However, based upon the review of engineering blueprints, there are discrepancies in some of the depicted elevations.

[1] K. Sejkora, "Temporal Comparison of Atmospheric Stability Classification Methods," 10th NUMUG Meeting, Wilmington, NC, 29-30 June 2005

The engineering blueprints for the reactor building construction use base elevations for the City of Lowell as a reference. The City of Lowell base elevation is 55.20ft less than the Coast and Geodetic elevation. The differences in base elevations and their conversions may have led to discrepancies in figures 3-2 and 3-3 when the figures were first developed for the initial licensing FSAR in 1974. Nonetheless, the true heights of the reactor building associated structures can be discerned from the blueprints. The height of the reactor building above finished grade has been determined to be 67ft – 10in. The height of the stack is confirmed to be 100ft as previously indicated. The stack is therefore 32ft-2in above the reactor building. Figures 3-2 and 3-3 will be corrected in a future update of the SAR. In addition, a review of additional data was made to verify the discrepancies in the heights presented in the figures do not affect the building volume of 335,000 ft^3 stated in SAR section 6.2.6.

Response to RAI-11.2.c.ii

The guidance in RG 1.145 refers to semi-empirical models based on theoretical and empirical correlations for elevated and non-elevated releases. As per RG 1.145, a release is elevated if the release point is 2.5 times above the adjacent structures and a theoretical formula is recommended (Eq. 4 in RG. 1.145) to calculate the corresponding χ/Q values. For ground releases, the guidance combines theoretical and empirical formulas to account for the effect of turbulence in building wakes (Eq. 1-3). For effluents released at a level higher than the adjacent structures, but lower than the elevated release points, the effluent plume may be considered as the combination of ground and elevated release based on the recommendations in RG 1.111. This methodology is implemented in the code ARCON96 (please see further Response to RAI-13.5.e)

ARCON96 treatment of vent releases depends on the vertical velocity of the effluent and the wind speed. If the vertical velocity is more than 5 times the wind speed, the release is treated as an elevated release with a stack height equal to the height of the vent. If the vertical velocity is less than the wind speed, the release is treated as a ground-level release. If the vertical velocity is between these values, the release is treated as a mixed-mode release based on the recommendations in Regulatory Guide 1.111. The χ/Q value for a mixed-mode release is a weighted average of the χ/Qs for the elevated and ground-level releases. The weights for the mixed-mode release are determined using a wind velocity dependent entrainment coefficient.

Response to RAI-11.2.d

Figure 3 shows the final wind rose data being used in all calculations both for the Ar-41 and MHA fission product releases. The previous figures were incorrectly given using an earlier version of the meteorological data.

Response to RAI-11.3.a

The reactor operations boundary is the reactor building.

Response to RAI-11.3.b

When liquid waste water from the reactor sump is transferred to the holding tanks in the attached classroom building (Pinanski Building) basement, the liquid shall be under the jurisdiction of the byproduct material license (BPML) for the university (MA License #60-0049).

Response to RAI-11.3.c

The reactor sump liquid is cycled and analyzed for the presence of radioactivity. If radioactivity is detected, it is identified by isotope and quantity, as determined within the detection limits of the instrumentation. The quantity of specific radioactive material identified is summed with the existing inventory under the BPML (broadscope type-A) to determine that the limits specified in the BPML are not exceeded. If within the limits of the BPML, the liquid shall be transferred from the reactor sump to the holding tanks. The process will conclude with a license transfer.

Response to RAI-11.3.d

Prior to discharge to the sewer, the tanks in the Pinanski Building basement are cycled and analyzed. The analysis consists of an evaporation to dryness followed by a subsequent gross alpha/beta activity analysis. As per our discharge permit with Lowell Regional Wastewater, a visual inspection is conducted of the sample to determine solubility. Additional physical and chemical evaluations of samples of wastewater discharged from the university are conducted at a state accredited lab and reported to the university.

Response to RAI-11.4:

The fixed area detectors within the reactor building have two alarm settings. The lower warning alarm settings are set at or below the radiation level that would constitute a radiation area as defined in 10CFR Part 20 ($\geq$5 mr/hr). The high alarm settings are set at or below the radiation level that would constitute a high radiation area as defined in 10CFR Part 20 ($\geq$100 mr/hr).

The continuous air monitors (CAMs) inside the reactor building are designed to measure airborne radioactive particulates. The CAMs are configurable with two alarm set points – a warning alarm as an alert for an above normal detection, and a high alarm for immediate response. The CAM alarm set points are set below the DAC (10CFR 20 Appendix B, Table 1) for Cs-138. Cs-138 is a decay product of Xe-138 and is considered to be a likely fission product indicator detected by the CAM.

The stack monitor has detectors to measure radioactive particulates and radioactive gases. Each is configurable with two alarm set points similar to the CAMs. The alarm set points for the particulate detector are set below the effluent concentration (10CFR 20 Appendix B, Table 2) associated with a Cs-138. The gaseous alarm set points are set below the activity level of Ar-41 that corresponds to a dose level of 100mrem/year from the effluent based upon continuous operation at full power and exposure to a member of the public for one year.

Response to RAI-11.5.a

The Canberra EcoGamma monitor indicated in Table 11-6 of the SAR was inadvertently included. This detector, while currently available, is used for trending purposes only and is not

part of the environmental monitoring program employed for both the reactor and byproduct materials licenses. The reference to this detector shall be removed from a future revision to the SAR. The "Environmental Gamma" monitors listed in table SAR 7-8 are gamma monitors within the reactor building used for monitoring specific remote facilities within the building such as thermal column beam line.

Response to RAI-11.5.b

The environment outside the reactor building is monitored by strategically located passive OSL dosimeters. The areas outside the reactor building where the dosimeters are located include the areas within the first and third floor airlocks as well as locations throughout the attached Pinanski Building (e.g., basement, first floor, second floor, third floor, and the roof). The numbers and placement of dosimeters are sufficient based upon historical data accumulated and analyzed from other dosimetry locations that were part of a previous comprehensive background study of areas around the UML campus. The OSL dosimeters are evaluated and reported by a NVLAP accredited vendor. The results are analyzed by the UML Radiation Safety Office to assure measured doses are below 10CFR 20 limits for the public and to monitor for trends that would indicate unusual or elevated exposures.

Response to RAI-13.5.a

The equilibrium nuclide concentration of fission products on page 13-8 contains a typographical error and the term "$3.1x10^{11}$" should read as "$3.1x10^{10}$". The nuclide concentrations used in the analysis are correct and the results are unaffected by the typographical error. The typographical error will be corrected in a future revision of the SAR.

Response to RAI-13.5.b

The statement on page 13-16 regarding the use of FGR dose conversion factors for "Scenarios A through D" contained a typographical error. The statement should have read "Scenarios A through E." The MHA dose calculations for Scenario E in the SAR were unaffected by the typographical error. However, for the reanalysis of the MHA presented in this document, Scenario D as presented in the SAR is no longer considered. A justification is provided in Response to RAI-13.5.j below. For this document, the SAR Scenario E has been designated as Scenario D.

As discussed in the responses to RAI-13.5.e and RAI-13.5.j below, the MHA has been reanalyzed using different assumptions resulting in different dose estimates. The corrections and changes based upon the responses in this document will be made to a future revision of the SAR.

Response to RAI-13.5.c

The dose conversion factor for iodine-135 in Table 13-3, shown as "3.32E10" contains a typographical error. The dose conversion factor should read as "3.32E-10." The whole-body inhalation dose calculations are unaffected by the typographical error. The typographical error will be corrected in a future revision of the SAR.

Response to RAI-13.5.d

The statement on page 13-16 "radioactive decay considered for the gamma shine component and the *ground* release" contains a typographical error. The MHA dose calculations for Scenario E (Scenario D in this document) has been reanalyzed without considering the effect of radioactive decay and using a mixed-mode approach for the vent release (see Response to RAI-13.5.e). The typographical error will be corrected in a future revision of the SAR.

Response to RAI-13.5.e

The MHA is defined as the removal of the cladding from one side of the fuel plate resulting in the release of volatile fission products from portions of the fuel meat. The analysis assumes that the UMLRR operates at full, 1 MW power with the minimum number of fuel plates. The resulting equilibrium fission product inventories with significant contribution to the radiological hazard are listed in Table 2. The fission product release fraction of 2.7% from the fuel plate into the reactor pool is based on the recommendation in NUREG/CR-2079 and the resulting pool radioactivity contents are also listed in Table 2 (third column).

RG 1.183 provides regulatory guidance regarding the quantity and release of radioactive material released into the coolant primarily from damaged nuclear power plant fuels, rather than low power research reactors. Most radionuclides released from the fuel matrix into the pool are in particulate form and not expected to be released into the atmosphere except noble gases and elemental and organic iodine.

RG 1.183, Appendix B, assumption #2 suggests that if the water height is 23 feet or greater above the reactor core then 99.5% of total iodine released from the fuel plate is retained by the water. UMLRR TS 2.1.1.2 requires that the water level in the pool is maintained at a minimum of 24 feet above the centerline of the reactor core resulting in a water level higher than 23 feet above the reactor fuel plates.

In addition, Appendix B, assumption #1.3 indicates that the organic iodine content is 0.15% of the total iodine release, which results in iodine composition above the water as 57% elemental and 43% organic. It is also assumed that noble gases are not retained by the water pool and 100% of all noble gases are released. Table 2 (fourth column) indicates the total amount of radioactive fission products released into the reactor building atmosphere that serves as the source term for the subsequent analysis. All potential release scenarios were reevaluated using the source term derived based on recommendations in Regulatory Guide 1.183.

The inhalation and submersion dose for facility personnel and the members of the public are given by:

Inhalation dose:

$$Dose = DCF_I \times A_I \times BR \times t \quad \text{(Internal)}$$
$$Dose = \frac{\chi}{Q} \times DCF_I \times A_E \times BR \times t \quad \text{(External)}$$

Submersion dose:

$$Dose = DCF_S \times A_I \times t \quad \text{(Internal)}$$
$$Dose = \frac{\chi}{Q} \times DCF_S \times A_E \times t \quad \text{(External)}$$

Where:

χ/Q	=	atmospheric dispersion factor
DCF_I	=	dose conversion factors for inhalation, FGR-11
DCF_S	=	dose conversion factors for air submersion, FGR-12
A_I	=	radionuclide concentration in the building
A_E	=	rate of radionuclide release from source
BR	=	breathing rate
t	=	exposure time

The total effective dose equivalents are calculated using FGR-11 and FGR-12 dose coefficients along the plume sector center lines. For three short lived isotopes, Kr-90, Xe-137, and Xe-139, the DFCs were obtained from other sources: DOE-EH-0700, "External Dose-Rate Conversion Factors for Calculation of Dose to the Public," and RG 1.109.

The atmospheric dispersion factor, χ/Q and consequent doses external to the facility were calculated using the ARCON96 code[2]. The code implements a straight-line Gaussian dispersion model with dispersion coefficients that are modified to account for low-wind-speed meander and building wake effects. The ARCON96 code uses hourly meteorological data applicable to the UMLRR site and calculates relative concentrations (χ/Q) at a specified location (in both distance and direction from the source) that would be exceeded no more than five percent of the time. The meteorological data file (.MET file) for ARCON96 was constructed from the data available for the Hanscom Air Force Base, January 1st 2013 – December 31st 2013. Since the meteorological data set did not include data of the atmospheric stability classes, the analysis was performed for three different stability classes, A, D, and F.

The respective χ/Q values were calculated at two locations: a) 200 m from the facility at the closest permanent, residential location, and b) the location with the maximum exposure where a member of a public may be exposed for a period of time after the release. Scenarios C and D analyzed fission product releases, which are eventually dispersed into the outside environment. Scenario C is a leakage through the large access truck door, while in Scenario D fission products are vented through the facility stack. The stack is 30 meter (100 feet) high that is less than 2.5 times the adjacent reactor building height, qualifying it as a vent release based on the recommendations in RG 1.145 and RG 1.111.

ARCON96 treats vent releases in addition to ground-level and elevated releases. The treatment of these releases depends on the vertical velocity of the effluent and the wind speed. If the vertical velocity is more than 5 times the wind speed, the release is treated as an elevated release with a stack height equal to the height of the vent.

[2] J.V. Ramsdell, C.A. Simonen, "Atmospheric Relative Concentrations in Building Wakes," NUREG/CR-6331, PNNL-10521, Rev. 1, June 1997.

If the vertical velocity is less than the wind speed, the release is treated as a ground-level release. If the vertical velocity is between these values, the release is treated as a mixed-mode release based on the recommendation in Regulatory Guide 1.111. The χ/Q value for a mixed-mode release is a weighted average of the χ/Qs for elevated and ground-level releases. The weights for the mixed-mode release are determined using a wind velocity dependent entrainment coefficient.

The original SAR analysis incorporated a simple decay model for both Scenario C and E, which is not necessarily a conservative assumption depending on the full chain of decay daughter products. In order to assure additional conservatism for both Scenario C and D in this document, it was assumed that there is no fission product decay and the activity level remains the same throughout the release period. The only exception is three quickly decaying isotopes, Kr-90, Xe-137, and Xe-139, which transmute into non-noble gas daughter products in less than 3 minutes. It is assumed that two of these isotopes, Kr-90 and Xe-137 would either plate out or be captured by the charcoal filter (see SAR section 6.2.4) and not disperse into the outside environment, while Xe-139 decays into a stable, non-radioactive component.

A summary of the reanalyzed doses for the various scenarios are given below. Again, note that the SAR Scenario E has been designated as Scenario D for this document. The response to RAI 13.5.j provides additional detail regarding the scenarios and the analyses.

Scenario A - Occupational Dose:
This scenario estimates the radiation exposure to workers inside the reactor building for the MHA. Under the condition whereby a radiation alarm indicates a fission product release, personnel would evacuate the reactor building in less than 10 minutes. The occupation dose (Table 3) results from the 10 minute inhalation and submersion in the semi-hemispherical gaseous cloud of the reactor building volume containing the fission products.

The calculated occupational whole-body TEDE of 540 mrem (5.4 mSv) is below the regulatory limit for occupational TEDE of 5,000 mrem (50 mSv) in 10 CFR 20.1201.

Scenario B - Pinanski Building Airlocks Doors and Reactor Building Truck Door:
This scenario estimates the radiation exposure to the general public located at or near the reactor building for the MHA. The scenario includes the unlikely and conservative assumption that the emergency exhaust system as described in SAR Section 6.2 fails to operate concurrent with the MHA. The resultant radiation exposure would be due to the direct and scattered gamma radiation from the decay of the fission products contained inside the reactor building air space.

The gamma fluxes and associated surface doses were calculated using the photon flux-to-dose rate conversion factors from ANSI/ANS 6.1.1 for three locations: a) outside the security doors leading to the airlocks (public access point), b) at positions outside the truck door, and c) at a location adjacent to the outside reactor building wall.

As show in Table 4, the highest dose occurs at the reactor building truck door. The truck door provides a large surface gamma source where the dose for a continuous 30-day stay at the truck door surface would exceed the 100 mrem (1 mSv) limit. In actuality, the truck door is separated from the outside environment by a roll-up metal garage door located on the exterior of the

building. The dose model does not consider the extra door and the separation it provides from the truck door. The 30-day dose at the surface of the truck door is provided for illustrative purposes as it is entirely unrealistic to assume a member of the public would stay positioned at the surface of the door for 24 hours per day for 30 days. In the highly unlikely event the conditions for this scenario were to occur, the area around the truck door would be posted and controlled in accordance to the requirements of 10CFR 20. As shown in Table 4, at a more reasonable distance of 2.5 meters from the door, the dose becomes 36 mrem (0.36 mSv) for a 30 day stay-time which is below the limit of 100 mrem (1 mSv). Locations further away from the door (driveway and parking lot areas) would reduce the radiation dose to even lower levels.

Scenario C - Leakage Around Reactor Building Truck Door:
This scenario estimates the radiation exposure to the general public due to leakage of fission products from the reactor building. The same conservative assumptions for Scenario B are applied with the additional assumption that a second concurrent failure has occurred whereby fission product leakage creates a ground level release. A postulated 1%/day leakage of fission products bypassing the truck door (see also response to RAI-13.5.n) is assumed in addition to the gamma radiation from the reactor building near the reactor building truck door. No decay of fission products is assumed. The ground level release is analyzed by the ARCON96 atmospheric dispersion code as described above. At the release point, the dose is dominated by the ground release (shown in Table 5 with a small contribution from the gamma ray radiation) resulting in a maximum dose of 36.2 mrem for a 30 day stay which is below the regulatory limit of 100 mrem (1 mSv). The radiation dose at the nearest residence is essentially negligible.

Scenario D - Public Areas Outside Reactor Building:
For this scenario (designated as Scenario E in the SAR), the ventilation and emergency exhaust systems as described in SAR Section 6 are assumed to operate as designed. The emergency exhaust system will discharge the fission products through the charcoal and HEPA filter train to the building stack as a vent release. No consideration is given for radioactive decay. The analysis was modeled with a weather pattern that is reflective of historical data, for the 18 hours duration of the scenario (time required for one complete exchange of the air in the building through the emergency exhaust system). The atmospheric relative concentration was calculated as a vent release that assumes a superposition of elevated and ground releases based on historical wind data. The results are shown in Table 6, with the maximum dose near the release point at 10m dominated by the vent release with a predominantly ground release component and a minor contribution from the gamma radiation. The TEDE levels for the maximum dose as well as the closest residential locations are well below the 10 CFR Part 20.1301 limit of 100 mrem.

Response to RAI-13.5.f

The SAR Table 13-2 contains typographical errors incorrectly stating the amount of xenon-133m and xenon-135m released into the reactor pool. In addition, the amount of xenon 131m, xenon-133m, and xenon-135m released into the reactor building atmosphere were also incorrectly stated. Table 2 below lists the corrected amount of fission products released into the reactor pool and the reactor building atmosphere. The typographical error will be corrected in a future revision of the SAR.

Response to RAI-13.5.g

The results of the occupational dose analysis, shown in Table 3 include the three short lived isotopes, Kr-90, Xe-137, and Xe-139. Though these isotopes are short lived, the total contribution from these isotopes is not insignificant, about 7% of the total.

Response to RAI-13.5.h

SAR Table 13-4 incorrectly labelled the columns "Thyroid Inhalation CEDE" and "Thyroid Submersion CEDE," which should have been labelled as committed dose equivalents (CDE). Table 3 of this document provides the corrected column labels. The submersion dose conversion factors (DCF) used in the analysis for I-131 through I-135 (based on FGR-12) are indicated below. Table 3 of this document provides the corresponding occupational dose values. Both the thyroid CDE and whole-body TEDE are below the regulatory limits for occupational dose in 10 CFR Part 20.1201. Corrections and changes to the SAR will be made in a future revision.

Isotopes	Thyroid DCF submersion	Whole-body DCF submersion
I-131	1.81E-14	1.82E-14
I-132	1.12E-13	1.12E-13
I-133	2.93E-14	2.94E-14
I-134	1.30E-13	1.30E-13
I-135	8.01E-14	7.98E-14

Response to RAI-13.5.i

The nearest residence is located approximately 200 m away in the north-west direction from the UMLRR facility. Both the MHA and Ar-41 analyses were extended to calculate the consequences of the exposure to a member of the public due to a potential radioactive fission product release. The response to RAI-13.5.e provides the details of the MHA analysis showing the TEDE at the closest residential location. The maximum TEDE values for Scenario C and D are listed in Table 5 and 6 for the nearest permanent residence.

Response to RAI-13.5.j

The SAR MHA analyses included 5 scenarios to evaluate the dose to workers and the public for various postulated conditions associated with the MHA. Scenario A evaluated dose to workers, while scenarios B through E evaluated dose to the public. For scenario B, the evaluation considered the gamma dose at each portal to the reactor building at a location where a member of the public may have access. The major assumptions were that the ventilation and emergency exhaust systems failed (i.e., all ventilation is shut down and the building is isolated, thus containing all the fission products), and there is radioactive decay for all isotopes. For Scenario C, the same assumptions used in scenario B were applied. In addition, a small amount of leakage (1% of building volume per day) was assumed around the truck door as a ground level release. The dose to a member of the public was evaluated from the gamma shine through the containment walls and truck door, as well as submersion and inhalation from the ground release. For Scenario D, the assumption was all automatic and manual operation of the ventilation failed

such that the ventilation remained operating and the fission products vent directly through the stack. For scenario E, the major assumption was the ventilation and emergency exhaust system operates as designed as described in SAR Section 6. Scenario E corresponds to the most likely evolution of the MHA.

Note that for scenarios B and D, the assumptions include system failures concurrent with the MHA, while scenario C assumes multiple failures. An MHA analysis concurrent with system failures is not required for research reactors (NUREG 1537-2, 13-3, 13-6). However, the consideration for such failures has been provided here to give added weight to the conclusion that even under extreme conditions, the MHA is within acceptable limits. The scenarios with system failures result in higher estimated doses but are still below 10CFR 20 limits for the public with the exception of the 30 day gamma dose at the truck door (see response to RAI 13.5e, Scenario B).

The MHA scenarios have been reanalyzed for this RAI response document. The SAR Scenario E, which corresponds to the most likely evolution of the MHA, is designated as Scenario D in this document. After further review, the SAR Scenario D was considered unrealistic since it assumed a failure such that the reactor building ventilation system could not be shut down by either automatic or manual means. In the unlikely event both automatic and remote manual controls fail, the ventilation shutdown and building isolation can be accomplished simply and easily by manually switching off electrical power to these systems.

As with the SAR Scenario E, Scenario D in this document assumes the ventilation and emergency exhaust systems as described in SAR section 6 are operating as designed. Air containing fission products in the reactor building airspace would be exhausted by the emergency exhaust fan, through the HEPA and charcoal filter train, and into the reactor facility stack.

The atmospheric discharge is treated as a vent release, which is a combination of ground and elevated release as per the guidance in Regulatory Guide 1.111 as implemented by the ARCON96 code. The maximum dose occurs near the facility building in the East direction and the TEDE values are listed in Table 6 “Scenario D” assuming three different stability classes. For conservatism, the gamma ray dose contribution corresponding to the location near the truck access door was also included, even though the door is not on the east side of the building. The resulting TEDE values are well below the regulatory limit of 100 mrem in 10 CFR Part 20.1301 and also the ALARA limit of 10 mrem in 10 CFR Part 20.1101. Even though the estimated dose due to the MHA fission product release event is below the ALARA limit, the UMLRR administration would be required to notify the NRC of a fission product release indicating an abnormal and significant degradation in reactor fuel and/or cladding.

Response to RAI-13.5.k

Scenario D has been eliminated since it is unrealistic to assume that all automatic and manual operation of the ventilation fails such that the ventilation remains operating and vents fission products directly out the stack. Scenario E (re-designated as Scenario D in these responses) was reanalyzed as a vent release using the ARCON96 code deriving relative concentration as a

function of distance and direction, using historical meteorological conditions (see response RAI-13.5.e) without considering radioactive decay. The results for Scenario D are listed in Table 6 assuming three different stability classes.

Response to RAI-13.5.l

The revised MHA analysis does not take credit for fission product isotope decay and the results for Scenario C and D are listed in Table 5 and 6 respectively.

Response to RAI-13.5.m

Scenario C was reanalyzed using the MHA assumption and methodology described in the Response to RAI-13.5.e. The maximum TEDE for Scenario C is near the release point as listed in Table 6.

Response to RAI-13.5.n

As noted in the response to RAI-13.5.j, Scenario C is not best representative of the MHA for determining dose since it assumes the systems as required by the technical specifications are not operable as designed and tested (i.e., Scenario D). Instead, Scenario C (and also B) provide added weight to the conclusion that even under extreme conditions, the MHA dose will be within the acceptable 10CFR 20 limits.

The 1% per day leakage rate value used for Scenario C was selected based on engineering judgement given the possibility of having a one inch gap around the truck door with a $\Delta p \sim 7kPa$ (for an extreme weather condition) resulting in a .005% leak rate. Using a factor of 200 is considered very conservative in estimating the potential leak along the truck door for this extreme circumstance given that in the most likely scenario (Scenario D) the exhaust fan keeps running resulting in a slightly negative building pressure with no out-leakage at the door.

Response to RAI-13.5.o.i

Figure 3 shows the final wind rose data being used in all calculations both for the Ar-41 and MHA fission product releases. The previous figure was incorrectly given using an earlier version of the meteorological data.

Response to RAI-13.5.o.ii

All scenarios were recalculated for the MHA analysis including Scenario C and D for three different stability classes, A, D, and F indicating the changes in dose rates due to atmospheric stability conditions. The results indicate that in general, no particular stability class is conservative and the local dose values are primarily influenced by the combination of distance, wind direction, and the stability class.

Response to RAI-13.5.p

The MHA model considered averaged χ/Q values representing two, 2-8, 8-24 hour, and 1-30 day time intervals based on the wind speed and direction data recorded throughout the year. The averaged χ/Q values were developed using the ARCON96 code for ground (Scenario C) and vent releases (Scenario D).

The treatment of these releases depends on the vertical velocity of the effluent and the wind speed. If the vertical velocity is more than 5 times the wind speed, the release is treated as an elevated release with a stack height equal to the height of the vent. If the vertical velocity is less than the wind speed, the release is treated as a ground-level release. If the vertical velocity is between these values, the release is treated as a mixed-mode release based on recommendations in RG 1.111 and RG 1.145. The χ/Q value for a mixed-mode release is a weighted average of the χ/Qs for elevated and ground-level releases. The weights for the mixed-mode release are determined using a wind velocity dependent entrainment coefficient.

(Figures and Tables are provided on Pages 14-18)

Figure 1 Nearest Residence Location

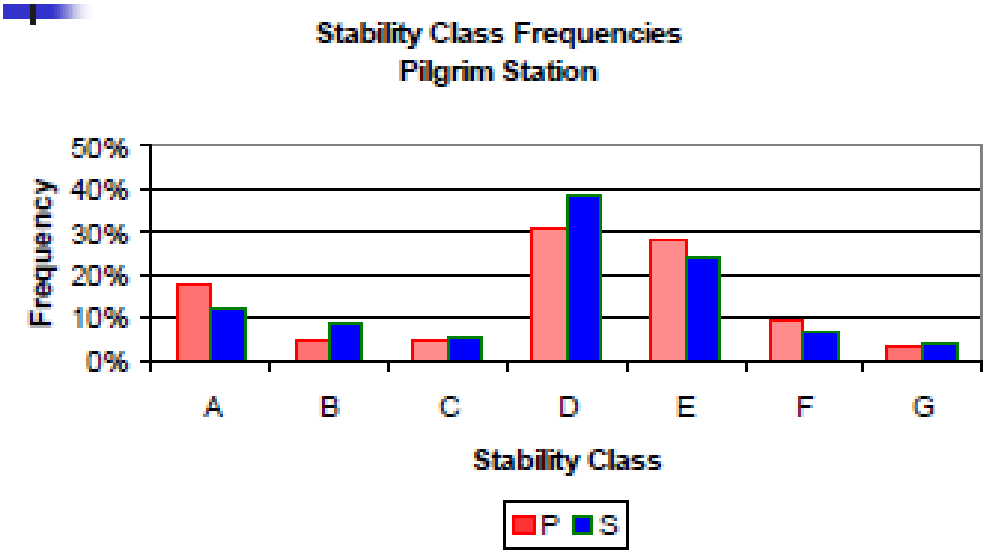

Figure 2 Pasquille Stability Class Frequency Distribution

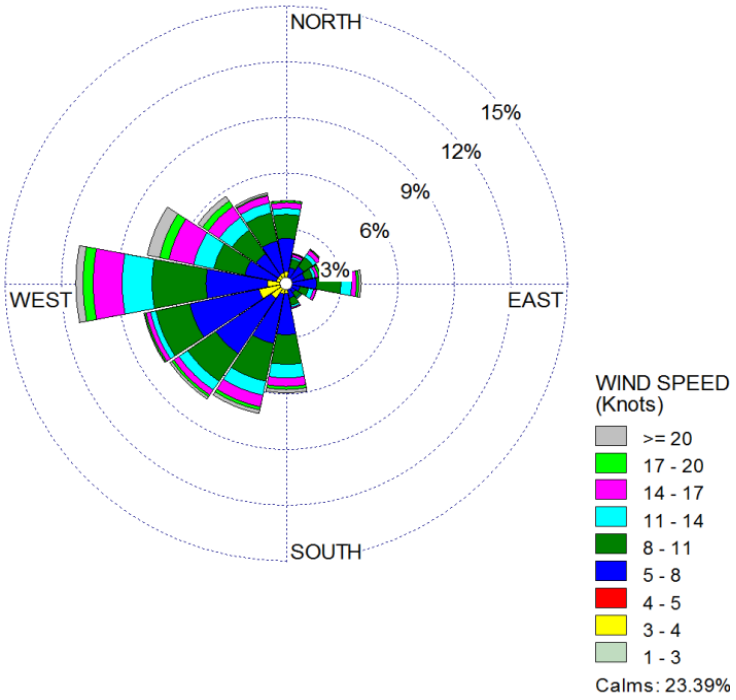

Figure 3 Wind Direction Distribution for Hanscom Air Force Base January 1st 2013 – December 31st 2013

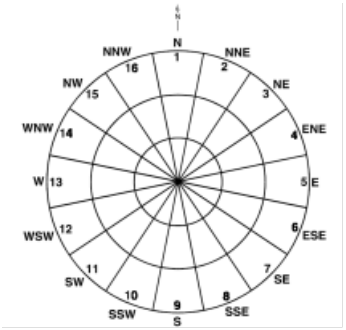

Figure 4 Sector Locations

Table 1 Ar-41 Total Effective Dose Equivalent, Stack Release

Distance/Direction	Ar-41 TEDE [mrem]			Stability Class Frequency Averaged TEDE (A/D/F) [mrem]
	Stability A	Stability D	Stability F	
Nearest Residence, 196 m Sector 14 (WNW)	3.2	.3	.4	.9
Maximum dose, 10 m Sector 13 (West)	2.6	8.9	14.5	8.3
Parking Lot Dose, 36 m Sector 5 (East)	2.4	8.6	13.2	7.9

Table 2 Fission Product Activity per Fuel Plate

Isotope	Fission Product Activity [Ci/plate]	Fission Product Activity Released into Fuel Pool [μCi]	Fission Product Activity Released into Reactor Building [μCi]
Kr-83m	3.36E+01	9.06E+05	9.06E+05
Kr-85	1.60E+01	4.31E+05	4.31E+05
Kr-85m	7.51E+01	2.02E+06	2.02E+06
Kr-87	1.49E+02	4.01E+06	4.01E+06
Kr-88	2.05E+02	5.53E+06	5.53E+06
Kr-89	2.32E+02	6.26E+06	6.26E+06
Kr-90	2.83E+02	7.63E+06	7.63E+06
Xe-131m	1.69E+00	4.55E+04	4.55E+04
Xe-133	3.90E+02	1.05E+07	1.05E+07
Xe-133m	9.31E+00	2.51E+05	2.51E+05
Xe-135m	1.05E+02	2.82E+06	2.82E+06
Xe-135	3.80E+02	1.03E+07	1.03E+07
Xe-137	3.53E+02	9.51E+06	9.51E+06
Xe-138	3.20E+02	8.63E+06	8.63E+06
Xe-139	2.93E+02	7.91E+06	7.91E+06
I-131	1.68E+02	4.54E+06	2.27E+04
I-132	2.50E+02	6.74E+06	3.37E+04
I-133	3.90E+02	1.05E+07	5.26E+04
I-134	4.54E+02	1.22E+07	6.12E+04
I-135	3.66E+02	9.88E+06	4.94E+04

Table 3 Occupational Dose Values
Scenario A

Isotope	Whole-body Inhalation TEDE (mrem)	Whole-body Submersion TEDE (mrem)	Thyroid Inhalation CDE (mrem)	Thyroid Submersion CDE (mrem)
Kr-83m		.0003		.0001
Kr-85		.012		.01
Kr-85m		3.5		3.5
Kr-87		38.7		38.8
Kr-88		132.0		133.0
Kr-89		140.0		190.0
Kr-90		8.6		8.8
Xe-131m		.004		.004
Xe-133		3.8		3.7
Xe-133m		.08		.08
Xe-135m		13.5		13.5
Xe-135		28.6		28.3
Xe-137		9.1		5.9
Xe-138		117.0		117.0
Xe-139		18.0		
I-131	15.6	.09	512.0	.09
I-132	.2	.88	4.53	.88
I-133	6.4	.36	198.0	.36
I-134	.2	1.9	1.36	1.9
I-135	1.3	.92	32.3	.92
Total	23.7	517	747.0	600.0
Whole-body TEDE		540	Total Thyroid CDE	1347

Table 4 Total Effective Gamma Dose Equivalent
Scenario B

Location	TEDE Dose [mrem]				
	1 hr	2 hr	24 hr	48 hr	720 hr
1st Floor Airlock security door	.02	.03	.14	.14	.15
3rd Floor airlock security door	.14	.21	.84	.84	.88
Containment wall, outside	.07	.11	.47	.47	.47
Outside truck door - .16 m	18.60	27.40	110.00	112.00	123.00
Outside truck door – 2.5 m	5.24	8.00	32.20	33.00	36.00
Outside truck door - 9.5 m	.84	1.24	4.00	4.10	4.51
Outside truck door – 19.5 m	.24	.37	1.49	1.52	1.63

Table 5 Total Effective Dose Equivalent
Scenario C

Stability Class	30 days TEDE Dose [mrem]					
	Near Source Release, 10 m			Nearest Residence, 200 m		
	Gamma	Ground	Total	Gamma	Ground	Total
A	4.5	15.1	19.6	-	.06	.06
D	4.5	31.7	36.2	-	.13	.13
F	4.5	31.7	36.2	-	.13	.13

Table 6 Total Effective Dose Equivalent
Scenario D

Stability Class	TEDE Dose 18 hours [mrem]					
	Max Dose Location, 10 m			Nearest Residence, 200 m		
	Gamma	Vent	Total	Gamma	Vent	Total
A	.3	1.1	1.4	-	.4	.4
D	.3	4.0	4.3	-	.07	.07
F	.3	6.3	6.7	-	.1	.1

End of Responses to RAI 13.5

Response to RAI-13.6.a

Both references are provided in Appendix B of this response. The first reference is the LOCA analysis description developed by RINSC. The second reference is the LOCA analysis report developed by Dr. E. Feldman at Argonne National Laboratory.

Response to RAI-13.6.b

While there are minor differences between the UMLRR and RINSC reactor core configurations, these differences have negligible impact on the applicability of the RINSC LOCA analysis. Most importantly, the UMLRR core is significantly larger than the RINSC core (21 elements vs 14 elements). The higher number of fuel plates (22 vs 16) per assembly and associated heat generation, in the RINSC core, can be compared to the UMLRR core, which leads to more distributed and lower volumetric power production in the UMLRR core. This provides larger convection cells with more coolant available to protect the reactor fuel during a LOCA event.

In terms of physical differences, both graphite and beryllium are exceptionally high thermal conductivity materials, k_{Ber} 200W/(mK) vs $k_{Graphite}$ 100W/(mK). From a thermal perspective, both materials are excellent conductors, producing little in terms of differential thermal gradients when comparing the cores. In addition, the peak flux in both cores is located around the central flux traps. Here, the difference between the two central flux traps is material construction. The UMLRR flux trap is solid aluminum, while the RINSC flux trap is beryllium. There is no internal heat production in the aluminum, while the beryllium has limited physical heat generation, via the n,2n reaction and gamma, n reactions. As with the graphite example above, the difference between the thermal conductivities of the beryllium and the aluminum are comparable (k_{Ber} 200W/(mK) vs k_{Al} 240W/(mK)).

Elements of this RAI were also addressed in In Facility Response RAI SAR 4.1[3] item (e): " The statement in the SAR that the UMLRR U_3Si_2-Al fuel is more limiting than the Worcester Polytechnic Institute (WPI) UAl_x-Al fuel is easily justified. The UMLRR fuel assembly is more reactive (i.e. has a higher k_∞) and it has fewer fuel plates per assembly. This leads to higher powered assemblies when placed into a given core configuration and, for a given assembly power, to a higher plate power since there are only 16 plates per element in the UMLRR assembly (versus 18 fuel plates per WPI element)." The lower uranium loading of the WPI aluminide fuel, when compared to both the UMLRR silicide and RINSC silicide fuel, results in a lower heat production and therefore falls within the envelope of the RINSC LOCA analysis. Taken together, these characteristics make the UMLRR comparison to RINSC an equivalent or more conservative comparison.

Response to RAI-13.6.c

The bottom of UMLRR core box is designed to be hydraulically connected to the reactor pool. This is achieved by an approximately 3/4" thru-hole located at the bottom-center of the lower core coolant plenum. This hole maintains a hydraulic connection between the core box and the

[3] UMass Lowell, Lic. No. R-125, Docket No. 50-223, Response to NRC RAI letter dated 02/01/17

remaining water in the reactor pool should the pool level drop to the bottom of the beam tube level.

Response to RAI-13.6.d

A final draft version of the Technical Specifications is to be submitted at a later date as part of this relicensing effort and shall include the following specifications:

1. The reactor shall not be operated with both the beam port lead shutter in the up (open) position and the beam-port shield plug removed.
2. The shield plug may be substituted or modified so long as the overall open diameter does not exceed 1-in.
3. In order to access the beam ports with both the lead shutter in the up position and shield plug removed, the reactor shall be positioned in the bulk pool.

The SAR Section 10.2.1 provides information on the beam port design. The following provide bases for the above proposed specifications. The 1-in diameter stated in the proposed TS #2 above allows for the production of a narrow radiation beam, useful for a wide range of potential research applications. The 1-in limit is well below the maximum diameter for a LOCA and drain time that could lead to the blister point fuel temperature. If a catastrophic damage event should occur to the in-pool portion of the beam tube (i.e., rupture) while the shutter is raised, one mitigating action would be to lower the shutter. The lead shutters are contained within the shutter housing which is located in the biological concrete shielding surrounding the pool. The shutters are roughly the length of the housing at 10-in. The shutters vary only in diameter and weight with the 6-in shutter at 150 pounds and the 8-in shutter at 244 pounds. Due to the high density of the lead, it will be able to displace any water that may be in the shutter assembly and effectively block and seal the tube from the rupture on the pool side. In such a case where the shutter was up and the shield plug removed, the reactor is also positioned in the bulk pool (via TS #3 above). If the tube rupture were to occur, the response to the event would also include placing the pool divider gate in place to protect the bulk pool from draining. The leak/damage to the beam port could then be appropriately addressed. Additionally, the beam ports can be covered with a 1" aluminum plate, bolted to the tube at the exit of the biological shield. Each of the three beam ports has an individual cover plate available. Used in conjunction -- closing the shutter, installing the pool gate, and installing the cover plate -- provides adequate defense-in-depth to mitigate this potential accident scenario.

Response to RAI-13.6.e

The primary cooling system is described in SAR Section 5.2. As discussed in this section, the preferred operating mode for forced convection cooling is the "cross-stall" mode due to vibration of the control blades in the "downcomer" mode. In cross-stall mode, the suction side of the primary pump draws the primary flow through the bottom of reactor core, while the reactor is located in the stall pool. Primary cooling water then passes thru the heat exchanger and is returned to the opposite side of the pool (bulk side). This cross pool flow pattern will only function with the pool divider gate for the two pools uninstalled. Therefore, the pool divider gate

by default cannot be in place when the reactor is operating in forced convection mode, negating the need for a TS requirement.

Response to RAI-13.7

As noted in the response to RAI 11-2.c.i, Figure 3-2 of the SAR provides an incorrect height for the top of the reactor building dome above the core centerline. As this measurement was used in the geometry assumptions used in the LOCA shine analyses in SAR Section 13.2.4.1, the LOCA shine has been reanalyzed based on the actual building height and cylindrical wall height data. This revised analysis has been submitted in Appendix C of this document.

Response to RAI-13.8

A combination of administrative controls and design features minimize the potential for Foreign Objects and Debris (FOD) to cause a coolant channel blockage.

As part of the reactor checkout procedure, the operator is required to perform a visual check of the reactor bridge and core area to include the following as stated in procedure RO-7:

- Inspect the core and remove any items that do not need to be there. Look for loose items such as tools, samples, bolts, etc.
- Inspect the ropes on any unsecured samples and make sure the rope and sample is secure.
- Clear all loose items from the bridge unless the item is necessary for sample movement.

Design features include the concrete pool wall extending 2-ft above the pool on the third floor level (SAR Figure 3-2). The wall extension above the floor provides an effective barrier from FOD being inadvertently kicked or knocked into the pool. The reactor bridge (see SAR 4.2.5 and figure 4-12) rests atop the wall and spans the width of pool to provide a platform for operators to observe the core, insert core samples, access the drive mechanisms for maintenance, etc. If an FOD should enter the pool while the operator is working above it, the operator would visually track the FOD to its final resting place. Operational experience has shown that an FOD inadvertently entering the pool has a strong tendency to drop to the pool floor where it can be recovered. A remote scram button located on the reactor bridge is also available to the operator should the FOD track to the top of the core.

The cross pool method of forced convection operation (SAR Section 5.2) requires bulk mixing of the pool water rather than a semi-closed loop design. If an FOD not noticed during the reactor checkout or inadvertently introduced unnoticed is drawn into the primary flow pathway, it would then need to transit the physical space between the fuel element end box and the fuel plates (SAR Section 4.2.1, figure 4-3) to cause a partial blockage. The fuel element end box, which contains the lifting handle (or bale), provides an effective physical barrier to inhibit an FOD from blocking the coolant flow pathway through the element. The end box is attached to aluminum side plates that are longer than the fuel element fuel plates. The resultant vertical gap between the end box and fuel plates at the front and back sides of the element provides an open channel for coolant flow should an FOD land on top of the end box.

APPENDIX A
UMLRR Storage Rack Criticality Analysis Result

UMLRR Storage Rack Criticality Analysis Results

Dr. John R. White

Chemical and Nuclear Engineering Department
University of Massachusetts Lowell
Lowell, MA 01854

August 11, 2016

Overview/Summary

The fresh and used fuel assemblies for the UMass-Lowell Research Reactor (UMLRR), when not in the reactor core, are stored in one of several storage racks that lie along the concrete pool wall. Each storage rack can hold up to nine (9) 3″×3″×30″ fuel elements in a linear array with a nominal center-to-enter spacing of about 3.78 inches (see the drawings identified in Ref. 1). One of the long sides of the aluminum storage rack is flush against the pool wall, but the pool-facing side has a thin Al/Boral plate structure as an additional reactivity hold-down device. However, there is some question as to the actual boron content of the poison plate and its effect on the reactivity level of a storage rack full of fresh fuel. The purpose of this brief study/report is to show that the reactivity credit associated with the Boral plate is not needed to assure that the storage rack configuration is always well subcritical. To support this conclusion, a series of MCNP[2] calculations were performed that confirm that the expected multiplication factor for a UMLRR storage rack full of fresh fuel, with no Boral in the model, is well below k = 0.7, which is substantially lower than the k < 0.9 limit quoted in ANSI Standard ANSI/ANS-15.1-2007 (R2013) for any fissionable storage configuration outside the reactor (see Ref. 3). The remainder of this brief report describes the models and methods used and summarizes the key results of the calculations performed -- with the primary goal of supporting the key conclusion that the UMLRR storage racks are significantly subcritical without the reactivity credit associated with the Boral sheet on one side of the rack geometry.

Models and Methods

A set of detailed MCNP models of the UMLRR have been used for several years now for general operational support and for evaluation of specific experiments within the facility. Overall, these MCNP models give a good representation of the physics behavior of the UMLRR, and ample evidence has been accumulated that support our confidence in the existing in-house computational tools/models. In particular, Refs. 4-5 give lots of detail concerning the base UMLRR MCNP model, along with several evaluations relative to actual measured data for the UMLRR. In most cases, the results are quite satisfactory and they certainly support the use of these computational models for routine UMLRR support.

The MCNP model for the current storage rack criticality safety analysis used the same base low enriched uranium (LEU) fuel element model as described in Refs. 4-5. This pre-existing model of a fresh fuel assembly represented the starting point for the current computational study. With this base, a series of storage rack models were developed which included a linear array of the fresh

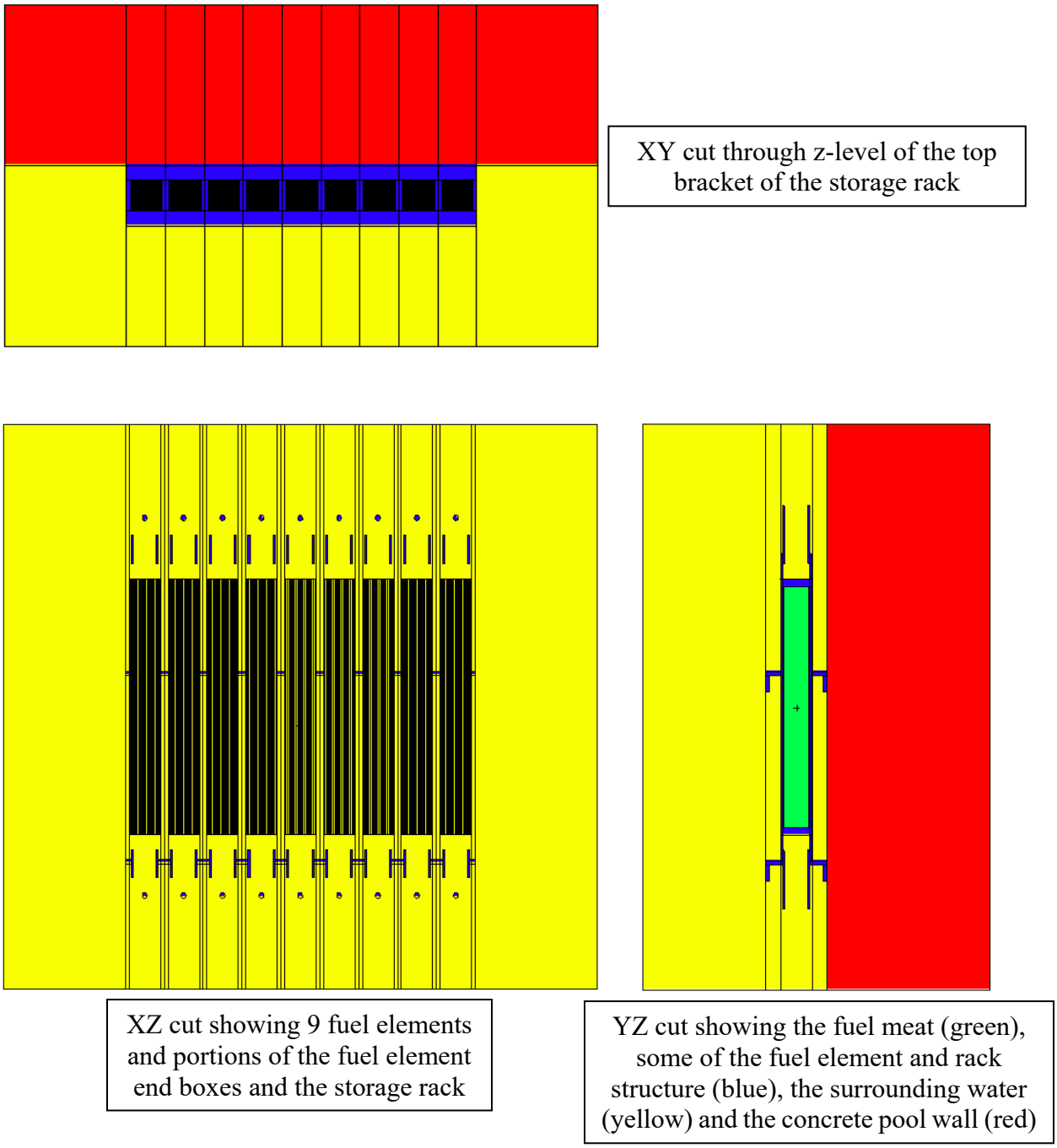

Fig. 1 Various views of the full storage rack model containing nine (9) fresh fuel elements.

fuel elements, surrounded by water, a combination of water and concrete, and a final model that even included some of the details of the Al rack structure. The complete set of calculations for this study included sensitivity analyses to address the effect of the center-to-center spacing, a check on the importance of including the concrete wall and/or the aluminum rack in the modeling, the effect on subcriticality of adding additional elements, one by one, to the rack, and even a quick check to make sure that the use of different cross sections libraries did not have any significant effect on the computed results.

For visual reference, Fig. 1 shows several views of the final MCNP geometry model for the nominal case of a full storage rack. As noted above, some of the parametric calculations did not include the rack structure, some had the concrete wall replaced by water, several cases had a reduced number of assemblies, and some runs even included variable center to center spacing between the fuel element. However, with reference to Fig.1 and a description of the specific cases of interest, one should be able to visualize the actual geometry used for the cases summarized here.

Summary Results

Center-to-Center Spacing: The first model addressed did not include the rack structure or the concrete wall -- only water reflectors were used. The model included a single fuel assembly with 20 cm of water above and below the fuel end boxes and 30 cm of water on the front and back sides (in the y-direction) -- these represent infinite water reflectors in these directions. In the x-direction, the gap between fuel elements (or center-to-center spacing) was varied and the outer boundaries used reflected boundary conditions to represent an infinite linear array of fuel elements. The results of this set of calculations are summarized in Fig 2.

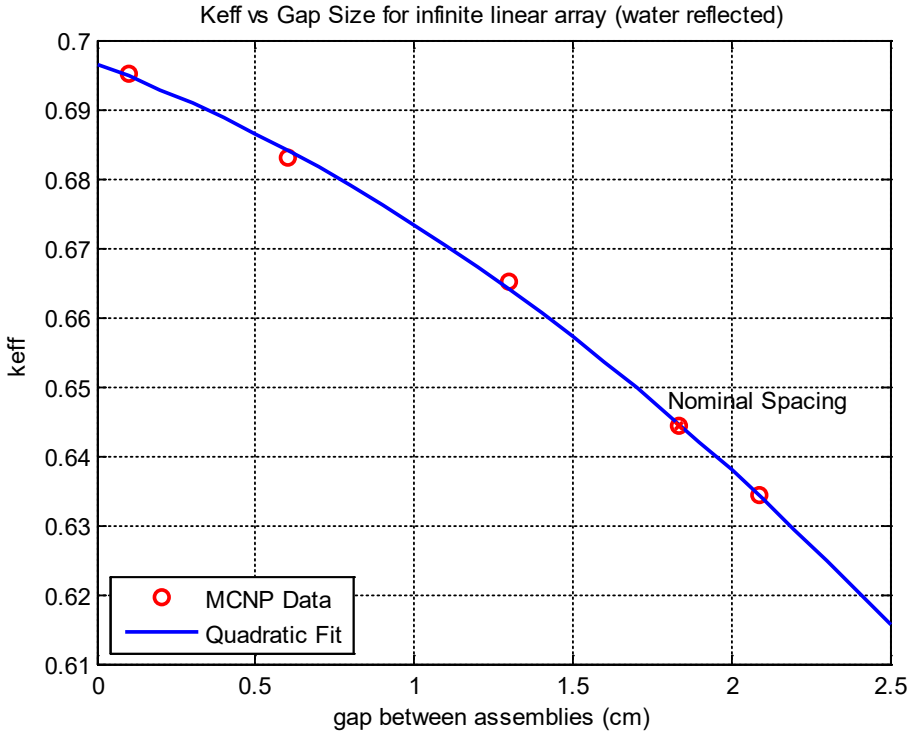

Fig. 2 Criticality level versus element spacing (water reflected model).

There are two important results illustrated here -- that the maximum multiplication factor for an infinite linear array of fuel elements is less than 0.7, and that the nominal spacing for the UMLRR storage rack of 3.78 inches (9.60 cm) even reduces this value further.

Note: The fuel assembly width is 3.06 inches (7.7724 cm), so the nominal gap size of 1.83 cm shown in Fig. 2 leads to a nominal center-to-center spacing of about 9.60 cm.

Reflector Effects: Although it was expected that explicitly adding the concrete wall and/or the aluminum rack into the MCNP model would have negligible effects on the above purely water-reflected results, MCNP models that included these components were developed anyway -- just to confirm and quantify the original expectations. Table 1 summarizes the results of this brief sensitivity study for the case of the nominal 3.78 inch center-to center spacing between elements for an infinite array of fuel elements. As apparent, both effects were indeed small (or negligible) and they do not change the conclusions obtained from the data in Fig. 2.

Table 1 Sensitivity effects of concrete wall and the aluminum rack structure.

Case Description	MCNP k_{eff}
purely water reflected with no rack structure	0.6442
40 cm of concrete wall included instead if water	0.6488
upper and lower rack structures included	0.6440

Note: In most of the MCNP calculations, the 1σ uncertainty in the value of k was between 0.0004 and 0.0005. Thus, values of k_{eff} that differ by less than about 0.0015 are essentially identical from a statistical perspective.

Cross Section Library Effects: Because the value of the computed subcriticality for the infinite linear array of fresh UMLRR U_3Si_2-Al fuel elements is so far below the regulatory limit of $k < 0.9$, a detailed sensitivity study to quantify all the model uncertainties is not really needed here. However, as an additional confirmatory check, three different MCNP cross section libraries were used to show that the sensitivity to this particular modeling option is indeed quite low. In particular, ENDF 7.0 data (i.e. with nuclide IDs ending in .70c) were used as the reference cross sections for most of the calculations. However, to evaluate the effect of different libraries, calculations for the case of the nominal 3.78 inch center-to center spacing between elements for an infinite array of fuel elements were also completed with ENDF 6.6 data and ENDF 7.1 data (i.e. with IDs ending in .66c and .80c, respectively). The results of this parametric exercise are given in Table 2 and, as apparent, there are no significant differences observed for the libraries used here.

Table 2 Sensitivity effects of cross section library for infinite linear array of fuel elements.

Case Description	MCNP k_{eff}
ENDF 7.0 data	0.6442
ENDF 7.1 data	0.6437
ENDF 6.6 data	0.6417

Number of Assemblies in Linear Array: All the MCNP calculations up to this point used reflected boundary conditions in the x-direction to simulate an infinite linear array of fuel elements. In practice, however, the UMLRR storage racks only hold a maximum of nine (9) elements. Thus it was of interest to determine how the subcriticality level changes when adding one element at a time, starting with only a single fuel assembly. In addition, this set of calculations should also validate that the infinite linear array modeling with the reflected boundary conditions was done properly since, as more and more elements are added, the value of the multiplication factor should approach the infinite array result.

For this series of calculations, the complete storage rack model, including the concrete wall and rack structure, was used (since the geometric modeling had already been performed for the above sensitivity calculations). This model is quite representative of the actual rack geometry as illustrated in Fig. 2 for the case of nine fuel elements. The computational results are summarized in Fig. 3, which shows the multiplication factor, k_{eff}, increasing rapidly up to five (5) assemblies to a k-value of nearly 0.6, but then the curve flattens as more elements are added to the linear array, eventually reaching a $k_{\infty} \approx 0.65$ for a large number of fuel elements (the value plotted at n = 25 is the infinite linear array value from the single assembly case with reflected boundary conditions). The results here are indeed as expected, with the subcriticality level stabilizing as predicted in the prior computations.

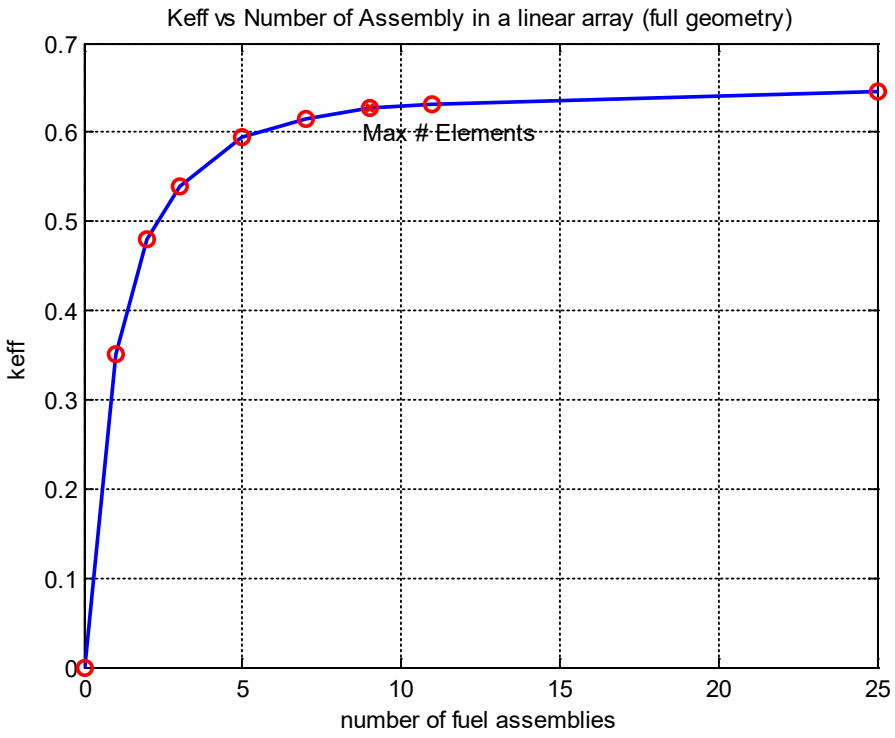

Fig. 3 Criticality level versus number of fuel elements (final rack model).

Number of Rows of Assemblies: Although not really pertinent to the single-row UMLRR storage rack design, a final set of calculations was performed to show that the given rack arrangement (with the assembly spacing of the actual UMLLR storage racks) would never

approach a critical mass even if the number of rows was increased. To do this calculation, the basic geometry shown in Fig. 2 was maintained (with slight modification within MCNP), except that the number of rows of fuel elements was increased -- this was done while maintaining the y-direction spacing of the original rack design. For illustration of the geometry, the top view of the 3-row model is shown in Fig. 4 and the summary results from the analysis are displayed in Fig. 5. For this hypothetical study, nine (9) elements in the x-direction were assumed.

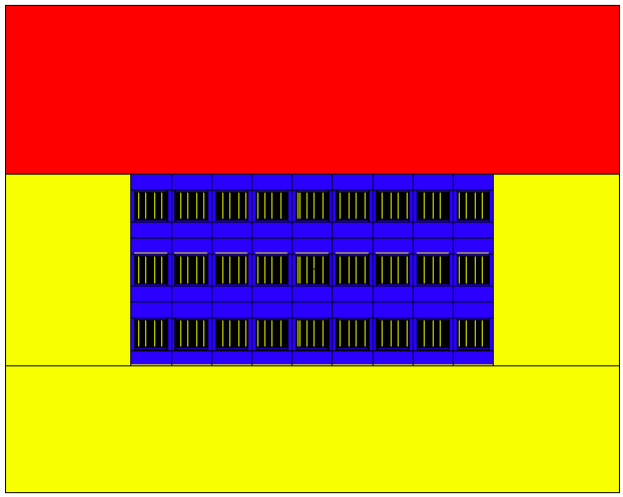

Fig. 4 XY cut through hypothetical 3×9 storage rack full of fresh UMLRR fuel elements.

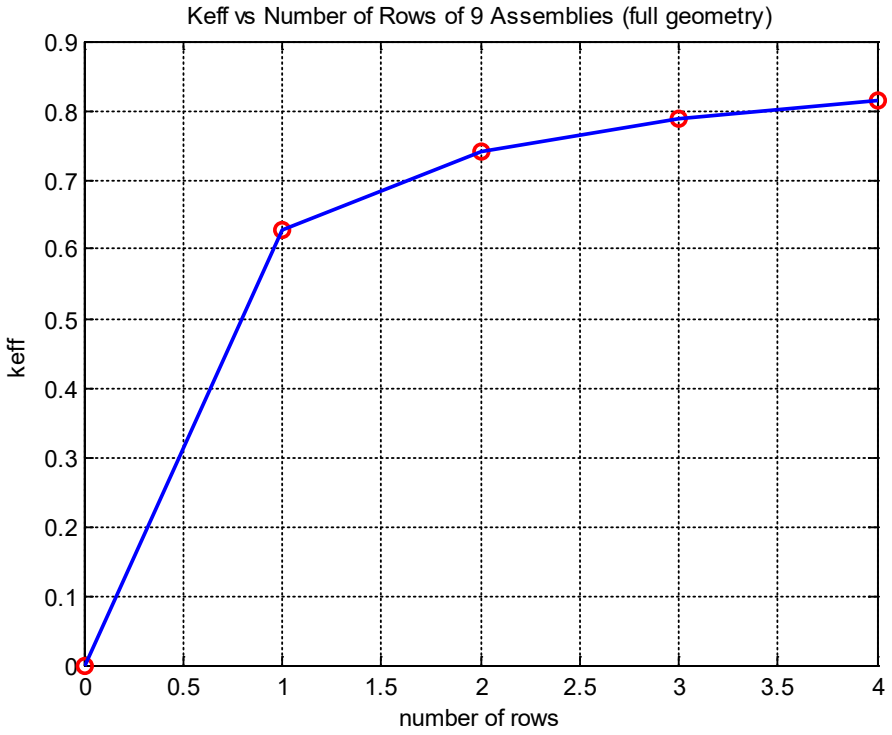

Fig. 5 Criticality level versus number of rows of nine (9) fuel elements (final rack model)

As apparent from Fig. 5, a 1×9 linear array (which is the UMLRR arrangement) is very subcritical, but even a 4×9 array has a k-value well below the regulatory limit of $k_{eff} < 0.9$ for a fuel storage geometry. This final analysis simply shows that there is essentially no way for the single-row UMLRR rack design to support a critical configuration. Even if multiple racks were placed side by side (which is simply not possible with the current rack design and placement along the walls of the UMLRR pool), the overall fuel storage arrangement stays well subcritical -- and none of the calculations performed in this study use any Boral poison material!

Conclusions

The purpose of this brief study was to show that the reactivity credit associated with the Boral plate that is part of the UMLRR storage rack design is not needed to assure that the storage rack configuration is always well subcritical. A series of MCNP calculations were performed that showed that the expected multiplication factor for a UMLRR storage rack full of fresh fuel, with no Boral in the model, is about $k = 0.63$, which is well below the regulatory $k < 0.9$ limit. A variety of other hypothetical geometries (infinite linear array and multiple rows of racks) and some sensitivity studies (effect of concrete wall, inclusion of Al rack, use of different cross section libraries, etc.) were modeled and, in all cases, the same conclusion was obtained -- that the fuel storage racks in the UMLRR always represent a substantially subcritical geometry without consideration of the Boral poison plate -- so no reactivity credit is used (or needed) for this extra reactivity hold-down feature of the UMLRR rack geometry.

References

1. Several General Electric Blueprints dated circa 1958 -- #192C580, #107C3552, and #218B992.
2. "MCNP6.1: Monte Carlo N-Particle Transport Code System," distributed through the Radiation Safety Information Computational Center, CCC-810 (Aug. 2013).
3. "American National Standard: The Development of Technical Specifications for Research Reactors," American Nuclear Society, ANSI/ANS-15.1-2007 (R2013) (April 2013).
4. J. R. White, R. Gocht, and M. Ducey "Final Report on MCNP Modeling for the UMLRR and Selected Gamma Irradiation Facilities," UMass-Lowell internal project documentation (Sept. 2011). Also see a series of internal Progress Reports that document the on-going development of the MCNP UMLRR model dated Nov. 2010, Jan. 2011, and Aug. 2011.
5. J. R. White, R. Gocht, M. Pike, and J. Marcyoniak, "Validation of the 3-D VENTURE and MCNP UMLRR Core Models used in Support of the WPI Fuel Transfer Project", Research Reactor Fuel Management Conference (RRFM2012), Prague, Czech Republic (March 2012).

APPENDIX B1

RINSC LOCA ANALYSIS

LOCA Analysis Addendum

Introduction

Dr. Earl Feldman from Argonne National Laboratory prepared a Loss of Coolant Accident Analysis for the Rhode Island Nuclear Science Center in 2004 entitled, "Section 13.2.3 Loss of Coolant Accident (LOCA) of Safety Analysis Report of the Rhode Island Nuclear Science Center Reactor, Submitted May 3, 2004". The drain model for this analysis has been refined to include the through port experimental facility as a potential pool water pathway, and to provide a more realistic and less limiting representation of the experimental facility drain piping. The decay power and heat transfer model are described in the original analysis document. The new drain model is presented in this addendum.

Accident Scenario

The Maximum Credible Accident (Design Basis Accident) is that a beam port extension is sheared off, which provides a path for the primary coolant to leak out of the pool. The through port is not considered to be credible for this accident because it passes underneath the thermal column extension, and therefore is not readily accessible for shearing as the following photograph of the high power section of the pool shows.

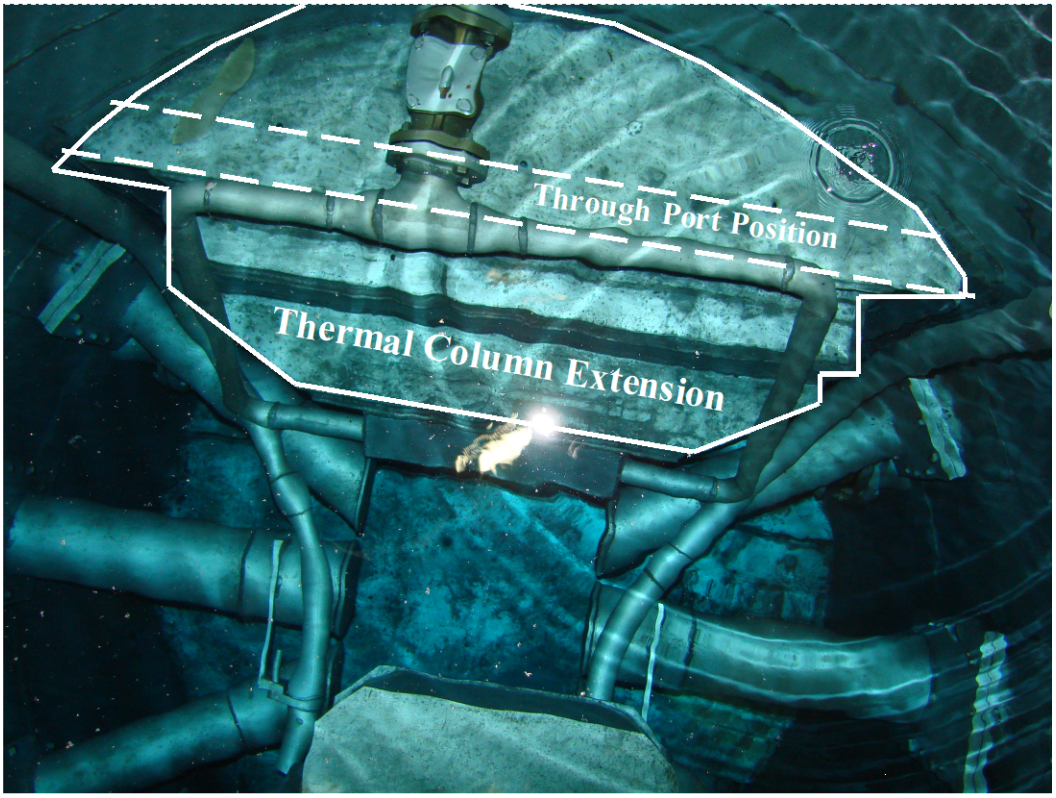

Experimental Facility Penetrations into the Reactor Pool

Of the six beam ports, four of the beam ports are six inch diameter ports, and two are eight inch diameter ports. All of the beam ports have the same center line elevation. Consequently, the most conservative accident scenario is one in which an eight inch diameter beam port is sheared off.

Drain Model

As shown in the following figure, each beam port has a one inch diameter drain line, and a one inch diameter vent line. These lines merge into a single one inch line at an elevation below the bottom of the beam port, extend out to the confinement edge of the reactor pool wall, and go through a manual drain valve. On the outlet side of the drain valve there is a one half inch diameter orifice plate welded onto the drain line. The one inch drain line connects to a two inch diameter drain line that is common to all of the beam ports, as well as the through port. This common line also connects to the one inch drain line for the through port, and the five inch off gas vent for the thermal column. The common drain line is well below the elevations of the beam ports, through port, and thermal column, and it connects to a five inch drain line that extends into the basement underneath the reactor. The five inch line is capped with a pipe tee that is positioned vertically. The upward facing vent ultimately ties into the Off Gas System. The downward facing drain diameter is reduced to a two inch line that empties into a five gallon bucket that is open to air.

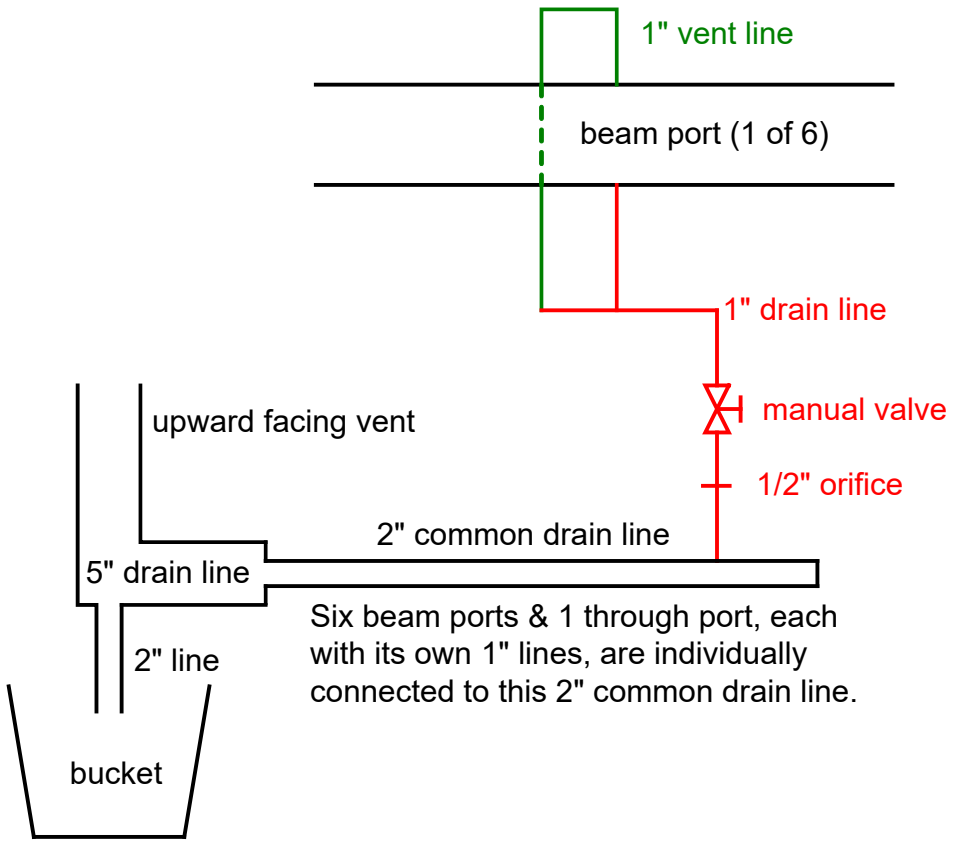

Experimental Drain System

Historically there has been an administrative control that requires that each of the ends of the beam ports and the through port that are open to the confinement room have an area of no more than a one half inch diameter hole open to confinement.

If an eight inch diameter beam port is sheared off, it will flood. The water will have two pathways:

1. Through the beam port drain lines
2. Though the open area at the confinement room end of the beam port

The most constrictive point of the beam port drain line is the one half inch diameter orifice. Since this opens into progressively larger pipe diameters that are at a lower elevation than all of the experimental facilities, there is no possibility that water from the sheared beam port will enter the other beam ports, through port, or thermal column. The original LOCA analysis assumed that the experimental drain system was a closed system, rather than a system that is open to the atmosphere. That analysis was more limiting in that the drain time was shorter because it allowed water to flow from the broken beam port, to the other five beam ports without any hydraulic resistance along the way, making each of them a potential pathway for pool water to drain in the event of a design basis accident.

The water that makes its way through the open area at the confinement room end of the beam port has historically been limited administratively to the area of a one half inch diameter hole.

Consequently, all of the water from the flooded beam port must pass through two, one half inch diameter holes. One of the holes is at the elevation of the bottom of the eight inch beam port, and the other can be taken conservatively at the elevation of the common two inch drain line. Therefore, a conservative model would be a tank in which water is draining out of two, one half inch diameter holes at the elevation of the centerline of the common two inch drain line. The difference in elevations between the pool level scram set point and the common two inch drain line is 28.06 ft as shown in the diagram that follows. It should be noted that the elevations shown in this diagram differ slightly from the comparable elevations used in the original LOCA analysis. These differences are fractions of an inch, and are negligible. They arise from the fact that the original information was based on the original General Electric Maintenance Manual for the facility, and the information used in this analysis was taken directly from the engineering drawings that are on the reference list that is on the following diagram.

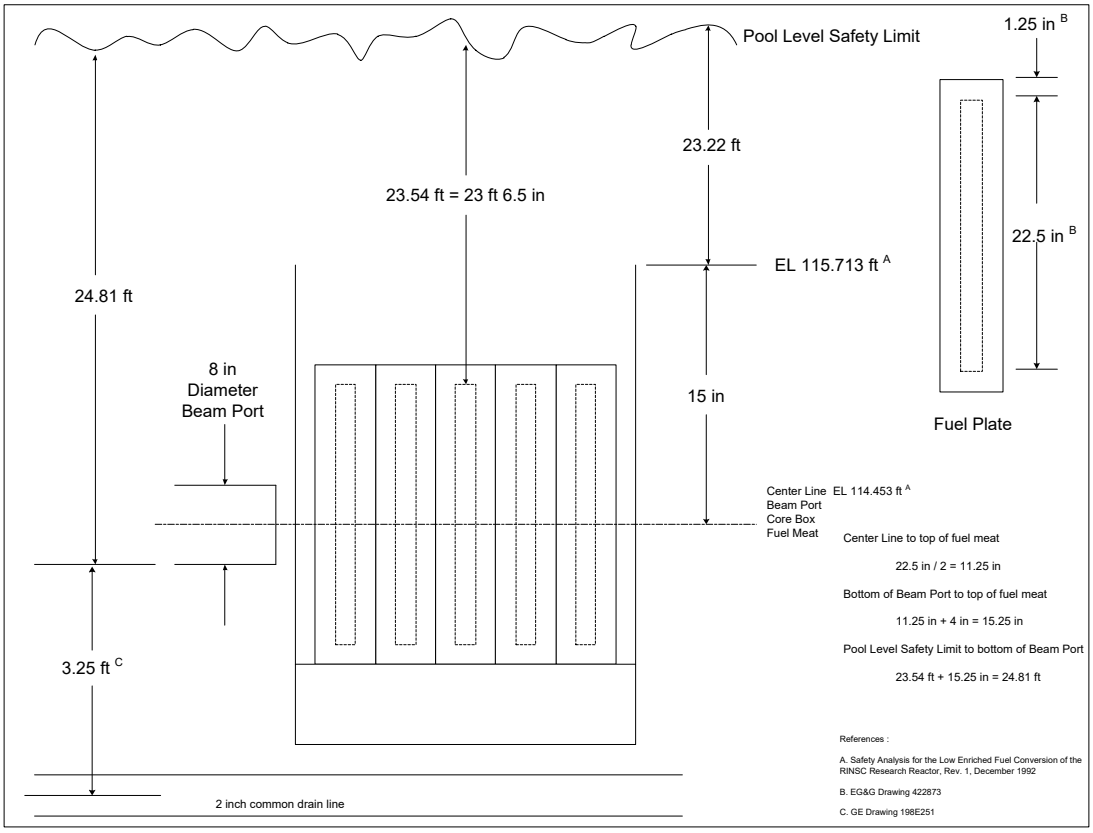

Elevations

As part of the analysis performed by Dr. Feldman, it was shown that as long as part of the fuel meat remains submerged in water at a level that is no lower than the elevation of the bottom of the eight inch beam ports, and the power fraction is no greater than 0.827%, then there is sufficient cooling capacity to prevent the fuel cladding temperature from reaching the blister point. The thermal analysis was a steady state problem with the water level at the bottom of the eight inch beam ports. Conservatively in that analysis, the drain time was taken to be the amount of time that it takes for the pool level to drop from the scram set point to the top of the grid box, which is well above the top of the fuel meat. The additional time for the water level to drop from the top of the grid box to the bottom of the eight inch beam ports was ignored

The difference in elevations between the pool level scram set point and the top of the grid box is 23.22 ft. Therefore, the difference in elevations between the top of the grid box and the common two inch drain line is:

28.06 ft – 23.22 ft = 4.84 ft

As a result, a conservative drain model is a tank with two, one half inch diameter holes at an elevation of 28.06 ft below the initial water level, and we are interested in the time that it takes for the water level to drop 23.22 ft to an elevation of 4.84 ft above the drain holes.

Drain Time

Bernoulli's Equation can be used to determine the drain time for the model.

Recall that Pressure can be put into terms of energy per volume:

$$P = \frac{Force}{Area} = \frac{F(d)}{A(d)} = \frac{Work}{Volume} = \frac{Energy}{Volume}$$

Bernoulli's equation is a consequence of the Law of Energy Conservation. The energy in a non-compressible liquid under laminar flow conditions is the sum of the static pressure, kinetic energy, and potential energy of the liquid. Therefore:

$$P + (1/2)\rho V^2 + \rho g Z = Cons\tan t$$

Where: P = Static Pressure

$(1/2)\ \rho V^2$ = Kinetic Energy

$\rho g Z$ = Potential Energy

Since at any given instant, the energy at the liquid surface in the tank is equivalent to the energy at the exit hole, we can say that:

$$\frac{V_1^2}{2} + \frac{P_1}{\rho} + gZ_1 = \frac{V_2^2}{2} + \frac{P_2}{\rho} + gZ_2$$

Where: V_1 = Velocity at which the liquid level is dropping

P_1 = Static pressure at the surface of the tank

Z_1 = Elevation of the liquid surface above the drain orifice

g = Acceleration due to gravity

V_2 = Velocity at which the liquid is exiting through the hole at the vena contracta

P_2 = Static pressure at the elevation of the drain hole

Z_1 = Elevation of the drain orifice

Since the water goes through a restriction:

$V_2 > V_1$

The increase in velocity is due to an increase in kinetic energy at the exit point. However, the total energy must be conserved, which means that the increase in kinetic energy of the fluid must come at the expense of either pressure energy or potential energy. In the model, the tank is open to atmosphere so P_1 is at atmospheric pressure. The drain also effectively opens to atmosphere because the liquid drains into a pipe system that has a sufficient diameter to prevent it from filling with fluid. This pipe system is also open to atmosphere, which means that P_2 is also at atmospheric pressure. This means that the increase in fluid velocity at the exit is due to the conversion of potential energy into kinetic energy, and that:

$P_1 = P_2 = 1$ atm

Consequently the P / ρ terms on both sides of the equation cancel reducing Bernoulli's equation to:

$$\frac{V_1^2}{2} + gZ_1 = \frac{V_2^2}{2} + gZ_2$$

$$\frac{V_1^2}{2} + gZ_1 - gZ_2 = \frac{V_2^2}{2}$$

$$\frac{V_1^2}{2} + g(Z_1 - Z_2) = \frac{V_2^2}{2}$$

But $(Z_1 - Z_2)$ is equivalent to the height (h) that the level of the liquid drops:

$$\frac{V_1^2}{2} + g(h) = \frac{V_2^2}{2}$$

$$\left[\frac{V_1^2}{2} + g(h) = \frac{V_2^2}{2}\right]2$$

$$V_1^2 + 2gh = V_2^2$$

$$V_2 = \sqrt{V_1^2 + 2gh}$$

The velocity at which the level of the liquid is dropping (V_1) is negligible in comparison to the velocity of the liquid in the jet stream so:

$$V_2 = \sqrt{2gh}$$

For a tank of liquid that has a hole below the level of the liquid, the relationship between the velocity at which the liquid level is dropping and the velocity at which the liquid is exiting the hole is:

The volume of liquid that exiting the hole per unit time is:

Volume (m^3 / s) = [Cross Sectional Area of Hole (M^2)] [Liquid Velocity (M / s)]

The same volume of liquid is removed from the surface of the tank, and can be calculated by:

Volume (m^3 / s) = [Cross Sectional Area of Tank (M^2)] [Liquid Velocity (M / s)]

These volumes are equal so:

$V_1A_1 = V_2A_2$

$$V_1 = \frac{A_2}{A_1} V_2$$

Where:

V_1 = Velocity at which the liquid level is dropping

V_2 = Velocity at which the liquid is exiting through the hole

A_1 = Cross sectional area of the tank

A_2 = Minimum cross sectional area (vena contracta) of the jet of liquid that is coming out of the drain hole

The ratio of the minimum cross sectional area (vena contracta) of the jet of liquid that is coming out of the drain hole (A_2), and the area of the hole that the jet is streaming from (A), is called the orifice coefficient (C_d):

$$C_d = \frac{A_2}{A}$$

Where:

C_d = Orifice coefficient

A = Cross sectional area of the hole that the liquid is draining through

A_2 = Minimum cross sectional area (vena contracta) of the jet of liquid that is coming out of the drain hole

The orifice coefficient for a sharp edged orifice that has water flowing though it has been found empirically, and is listed in references as:

$C_d = 0.61$

We can put A_2 in terms of C_d and A:

$$C_d = \frac{A_2}{A}$$

$A_2 = C_d A$

Therefore:

$$V_1 = \frac{A_2}{A_1} V_2 = \frac{C_d A}{A_1} V_2$$

Plugging in our equation for V_2:

$$V_1 = \frac{C_d A}{A_1} \sqrt{2gh}$$

V_1 is the velocity at which the level of the liquid in the tank is dropping, which is the rate at which the height of the liquid is decreasing. Therefore:

$$V_1 = -\frac{dh}{dt}$$

Plugging in our equation for V_1:

$$-\frac{dh}{dt} = \frac{C_d A}{A_1} \sqrt{2gh}$$

This equation can be separated into factors that are related to time, and factors that are related to the height of the liquid:

$$dt = -\frac{A_1}{C_d A \sqrt{2gh}} dh$$

This equation can be integrated from t = 0 to $t = t_{final}$ in which these times correspond to the initial and final heights of the liquid in the tank:

$$\int_0^{t\ final} dt = \int_{h\ initial}^{h\ final} -\frac{A_1}{C_d\ A\sqrt{2gh}}\,dh$$

$$t_{\ final} = -\frac{A_1}{C_d\ A}\int_{h\ initial}^{h\ final}\frac{dh}{\sqrt{2gh}}$$

$$t_{\ final} = -\frac{A_1}{C_d\ A\sqrt{2g}}\int_{h\ initial}^{h\ final}\frac{dh}{\sqrt{h}}$$

$$t_{\ final} = -\frac{A_1}{C_d\ A\sqrt{2g}}\left[\frac{\sqrt{h}}{1/2}\right] evaluated\ between\ h_{\ final}\ and\ h_{\ initial}$$

$$t_{\ final} = -\frac{2A_1}{C_d\ A\sqrt{2g}}\left[\sqrt{(h_{\ final})} - \sqrt{(h_{\ initial})}\right]$$

$$t_{\ final} = \frac{2A_1}{C_d\ A\sqrt{2g}}\left[\sqrt{(h_{\ initial})} - \sqrt{(h_{\ final})}\right]$$

$$t_{\ final} = \frac{2A_1\sqrt{h_{initial}}}{C_d\ A\sqrt{2g}}\left[\frac{\sqrt{(h_{\ initial})}}{\sqrt{(h_{\ initial})}} - \frac{\sqrt{(h_{\ final})}}{\sqrt{(h_{\ initial})}}\right]$$

$$t_{\ final} = \frac{2A_1}{C_d\ A}\left[\sqrt{\frac{h_{initial}}{2g}}\right]\left[1 - \frac{\sqrt{(h_{\ final})}}{\sqrt{(h_{\ initial})}}\right]$$

This is the equation that describes how long it takes for liquid in a tank to drain from $h_{\ initial}$ to $h_{\ final}$ out of a hole in the tank. It is equivalent to equation 5 in Dr. Feldman's report.

For the drain model in which there are two, one half inch holes at an elevation of 28.06 ft below the initial water level, and in which we are interested in the time that it takes for the water level to drop 23.22 ft to an elevation of 4.84 ft above the drain holes, the data for this model is summarized as:

Variable	Representation	Value
A	Combined cross sectional area of the two holes that the liquid is draining through	2.727×10^{-3} ft^2
A_1	Cross sectional area of the tank	150 ft^2
C_d	Orifice coefficient	0.61
g	Acceleration due to gravity	32.2 ft / s^2
$h_{initial}$	Initial liquid level in the tank	28.06 ft
h_{final}	Final liquid level in the tank	4.84 ft

Where A is determined by limiting the diameter of both drain holes to 0.5 inches each, which means that each radius is 0.25 inches. Therefore the cross sectional area through which the pool water drains is:

Radius of each hole is:

0.25 in (ft / 12 in) = 0.020833 ft

Cross sectional area of each hole is:

Area = $\pi r^2 = 1.3635 \times 10^{-3}$ ft^2

Total cross sectional area is:

A = $2(1.3635 \times 10^{-3}$ ft$^2) = 2.727 \times 10^{-3}$ ft^2

A_1 is based on data from GE Drawing 198E273

Therefore the drain time for the model is:

$$t_{final} = \frac{2A_1}{C_d A}\left[\sqrt{\frac{h_{initial}}{2g}}\right]\left[1 - \frac{\sqrt{(h_{final})}}{\sqrt{(h_{initial})}}\right]$$

$$t_{final} = \left[\frac{(2)(150\,ft^2)}{(0.61)(2.727X10^{-3}\,ft^2)}\right]\sqrt{\left[\frac{(28.06\,ft)}{(2)(32.2\,ft/s^2)}\right]}\left[1 - \sqrt{\frac{(4.84\,ft)}{(28.06\,ft)}}\right]$$

t_{final} = 69604 seconds = 19.34 hr

Therefore for our drain time model, it takes 19.34 hours for the pool level to drop from the scram set point level to the top of the grid box.

Power Fraction Effect on Fuel Plate Temperature

As previously stated, the analysis performed by Dr. Feldman shows that as long as part of the fuel meat remains submerged in water at a level that is no lower than the elevation of the bottom of the eight inch beam ports, and the power fraction is no greater than 0.827%, then there is sufficient cooling capacity to prevent the fuel cladding temperature from reaching the blister point. Conservatively, the drain time has been taken to be the amount of time that it takes for the pool level to drop from the scram set point to the top of the grid box, which is well above the top of the fuel meat.

Decay Power

The analysis done by Dr. Feldman made use of decay power data provided by Stillman. Decay power is dependent on operating history. The most conservative operating history is infinite operation. For an infinite operating history, the Stillman table provides data for the following power fractions close to 0.827%:

15000 seconds	0.844%
20000 seconds	0.775%

Therefore, using linear interpolation to determine the amount of decay time necessary for the power fraction to reach 0.827%:

15000 seconds	0.844%
x	0.827%
20000 seconds	0.775%

$$\frac{(x-15000)\,\text{sec}}{(20000-15000)\,\text{sec}}=\frac{(0.827-0.844)\%}{(0.775-0.844)\%}$$

$$\frac{(x-15000)\,\text{sec}}{5000\,\text{sec}}=\frac{-0.017}{-0.069}$$

$$x-15000 = 5000\left[\frac{-0.017}{-0.069}\right]$$

x = 16232 seconds

This means that the amount of time that it would take for the power fraction to drop below the point at which blister temperature of the cladding cannot be reached with a coolant level no lower than the elevation of the bottom of the eight inch beam ports, after infinite reactor operation is 16232 seconds (4.5 hrs).

Conservative Assumptions

The drain time model does not take into consideration the fact that when the pool level is one inch above the pool level safety limit, the Pool Make-Up System starts adding make-up water to the pool.

The drain time model assumes that all of the drain pathways are at an elevation that is at the centerline of the common drain line between the beam ports and the through port. This elevation is well below the elevations of all of the experimental facilities.

The drain time model only considers the amount of time that it takes for the pool level to drop to the elevation at the top of the grid box, even though the heat transfer model is based on the water level being at the elevation of the bottom of the eight inch beam ports.

The operating history assumed for the decay power determination is infinite.

Maximum Beam Port Area Open to Confinement

It takes 16232 seconds for the power to drop below the point at which the fuel cladding may be damaged. The maximum area of the beam port that can be open to confinement while still providing 16232 seconds of drain time between the level at which the pool level scram trips, and the top of the grid box is:

$$t_{final} = \frac{2A_1}{C_d A}\left[\sqrt{\frac{h_{initial}}{2g}}\right]\left[1 - \frac{\sqrt{(h_{final})}}{\sqrt{(h_{initial})}}\right]$$

$$A = \frac{2A_1}{C_d t_{final}}\left[\sqrt{\frac{h_{initial}}{2g}}\right]\left[1 - \frac{\sqrt{(h_{final})}}{\sqrt{(h_{initial})}}\right]$$

$$A = \left[\frac{(2)(150\,ft^2)}{(0.61)(16232\,\mathrm{sec})}\right]\sqrt{\left[\frac{(28.06\,ft)}{(2)(32.2\,ft/s^2)}\right]}\left[1 - \sqrt{\frac{(4.84\,ft)}{(28.06\,ft)}}\right]$$

$A = 1.169 \text{ X } 10^{-2} \text{ ft}^2 = 1.68 \text{ in}^2$

Therefore the total cross sectional area through which pool water can drain while keeping the fuel meat submerged for the 16232 seconds that it takes for the power level to drop to a point where there is not enough heat being produced to damage the fuel cladding is 1.68 square inches.

Of this area, the beam port drain is a one half inch diameter hole, which corresponds to an area of:

Diameter = 0.5 in

r = (1/2) Diameter = (1/2)(0.5 in) = 0.25 in

$A = \pi r^2 = \pi (0.25 \text{ in})^2 = 0.2 \text{ in}^2$

Subtracting the beam port drain cross sectional area from the total drain area available:

Beam Port Area Open to Confinement = Total Area – Beam Port Drain Area

$= 1.68 \text{ in}^2 - 0.2 \text{ in}^2$

$= 1.48 \text{ in}^2$

This corresponds to a circular hole in the beam port cover that has a diameter of:

$A = \pi r^2$

$1.48 \text{ in}^2 = \pi r^2$

$r^2 = (1.48 \text{ in}^2) / \pi$

$r = [(1.48 \text{ in}^2) / \pi]^{1/2} = 0.68 \text{ in}$

Diameter = 2r = 2(0.68 in) = 1.37 in

Conclusions

The maximum credible accident scenario for the Rhode Island Nuclear Science Center is that a beam port extension is sheared off during operation of the reactor. If the reactor has been in operation for an infinite amount of time at full power, it would take 16232 seconds (4.5 hr) for the decay power to drop to a level that does not produce enough heat to cause fuel cladding damage. Given that the diameter of the beam port drain is one half inch, this means that as long as the area of the beam port that is open to the confinement room is no greater than 1.48 in^2, the amount of time that it would take for the pool to drain down to the level of the top of the grid box would be greater than the amount of time necessary for power to decay to a level that does not produce enough heat to cause fuel cladding damage. This corresponds to a circular hole in the beam port cover plate that has a 1.37 in diameter.

Since the beam port drains empty into progressively larger diameter pipes that ultimately open to atmosphere at a level below the level of the pool floor, the common drain pipe will never fill, and will always be at atmospheric pressure. This means each beam port and the through port act independently from the others, and that the un-damaged ports do not become contributing pathways for pool water to drain in the event that one beam port extension is sheared off.

Shearing the through port is not considered to be a credible accident because it passes underneath the thermal column extension.

APPENDIX C

LOCA SHINE ANALYSIS

13.2.4.1 Analysis of Unshielded Sources

Though a LOCA scenario is highly improbable and the consequences would not lead to fuel damage, it is assumed for the analysis in this section that the water shield above the reactor core and the Co-60 sources would be removed completely, creating the potential for both direct and indirect doses from these sources. As described in Section 4.3, the reactor pool is divided into two sections – a bulk irradiation side and a reactor stall side. The bulk irradiation side houses the Co-60 sources and the stall side houses the reactor. However, the reactor can be moved on a rail system to the bulk side within minutes if needed. The two sides can be isolated by means of a water-tight pool divider gate which provides a means of isolating one side of the pool should a leak occur. In the unlikely event that the pool completely drains, a direct dose would occur for individuals in the reactor containment building who are exposed to the primary gamma rays emerging from the top of the open and empty pool. The indirect dose is attributed mainly to primary gamma rays that emerge from the open pool and then scatter off the reactor building dome. The resultant scattered photons then can irradiate individuals at locations of interest.

The scope of the approach for this analysis is consistent with license documentation produced for other research reactors licensed by the NRC. This section provides a methodology for estimating the direct and indirect absorbed dose rates to tissue which are assumed to be equal to collision kerma rates to water. For the indirect dose assessment, values for absorbed dose were converted to dose equivalent using a quality factor of one. Furthermore, these dose equivalent values represent the "deep-dose equivalent" as defined in 10 CFR Part 20[i]. Dose related quantities, such as attenuation coefficients, energy absorption coefficients, and buildup parameters were obtained from the textbook *Radiation Shielding*[ii] by Shultis and Faw.

The major assumptions used in this section are:

1. The bottom of the reactor pool is assigned a vertical height of zero, and all vertical distances are measured relative to this value.
2. The Co-60 source and the reactor core are treated as unshielded point sources at a specified vertical distance above the bottom center of the reactor pool.

3. The pool enclosure is approximated as a cylinder, with a radius that provides a surface area that is similar to the actual rectangular pool, thus providing a comparable irradiation of the reactor dome by primary gamma rays that emerge from the pool surface.
4. Scattered or annihilation photons that arise from interactions of primary gamma rays within the pool enclosure were neglected.
5. Attenuation in the pool enclosure was neglected for scattered photons that traverse any part of the pool enclosure before reaching the truck door exterior.
6. The central portion of the reactor dome is treated as a segment of a spherical shell, constructed of iron with a uniform thickness of 1 inch rather than the actual thickness of 5/8 inches. The enhanced thickness of the dome also accounts for indirect dose due to scattered photons that emerge from the reactor dome and subsequently scatter off other surfaces within the containment vessel.
7. For the estimation of indirect dose rate, attenuation of primary gamma rays was neglected in both the air and in the reactor dome. Likewise, attenuation of scattered photons in the intervening air was neglected for estimating indirect dose rate at the truck door exterior.
8. Scattered photons, fluorescent x-rays, and annihilation photons that originate in the reactor dome escape the reactor dome without interacting.
9. Absorbed dose to tissue is equal to collision kerma in water.
10. The quality factor for photons is one, and dose equivalent estimates for indirect dose are for the regulatory quantity “deep-dose equivalent”.
11. Buildup for the quantity air-kerma also is applicable to absorbed dose to tissue.
12. Buildup in air or iron for scattered photons is assumed to be similar to buildup for monoenergetic photons that traverse these materials.
13. The typical duration for reactor operations is 6 hours at a power level of 1 MW.
14. The reactor truck door has no curvature.
15. Spontaneous neutron emissions from the uncovered reactor core do not contribute significantly to dose.

Table 13-10 provides the relative vertical distances for a specified object or location within the reactor containment vessel. These distances were obtained from the original technical drawings for the reactor containment vessel, and were used for direct and indirect dose calculations for the LOCA scenario. Also provided in the table is the notation used in the dose calculations for the vertical distance of a specified object or location.

Table 13-10: Relative vertical distances used for dose calculations that pertain to the LOCA scenario.

Object or location	Relative vertical distance, (ft)
Bottom of the reactor pool (xy plane)	0
First floor (H_1)	3.5
Horizontal center-line of the reactor core (H_S)	6.0
Co-60 source (H_S)	6.0
Third floor (H_3)	30.5
Top of the pool wall (H_P)	33.0
Top of the reactor dome (R)	71.0

The Co-60 source is assumed to be at the same vertical distance as the horizontal center-line of the reactor core. This assumption is based on the practice of having some portion of the Co-60 activity on an elevated platform for high-dose rate material irradiations. Although the vertical distance of this platform is less than 6 ft, it was assumed for conservatism that the entire Co-60 source is located at a vertical distance H_S of 6 ft. The central portion of the reactor dome is a segment of a spherical shell of radius R = 71 ft as measured from the bottom of the reactor pool, hence the vertical distance to the top of the reactor dome is 71 ft.

13.2.4.2 Direct Dose Rates

The primary source terms for direct dose rate are the Co-60 source and the reactor core, and each will be treated individually. The Co-60 activity A is assumed to be 3.7×10^{15} Bq (100 kCi) which is the activity limit under the current license application. The Co-60 activity is treated as a point source at vertical distance H_S above the bottom of the pool, which emits gamma rays with an average energy E of 1.25 MeV and yield Y of 2. The distance of closest approach for direct dose is assumed to be the top of the pool wall, H_P, and the intervening material is air at normal pressure (1 atm) and temperature (22 °C or 295 °K) resulting in an air density of 1.2×10^{-3} g cm^{-3}. The direct dose rate due to the Co-60 source is given by:

$$D = \frac{AYE}{4\pi(H_P - H_S)^2}\left(\frac{\mu_{en}}{\rho}\right)\exp\left(-\mu(H_P - H_S)\right)B(\mu(H_P - H_S)) \quad ,$$

where (μ_{en}/ρ) = 2.965×10^{-2} cm^2 g^{-1} is the mass energy absorption coefficient for 1.25 MeV gamma rays in water (tissue), μ = 6.802×10^{-5} cm^{-1} is the linear attenuation coefficient for 1.25 MeV gamma rays in air, and $B\left(\mu(H_P - H_S)\right)$ accounts for buildup in the intervening air of thickness of $H_P - H_S$. For this analysis it was convenient to use Berger's formula for buildup:

$$B\left(\mu(H_P - H_S)\right) = 1 + a\mu(H_P - H_S)\exp\left(+b\mu(H_P - H_S)\right) \quad ,$$

where a = 1.33 and b = 0.028 are parameter values for buildup of the quantity air-kerma for 1.25 MeV gamma rays that traverse the intervening air. It was assumed here and elsewhere in this section that buildup parameters for air-kerma are applicable to dose to tissue because the mass energy absorption coefficients for air and water are approximately equal over a broad range of photon energies.

The reactor core also will be treated as a point source, with primary gamma ray emissions from a large inventory of fission products accumulated over some prior operating schedule. In this case, it is convenient to consider the dynamic behavior of energy groups rather than to track individual fission products over time. This approach is described in Appendix G of the reference by Shultis and Faw[ii]. The gamma ray energy emission rate $\Gamma_j(T,t)$ from fission products in the jth group, produced by the thermal fission of U-235 and accumulated over operating duration T, is expressed as a function of time t after reactor shutdown by:

$$\Gamma_j(T,t) = \sum_{i=1}^{N_j}\frac{\alpha_{i,j}}{\lambda_{i,j}}\left(1 - e^{-\lambda_{i,j}T}\right)e^{-\lambda_{i,j}t} \quad ,$$

where $\alpha_{i,j}$ and $\lambda_{i,j}$ are magnitude and decay parameters, respectively, for the ith source term in the jth group, and N_j is the number of source terms in the jth group. The value of N_j ranges from 9 to 14, and there are six energy groups (j = 1 to 6). The units for $\Gamma_j(T,t)$ are MeV fission^{-1}, the units for $\alpha_{i,j}$ are MeV s^{-1} fission^{-1}, the unit for $\lambda_{i,j}$ is s^{-1}, and the unit for T and t is seconds ($10^{-4} \le t \le 10^9$). For a constant fission rate S_F (in units of fissions s^{-1}) and

the same distance of closest approach used for the Co-60 source, the direct dose rate due to the jth group of fission products in the reactor core is given by:

$$D_j(T,t) = \frac{S_F\,\Gamma_j(T,t)}{4\pi(H_P - H_S)^2}\left(\frac{\mu_{en}}{\rho}\right)_j \exp\left(-\mu_j(H_P - H_S)\right) B_j(\mu_j(H_P - H_S)) \quad ,$$

where $(\mu_{en}/\rho)_j$ is the mass energy absorption coefficient in water (tissue) for the jth group, μ_j is the linear attenuation coefficient for air for the jth group, and:

$$B_j\left(\mu_j(H_P - H_S)\right) = 1 + a_j\mu_j(H_P - H_S)\exp\left(+b_j\mu_j(H_P - H_S)\right) \quad ,$$

is Berger's formula for buildup in the intervening air, where a_j and b_j are parameters for buildup of the quantity air-kerma for the jth group. Each of the quantities: $(\mu_{en}/\rho)_j$, μ_j, a_j, and b_j were evaluated for the average gamma ray energy of the jth group. The direct dose rate for all fission product groups is given by:

$$D(T,t) = \sum_{j=1}^{6} D_j(T,t) \quad .$$

Assuming an energy recovery of 200 MeV per fission of U-235 and a reactor power level of 1 MW or 6.242×10^{18} MeV s^{-1}, the fission rate S_F is 3.121×10^{16} fissions s^{-1}. The group number and corresponding average gamma ray energy for fission products are provided in Table 13-11 below, and values for the quantities used to determine direct dose rate are provided in Table 13-12. The $\alpha_{i,j}$ and $\lambda_{i,j}$ values are provided in the reference by Shultis and Faw[ii].

13.2.4.3 Direct Dose Rate Results

All distances were converted to the unit of cm for calculations, and a conversion factor of $10^3(3.6\times10^3/6.242\times10^7)$ mrad g MeV^{-1} s hr^{-1} was used to obtain suitable units for the direct dose rates. The direct dose rate at the top of the pool wall due to the Co-60 source is 1.888×10^6 mrad hr^{-1}, and the direct dose rate for the reactor core depends on the previous duration of operations T and the elapsed time t after reactor shutdown. For this analysis, there were two durations chosen for reactor operations: 6 hours (2.16×10^4 s) and infinity. The first duration is indicative of typical reactor operations, and the second duration represents a saturation condition for fission product activities in the reactor core. The use of

an infinite duration for reactor operations is consistent with the Maximum Hypothetical Accident (MHA) scenario described in Section 13.2.1. The direct dose rates are listed in Table 13-13 for several values of t to indicate the trend over time, and for convenience values for t and T in the table do not have the unit of seconds. The first value for t of 27 minutes has significance as the approximate time required for a rupture in an eight-inch beam tube to cause the reactor pool to drain to the level of the horizontal center-line of the reactor core, thus exposing a significant portion of the reactor core to air[iii].

Table 13-11: Group Number and average gamma ray energy based on fission products from the thermal fission of U-235.

Group number (j)	Average energy, E_j (MeV)
1	6.25
2	4.5
3	3.5
4	2.5
5	1.5
6	0.5

Table 13-12: Values used to determine direct dose rate based on fission products from the thermal fission of U-235.

Average energy, E_j (MeV)	$\left(\frac{\mu_{en}}{\rho}\right)_j$ for water ($\text{cm}^2\ \text{g}^{-1}$)	μ_j for air (cm^{-1})	a_j for air	b_j for air
6.25	1.788×10^{-2}	2.974×10^{-5}	0.458	−0.004
4.5	1.991×10^{-2}	3.489×10^{-5}	0.57	−0.0005
3.5	2.174×10^{-2}	3.985×10^{-5}	0.68	+0.003
2.5	2.445×10^{-2}	4.803×10^{-5}	0.86	+0.009
1.5	2.833×10^{-2}	6.190×10^{-5}	1.16	+0.021
0.5	3.299×10^{-2}	1.040×10^{-4}	2.29	+0.067

Table 13-13: Direct dose rates for fission products. The direct dose rates from the thermal fission of U-235 were evaluated at a distance $H_P - H_S$ from the reactor core and for the specified elapsed time t and duration T of reactor operations.

Elapsed time, t	Direct dose rate (mrad hr^{-1})	
	T = 6 hours	$T \rightarrow \infty$
27 min	7.143×10^{6}	1.259×10^{7}
1 hour	4.621×10^{6}	9.953×10^{6}
1 day	2.208×10^{5}	3.890×10^{6}
7 days	2.579×10^{4}	2.266×10^{6}
30 days	4.704×10^{3}	1.261×10^{6}
90 days	1.150×10^{3}	7.421×10^{5}

The inclusion of attenuation and buildup for direct dose rate calculations was necessary only for fission product group 6 (with an average gamma ray energy of 0.5 MeV). For all other groups, and for the Co-60 source, the calculated values for direct dose rate were not affected significantly by the inclusion of attenuation and buildup, but these factors were included to be consistent. In addition, any scattered photons or annihilation photons that arise from interactions of primary gamma rays within the pool enclosure were neglected.

13.2.4.4 Indirect Dose Rates

The indirect dose is due mainly to primary gamma rays that interact in the reactor dome by Compton scatter, thus producing scattered photons that can irradiate individuals at locations of interest. In addition, a relatively smaller contribution to indirect dose was determined due to annihilation photons produced as a consequence of the pair-production interaction of primary photons in the reactor dome. The methodologies for these indirect dose assessments are provided below.

13.2.4.5 Geometry

The geometry used to estimate indirect dose rates is provided in Figure 13-19. The base of the reactor containment vessel is modeled as a cylinder with an outer radius R_C equal to 42 feet (12.80 m). The bottom of this cylindrical base coincides with the bottom of the reactor pool (i.e., the xy plane), and the top joins with the curved dome ceiling. The central portion of the dome ceiling is modeled as a segment of a spherical shell, with a radius R of 71 ft (21.64 m) and origin at the bottom center of the cylindrical base. The pool enclosure also is modeled as a cylinder with radius R_P equal to 4 m and height H_P equal to 33 ft (10.06 m), which is centered at the bottom of the containment vessel. The actual pool enclosure is rectangular, with a total area of 384 ft^2 or about 36 m^2 at the pool surface. For the cylindrical pool model, the pool surface area is πR_P^2 or about 50 m^2 which provides a comparable irradiation of the reactor dome by primary gamma rays that emerge from the pool surface. The asterisk in Figure 13-19 indicates the location of the radiation sources, either of the Co-60 source or the reactor core, which is a vertical distance H_S above the bottom of the pool. The distance from the radiation source to an arbitrary location on the reactor dome is denoted by w.

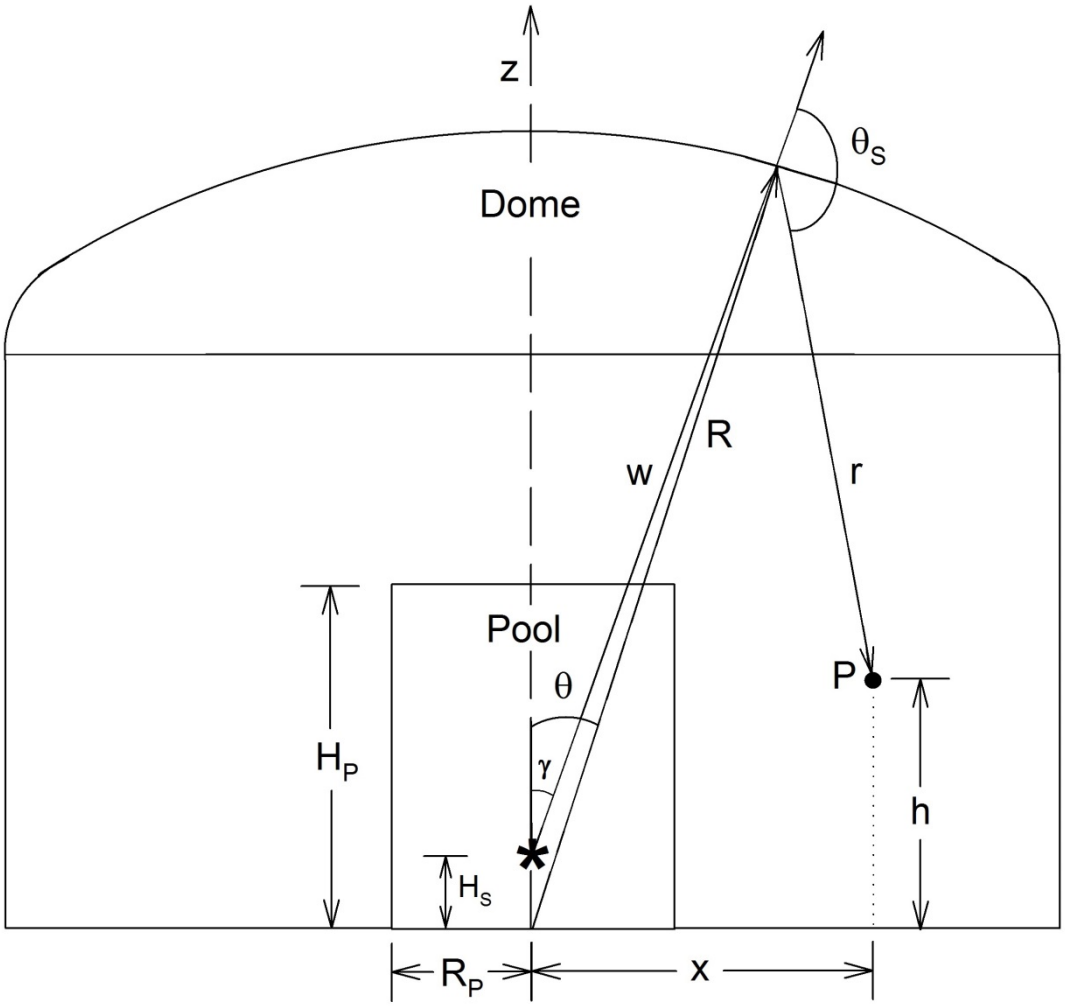

Figure 13-19. Containment vessel and pool geometry for estimating indirect dose rates.

Three angles are shown in Figure 13-19: θ_S, θ, and γ. The angle θ_S pertains to the Compton scatter interaction, which indicates the angle of scatter for primary gamma rays that interact at an arbitrary location on the reactor dome resulting in a scattered photon that travels toward the location of interest P, and the length r indicates the distance between the location of Compton scatter and the location P. The polar angle θ as measured from the vertical z-axis is used to locate an arbitrary increment of area on the reactor dome, and the angle γ is used to define the maximum value for θ. The location of interest P for calculating indirect dose rates is a horizontal distance x from the center of the cylindrical base and a height h above the bottom of the reactor pool.

13.2.4.6 Primary Gamma Ray Fluence Rates Incident on the Reactor Dome

The primary source terms for indirect dose are the Co-60 source and the reactor core, and each will be treated individually. The Co-60 activity A is assumed to be 3.7×10^{15} Bq as was the case for the direct dose rate determination, and the Co-60 activity is treated as a point source located at the asterisk in Figure 13-19. The primary gamma ray fluence rate φ incident at an arbitrary location on the reactor dome from the Co-60 source therefore is:

$$\varphi = \frac{AY}{4\pi w^2} \ .$$

The reactor core also will be treated as a point source at the location of the asterisk in Figure 13-19 and the fission product emissions will be characterized using energy groups as were used to determine direct dose rate. For a constant fission rate S_F of 3.121×10^{16} fissions s^{-1} and average group energy E_j (in MeV), the primary gamma ray fluence rate incident at an arbitrary location on the reactor dome for the jth group of fission products is given by:

$$\varphi_j(T,t) = \frac{S_F\ \Gamma_j(T,t)}{E_j}\left(\frac{1}{4\pi w^2}\right) \ .$$

The previous expressions do not include attenuation in the intervening air of the primary gamma rays for either the Co-60 source or the reactor core, which is intended to maximize the primary gamma ray fluence rate that irradiates the reactor dome.

13.2.4.7 Secondary Photon Fluence Rates Incident on the Locations of Interest

The major secondary source terms for indirect dose are scattered photons produced by the primary gamma rays from Co-60 or the reactor core that interact by Compton scatter in the reactor dome. For primary gamma rays with energy E (in MeV) that interact by Compton scatter in the reactor dome, the energy E' (in MeV) of the scattered photon is given by:

$$E' = \frac{E}{1 + \frac{E}{0.511}(1 - \cos\theta_S)} \ ,$$

where 0.511 MeV is the rest mass energy of an electron, and θ_S is the scattering angle. The differential cross-section for the Compton scatter interaction, which provides the probability for the scattered photon with energy E' to emerge within a differential solid angle $d\Omega$ that encompasses the location of interest, also is dependent on E and θ_S and is given by:

$$\left(\frac{d\sigma}{d\Omega}\right) = \frac{r_0^2}{2}\left(\frac{E'}{E}\right)^2\left[\frac{E}{E'} + \frac{E'}{E} - 1 + (\cos\theta_S)^2\right],$$

where r_0 = 2.818×10^{-13} cm is the classical electron radius. The units for $(d\sigma/d\Omega)$ are cm^2 steradian^{-1} electron^{-1}.

The central portion of the reactor dome is 5/8 inch steel which increases in thickness to 1 inch where the curvature of the dome increases to connect smoothly with the cylindrical base. For purposes of estimating indirect dose, the reactor dome is assumed to be iron with a uniform thickness of 1 inch, resulting in an electron areal density n_e of 5.606×10^{24} electrons cm^{-2}. The assumed composition of the dome is reasonable because iron is the major component of steel. The assumed thickness of the dome is conservative because the geometry dictates that only the central portion of the dome is irradiated by primary gamma rays. The enhanced dome thickness, however, is assumed to account for indirect dose due to the subsequent scatter from other surfaces (e.g., floors and walls) within the containment vessel of other scattered photons that emerge from the reactor dome.

For a spherical coordinate system with the same origin as the spherical shell segment, an increment of reactor dome area is given by: $R^2 \sin\theta \, d\theta \, d\beta$, where θ is the polar angle and β is the planar angle (the angle β is not shown in Figure 13-19). The differential number of electrons available for Compton scatter at an arbitrary location on the reactor dome therefore is $n_e R^2 \sin\theta \, d\theta \, d\beta$. Furthermore it is assumed that all these electrons are subject to the same primary gamma ray fluence rate (i.e., the attenuation of primary gamma rays in the reactor dome is neglected).

The cosine of the scattering angle θ_S can be determined using vector relationships. If $\vec{w}$ denotes a vector that originates at the radiation source and points to an arbitrary location on the reactor dome where Compton scatter occurs, and $\vec{r}$ denotes a vector that originates at the location of Compton scatter and points to the location of interest P, then the cosine of the scattering angle is given by:

$$\cos\theta_S = \frac{\vec{w} \cdot \vec{r}}{|\vec{w}|\,|\vec{r}|}.$$

There are two locations of interest in the reactor containment vessel for estimating indirect dose rates: the edge of the reactor pool ($x = R_P$ and $h = H_3 + 150\text{cm}$) and at the truck door exterior ($x = R_C$ and $h = H_1 + 150\text{cm}$), and the resultant geometry dictates that the magnitude of the scattering angle is bounded by ($\pi/2 < \theta_S \leq \pi$).

In the absence of attenuation, the differential scattered photon fluence rate at the location P due to the Compton scatter of Co-60 gamma rays in the reactor dome is given by:

$$\varphi \left(\frac{d\sigma}{d\Omega}\right) \frac{n_e}{r^2} R^2 \sin\theta \, d\theta \, d\beta \, ,$$

and the same quantity for the jth group of fission products is given by:

$$\varphi_j(T,t) \left(\frac{d\sigma}{d\Omega}\right) \frac{n_e}{r^2} R^2 \sin\theta \, d\theta \, d\beta \, .$$

These expressions were integrated numerically over the irradiated surface of the reactor dome to estimate the indirect dose rates due to Compton scatter in the dome, with additional factors accounting for energy fluence rate, attenuation, buildup, and energy absorption in water (tissue).

Additional secondary source terms to consider for indirect dose are fluorescent x-rays and annihilation photons produced in the reactor dome as a result of the photoelectric effect and pair-production interactions of primary gamma rays. The photoelectric effect was assumed to occur with K-shell electrons in iron, and the subsequent atomic de-excitation would result in the emission of one fluorescent x-ray with an energy equal to the K-shell binding energy for iron, which is about 10 keV. It also was assumed that these fluorescent x-rays escaped the reactor dome without attenuation. In this case the reactor dome becomes a source of 10 keV fluorescent x-rays. These x-rays, however, are attenuated readily in the intervening materials and therefore do not contribute to indirect dose rate at the locations of interest defined previously, for either the Co-60 source or the reactor core.

The pair production interaction for primary gamma rays can occur for Co-60 and for fission product groups 1 - 5. It was assumed that the resultant positron annihilated at rest in the reactor dome, and that the resultant annihilation photons escaped the dome without attenuation. In this case the reactor dome becomes a source of 0.511 MeV annihilation photons. The contribution to indirect dose due to annihilation photons produced in the dome by the pair-production interaction of primary gamma rays from Co-60 was determined to be

negligible (compared to that for scattered photons) at the locations of interest defined previously, which is attributed to the small cross-section for the pair-production interaction in iron at 1.25 MeV. The contribution to indirect dose due to annihilation photons produced in the dome by the pair-production interaction of primary gamma rays from the reactor core was found to be significant (compared to that for scattered photons) at the truck door exterior only, which is attributed to the increased penetrating ability of annihilation photons in iron compared to the lower-energy photons produced in the reactor dome by Compton scatter.

In the absence of attenuation, the differential annihilation photon fluence rate at the location P due to pair-production at an arbitrary location in the reactor dome for the jth group of fission products is given by:

$$\varphi_j(T,t)\left(1-\exp(-\mu_j d)\right)\left(\frac{\mu_{PP,j}}{\mu_j}\right)\frac{Y_{PP}}{4\pi r^2}R^2\sin\theta\,d\theta\,d\beta\ ,$$

where μ_j is the linear attenuation coefficient for iron for the jth group, d = 2.54 cm is the enhanced thickness of the dome, $\mu_{PP,j}$ is the linear attenuation coefficient for the pair-production interaction for iron for the jth group, and Y_{PP} = 2 is the yield for annihilation photons. This expression was integrated numerically over the irradiated surface of the reactor dome to estimate the indirect dose rates due to annihilation photons, with additional factors accounting for energy fluence rate, attenuation in the truck door, buildup in the truck door, and energy absorption in water (tissue).

13.2.4.8 Indirect Dose Rates at the Edge of the Reactor Pool

For the indirect dose rates due to scattered photons at the edge of the reactor pool, the scattered photons traverse only the air in the reactor containment vessel before reaching this location of interest. In this case, attenuation and buildup in air was considered for these scattered photons.

The indirect dose rate at the edge of the reactor pool due to scattered photons associated with the Co-60 source is estimated by:

$$D\ =\ \int_0^{\pi} 2\int_0^{\theta_{max}} \varphi\left(\frac{d\sigma}{d\Omega}\right)\frac{n_e}{r^2}\,E'\left(\frac{\mu'_{en}}{\rho}\right)\exp(-\mu' r)\,B(\mu' r)\,R^2\sin\theta\,d\theta\,d\beta\ ,$$

where the factor E' defines an energy fluence rate for the scattered photons, (μ'_{en}/ρ) accounts for energy absorption in water (tissue) for the scattered photons, $\exp(-\mu' r)$ accounts for attenuation in air, and $B(\mu' r)$ accounts for buildup in air. Although it is not shown explicitly, the primary gamma ray fluence rate φ depends on w which is a function of θ, and the distance r is a function of θ, β, x, and h. The initial factor of 2 accounts for symmetry with respect to the planar angle β. The upper limit of integration θ_{max} is defined as follows. The cosine of the maximum value for angle γ shown in Figure 13-19 is given by:

$$\cos(\gamma_{max}) = \frac{H_P - H_S}{\sqrt{R_P^2 + (H_P - H_S)^2}} .$$

A quadratic relationship between angles γ and θ can be used to define the maximum value for the angle θ:

$$\theta_{max} = \cos^{-1}\left(\frac{H_S(\sin(\gamma_{max}))^2 \pm \cos(\gamma_{max})\sqrt{R^2 - H_S^2(\sin(\gamma_{max}))^2}}{R}\right) ,$$

which evaluates to 23.8 degrees using the positive root.

Berger's formula was used to describe buildup in the intervening air for the scattered photons as they travel toward the edge of the pool:

$$B(\mu' r) = 1 + a'\mu' r \exp(+b'\mu' r) ,$$

where a' and b' are parameters for buildup of the quantity air-kerma, which is assumed to be equal in magnitude to buildup for absorbed dose to tissue.

Because the scattered photons have variable energy E' which depends on the scattering angle, the following general fitting function was used to calculate the various dose quantities (μ'_{en}/ρ), μ', a', and b':

$$f(E') = c_0 + c_1 E' + c_2 (E')^2 + c_3 (E')^3 ,$$

where c_0, c_1, c_2, and c_3 are fitting parameters. Values for the fitting parameters for each relevant dose quantity are listed in Table 13-14 for the energy range ($0.15 \leq E' \leq 0.6$) MeV which includes all scattered photon energies traveling toward the locations of interest defined previously.

Table 13-14: Fitting parameters for various dose quantities used to estimate indirect dose rate at the edge of the reactor pool due to scattered photons.				
Fitting parameter	Dose quantity			
	$\left(\frac{\mu'_{en}}{\rho}\right)$ for water ($cm^2\ g^{-1}$)	μ' for air (cm^{-1})	a' for air (dimensionless)	b' for air (dimensionless)
c_0	+0.018013	$+2.1403\times10^{-4}$	+7.9539	+0.15035
c_1	+0.087286	-4.5885×10^{-4}	−29.098	−0.19283
c_2	−0.168143	$+6.8469\times10^{-4}$	+53.543	−0.02010
c_3	+0.106503	-4.1233×10^{-4}	−35.785	+0.14213

The indirect dose rate at the edge of the reactor pool due to scattered photons associated with the jth group of fission products is estimated by:

$$D_j(T,t) = \int_0^{\pi} 2 \int_0^{\theta_{max}} \varphi_j(T,t) \left(\frac{d\sigma}{d\Omega}\right) \frac{n_e}{r^2} E' \left(\frac{\mu'_{en}}{\rho}\right) \exp(-\mu' r)\, B(\mu' r) R^2 \sin\theta \, d\theta \, d\beta \ ,$$

and the indirect dose rate due to scattered photons for all fission product groups is given by:

$$D(T,t) = \sum_{j=1}^{6} D_j(T,t) \ .$$

Similar statements regarding the dependence of quantities in the integrand on the integration variables and distances x and h also apply to the previous integral expression. The scattered photons that are produced in the reactor dome are assumed to escape the reactor dome without interacting. Also, typical values for buildup are determined for monoenergetic sources, and it is assumed that buildup for the scattered photons that emerge from the reactor dome is similar to buildup for monoenergetic sources. As stated previously, the indirect dose rates at the edge of the reactor pool due to annihilation photons was determined to be negligible for either the Co-60 source or the reactor core.

13.2.4.9 Indirect Dose Rates at the Truck Door Exterior

For the indirect dose rates at the truck door the location P is assumed to be on the exterior of the truck door, such that the secondary photons traverse the air in the reactor containment vessel and then the truck door itself, which is steel with a thickness of 3/8

inches, before reaching the location of interest. In this case, attenuation of secondary photons in the intervening air was neglected to maximize the secondary photon fluence rate incident on the truck door. Attenuation and buildup in iron was considered for secondary photons that are incident on the truck door. For simplicity, it was assumed that the truck door has no curvature. The path length δ through the truck door traversed by scattered photons can be determined by similar triangles, and in general is dependent on the thickness of the truck door and on R, θ, β, x, and h.

The indirect dose rate at the truck door exterior due to scattered photons associated with the Co-60 source is estimated by:

$$D = \int_0^{\pi} 2 \int_0^{\theta_{max}} \varphi \left(\frac{d\sigma}{d\Omega}\right) \frac{n_e}{r^2} E' \left(\frac{\mu'_{en}}{\rho}\right) \exp(-\mu'\delta)\, B(\mu'\delta) R^2 \sin\theta \, d\theta \, d\beta \ ,$$

where $\exp(-\mu'\delta)$ accounts for attenuation in the truck door and $B(\mu'\delta)$ accounts for buildup in the truck door. Berger's formula was used to describe buildup in the truck door:

$$B(\mu'\delta) = 1 + a'\mu'\delta \exp(+b'\mu'\delta) \ ,$$

where a' and b' are parameters for buildup of the quantity air-kerma for scattered photons that traverse the truck door. Likewise, the following general fitting function was used to calculate the dose quantities μ', a', and b' for iron:

$$f(E') = c_0 + c_1 E' + c_2 (E')^2 + c_3 (E')^3 \ ,$$

where c_0, c_1, c_2, and c_3 are fitting parameters. Values for the fitting parameters for each dose quantity are listed in Table 13-15 for the energy range ($0.15 \leq E' \leq 0.6$) MeV. The fitting parameters for (μ'_{en}/ρ) were given previously in Table 13-14.

Table 13-15: Fitting Parameters for various dose quantities used to estimate indirect dose rate at the truck door exterior due to scattered photons.

Fitting parameter	Dose quantity		
	μ' for iron (cm^{-1})	a' for iron (dimensionless)	b' for iron (dimensionless)
c_0	+2.8464	−0.75149	−0.093109
c_1	−13.686	+11.626	+0.70049
c_2	+29.373	−23.181	−1.2752
c_3	−21.389	+15.103	+0.77800

The indirect dose rate at the truck door exterior due to scattered photons associated with the jth group of fission products is estimated by:

$$D_j(T,t) \;=\; \int_0^{\pi} 2 \int_0^{\theta_{max}} \varphi_j(T,t) \left(\frac{d\sigma}{d\Omega}\right) \frac{n_e}{r^2}\; E' \left(\frac{\mu'_{en}}{\rho}\right) \exp(-\mu'\delta)\; B(\mu'\delta) R^2 \sin\theta \; d\theta \; d\beta \;\; ,$$

and the indirect dose rate due to scattered photons for all fission product groups is given by:

$$D(T,t) = \sum_{j=1}^{6} D_j(T,t) \;\; .$$

Likewise, the scattered photons that are produced in the reactor dome are assumed to escape the reactor dome without interacting, and buildup for the scattered photons that are incident on the truck door is assumed to be similar to buildup for monoenergetic sources.

The indirect dose rate at the edge of the reactor pool due to annihilation photons associated with the jth group of fission products is estimated by:

$$D_j(T,t) \;=\; \int_0^{\pi} 2 \int_0^{\theta_{max}} \varphi_j(T,t)\; G_j\; R^2 \sin\theta \; d\theta \; d\beta \;\; ,$$

where:

$$G_j \;= \left(1 - \exp\left(-\mu_j d\right)\right) \left(\frac{\mu_{PP,j}}{\mu_j}\right) \frac{Y_{PP}}{4\pi r^2}\; E_{PP} \left(\frac{\mu_{en}}{\rho}\right) \exp(-\mu\delta)\; B(\mu\delta) \;\; ,$$

and where E_{PP} = 0.511 MeV is the energy of the annihilation photons, (μ_{en}/ρ) = 0.03297 cm^2 g^{-1} is the energy absorption coefficient in water (tissue) for the annihilation photons, μ = 0.6432 cm^{-1} is the linear attenuation coefficient for annihilation photons in iron, δ is the slant distance through the truck door, and $B(\mu\delta)$ accounts for buildup in the truck door. Berger's formula was used to describe buildup in the truck door:

$$B(\mu\delta) \;=\; 1 + \; a\, \mu\, \delta \exp(+\mathrm{b}\, \mu\, \delta) \;\; ,$$

where a = 1.16 and b = 0.036 are parameters for buildup of the quantity air-kerma for annihilation photons that traverse the truck door. The indirect dose rate due to scattered photons for all fission product groups is given by:

$$D(T,t) = \sum_{j=1}^{6} D_j(T,t) \ .$$

The dose quantities μ_j and $\mu_{PP,j}$ for the annihilation photons associated with the jth group of fission products are provided in Table 13-16.

Table 13-16: Dose quantities for the annihilation photons associated with the jth group of fission products from the thermal fission of U-235.

Average energy, E_j (MeV)	μ_j for iron (cm^{-1})	$\mu_{PP,j}$ for iron (cm^{-1})
6.25	2.400×10^{-1}	8.140×10^{-2}
4.5	2.541×10^{-1}	5.594×10^{-2}
3.5	2.726×10^{-1}	3.889×10^{-2}
2.5	3.098×10^{-1}	2.030×10^{-2}
1.5	3.829×10^{-1}	2.819×10^{-3}
0.5	6.489×10^{-1}	0

As stated previously, the indirect dose rate at the truck door exterior due to annihilation photons was determined to be negligible (compared to that for scattered photons) for the Co-60 source.

13.2.4.10 Indirect Dose Rate Results

All distances were converted to the unit of cm for calculations, and a conversion factor of $10^3(3.6\times10^3/6.242\times10^7)$ mrem g MeV^{-1} s hr^{-1} was used to obtain suitable units for the indirect dose rates. The indirect dose rate at the edge of the reactor pool ($x = R_P$ and $h = H_3 + 150$cm) due to scattered photons associated with the Co-60 source is 5.31×10^3 mrem hr^{-1}, and the indirect dose rate at the truck door exterior ($x = R_C$ and $h = H_1 + 150$cm) due to scattered photons associated with this source is 4.62×10^2 mrem hr^{-1}.

Table 13-17 contains the indirect dose rates due to scattered photons at the edge of the reactor pool for all fission product groups and for the two durations of reactor operations considered here. Table 13-18 contains the indirect dose rates due to scattered photons at the truck door exterior for all fission product groups and for the same durations of reactor operations.

Table 13-17: Indirect dose rates at the edge of the reactor pool ($x = R_P$ and $h = H_3 + 150\text{cm}$) due to scattered photons associated with fission products produced by the thermal fission of U-235 and for the specified elapsed time t and duration T of reactor operations.

Elapsed time, t	Indirect dose rate (mrem hr^{-1})	
	T = 6 hours	$T \rightarrow \infty$
27 min	4.34×10^{4}	8.65×10^{4}
1 hour	2.81×10^{4}	7.06×10^{4}
1 day	1.85×10^{3}	3.23×10^{4}
7 days	1.97×10^{2}	1.85×10^{4}
30 days	3.16×10^{1}	1.15×10^{4}
90 days	1.09×10^{1}	7.36×10^{3}

Table 13-18: Indirect dose rates at the truck door exterior ($x = R_C$ and $h = H_1 + 150\text{cm}$) due to scattered photons associated with fission products produced by the thermal fission of U-235 and for the specified elapsed time t and duration T of reactor operations.

Elapsed time, t	Indirect dose rate (mrem hr^{-1})	
	T = 6 hours	$T \rightarrow \infty$
27 min	2.43×10^{3}	4.70×10^{3}
1 hour	1.58×10^{3}	3.81×10^{3}
1 day	9.62×10^{1}	1.68×10^{3}
7 days	1.05×10^{1}	9.67×10^{2}
30 days	1.75×10^{0}	5.82×10^{2}
90 days	5.49×10^{-1}	3.66×10^{2}

Table 13-19 contains the indirect dose rates due to annihilation photons at the truck door exterior for all fission product groups and for the two durations of reactor operations considered here. Table 13-20 contains the total indirect dose rates due to both scattered photons and annihilation photons at the truck door exterior for all fission product groups and for the same durations of reactor operations.

Table 13-19: Indirect dose rates at the truck door exterior ($x = R_C$ and $h = H_1 + 150\text{cm}$) due to annihilation photons associated with fission products produced by the thermal fission of U-235 and for the specified elapsed time t and duration T of reactor operations.

Elapsed time, t	Indirect dose rate (mrem hr^{-1})	
	T = 6 hours	$T \rightarrow \infty$
27 min	1.49×10^{2}	1.86×10^{2}
1 hour	9.64×10^{1}	1.31×10^{2}
1 day	9.48×10^{-1}	1.89×10^{1}
7 days	1.75×10^{-1}	1.20×10^{1}
30 days	4.25×10^{-2}	3.59×10^{0}
90 days	1.84×10^{-3}	5.52×10^{-1}

Table 13-20: Total indirect dose rates at the truck door exterior ($x = R_C$ and $h = H_1 + 150\text{cm}$) due to both scattered photons and annihilation photons associated with fission products produced by the thermal fission of U-235 and for the specified elapsed time t and duration T of reactor operations.

Elapsed time, t	Total indirect dose rate (mrem hr^{-1})	
	T = 6 hours	$T \rightarrow \infty$
27 min	2.58×10^{3}	4.89×10^{3}
1 hour	1.67×10^{3}	3.94×10^{3}
1 day	9.71×10^{1}	1.70×10^{3}
7 days	1.07×10^{1}	9.79×10^{2}
30 days	1.79×10^{0}	5.86×10^{2}
90 days	5.51×10^{-1}	3.67×10^{2}

The indirect dose rates at the truck door exterior due to annihilation photons associated with the fission product groups represent about 6% at most of the indirect dose rates due to scattered photons. Even though this contribution is relatively small, the results were tabulated in this section because the indirect dose rate due to annihilation photons is independent of the indirect dose rate due to scattered photons. The indirect dose rates at the edge of the reactor pool due to annihilation photons associated with the fission product groups represent about 2% at most of the indirect dose rates due to scattered photons, and therefore were not reported in this section.

Furthermore, indirect dose rates were evaluated for primary gamma rays that undergo an initial Compton scatter in the reactor dome and a subsequent Compton scatter with the concrete floor: either on the third floor near the reactor pool, or on the first floor near the truck door. The resultant dose rates from these double-scatter events contributed an

additional 5 - 10% to the indirect dose rates due to single Compton scatter events with the reactor dome. Given that the magnitude of all indirect dose rates due to scattered photons is directly proportional to the thickness of the reactor dome, the use of 1 inch for the dome thickness as stated previously results in an increase in indirect dose rate of 60% compared to that obtained using the actual dome thickness of 5/8 inches. This additional 60% of indirect dose rate therefore is assumed to account for double-scatter events from other surfaces in the vicinity of the locations of interest.

13.2.4.11 Summary

In the improbable event of a complete loss of coolant accident the direct dose rates were found to be quite large, with initial values on the order of 10^3 to 10^4 rad hr^{-1}. These direct dose rates, however, should not be realized in practice because the reactor containment building would be evacuated before the water completely drained from the reactor pool. In addition, a loss of coolant accident attributed to a beam tube rupture would drain the reactor pool to the level of the horizontal center-line of the reactor core. At this level, some water shielding would be present for the lower portion of the reactor core, and likewise some water shielding also would be present for a significant portion of the Co-60 activity. In this case, the direct and indirect dose rates should be reduced to some extent.

The Compton scatter interactions were found to dominate the indirect dose rates, and a relatively smaller component was determined for annihilation photons that are associated with fission products in the reactor core. The initial indirect dose rates due to scattered photons were on the order of 10^0 to 10^1 rem hr^{-1} at the edge of the reactor pool, and on the order of 10^{-1} to 10^0 rem hr^{-1} at the exterior of the truck door. The initial indirect dose rates due to annihilation photons were on the order of 10^{-1} rem hr^{-1} at the exterior of the truck door. The direct and indirect dose rates for fission products indicate a significant increase in longer-lived fission products as $T \rightarrow \infty$. The indirect dose rates from fission products due to a loss of coolant accident following a typical reactor operating schedule, however, would decay significantly after about one month, and the Co-60 source therefore presents the most significant long-term radiation hazard. Long-term indirect dose rates therefore would be on the order of 10^0 rem hr^{-1} at the edge of the reactor pool, and on the order of 10^{-1} rem hr^{-1} at the exterior of the truck door.

Furthermore, the indirect dose rates must decrease dramatically outside the truck door, because as distance from the truck door increases the proportion increases of scattered photons and annihilation photons from the reactor dome that intercept the wall of the containment vessel above the truck door. The wall of the containment vessel in general is poured concrete with a thickness of 2 feet, and with an exterior steel lining. For all cases of indirect dose considered here, the effective energy of the scattered photons is less than 0.3 MeV, and photons of this energy that are obliquely incident on the containment wall (at the fluence rates considered here) will be attenuated to negligible levels. The same argument also can be applied to the annihilation photons that are obliquely incident on the containment wall. Based on the geometry used here, at a distance of about 24 ft from the truck door, at ground level, all scattered photons and annihilation photons from the reactor dome are intercepted at an oblique angle by the wall of the containment vessel. The total indirect dose rates at this distance therefore would be negligible (i.e., much less than 2 mrem hr^{-1}).

13.3 References

[i] U.S. Nuclear Regulatory Commission. Standards for Protection Against Radiation. Washington, DC: U.S. Government Printing Office; 10 CFR Part 20; 1992.

[ii] Shultis J. and Faw R. Radiation Shielding. La Grange Park, IL: American Nuclear Society; 2000.

[iii] University of Massachusetts Lowell Research Reactor. Final Safety Analysis Report (updated). Lowell, MA: UMLRR (NRC-50223); 1985.

APPENDIX B2
RINSC SAR LOCA

Replacement for:

> "Section 13.2.3 Loss of Coolant Accident (LOCA)" of *Safety Analysis Report of the Rhode Island Nuclear Science Center Reactor*, Submitted May 3, 2004.

This replacement has been prepared by:

Earl E. Feldman
Argonne National Laboratory
Argonne, Illinois
August 2010

13.2.3 Loss of Coolant Accident (LOCA)

13.2.3.1 Accident Scenario

The loss of coolant accident is the Design Basis Accident for the RINSC and is based upon an assumption that a beam port end in the pool is severed and the coolant drains into the beam port and leaks out on the reactor main floor. The coolant will also go down the drain line within the severed beam port and reemerge in the other beam ports because the drain lines of all of the beam ports are connect together and to a common closed volume. Since this common volume is relatively small compared with the volume of the pool, a single severed beam port will cause water to flow simultaneously from all of the beam ports to the reactor main floor.

There are four six inch diameter and two eight inch diameter aluminum beam ports which extend from outside the concrete wall through the pool wall liner at the mid-level of the reactor core. If the pool water drained to this level, active fuel would still remain immersed in about eight inches of water. A typical beam port, as shown in Figure 13.2.3-1 has four basic barriers that can prevent or impede leakage between the pool and the reactor room ends. The first is a welded cap assembly (thimble) at the beam port end in the pool. The second is the beam port shutter, which can be lowered to close-off the beam port. A third barrier, concrete shielding plugs with a one inch spiral hole for instrument leads, sits at the reactor room end of the beam port. During experiments these plugs may be in place or may be replaced with an experimental facility of similar design. The final barrier is a cover flange that bolts to the end of the beam port. This flange is in place while the beam port is not in use for experiments. When an experiment is placed in a beam port end, it will be designed to restrict flow so that in the event of a beam port failure the flow from the beam port to the reactor room will be no more than would occur if the experiment were not present and there were a ½" diameter hole extending to the reactor room. All experiments must be designed to withstand a backpressure equivalent of the hydraulic head of the pool, or about 25 feet of water pressure.

The assumptions used to calculate the drainage time are shown below.

- A guillotine cutoff occurs at the beam port and floods a beam port. Although a 2-inch drop in pool level scrams the reactor, the water level at scram will be taken to be the lowest level allowed by the Safety Limit of the Technical Specifications, which is 23.54 feet above the active core.
- All beam port shutters are fully open.
- The drain line manual valve is open.
- During the LOCA event there are no restrictions to flow within any of the beam ports except for a ½-inch diameter hole at the exterior end of each of the six beam ports. These six holes are modeled as six sharp-edged holes through which the pool water simultaneously drains as a result of the failure of only one beam port.
- The pool fill valve does not open automatically.
- No operator action is taken to reduce or stop the flow.

It will be assumed that one beam port is severed. Because of the common interconnected drain lines, all six beam ports are flooded. Water flows from each of the six beam ports onto the

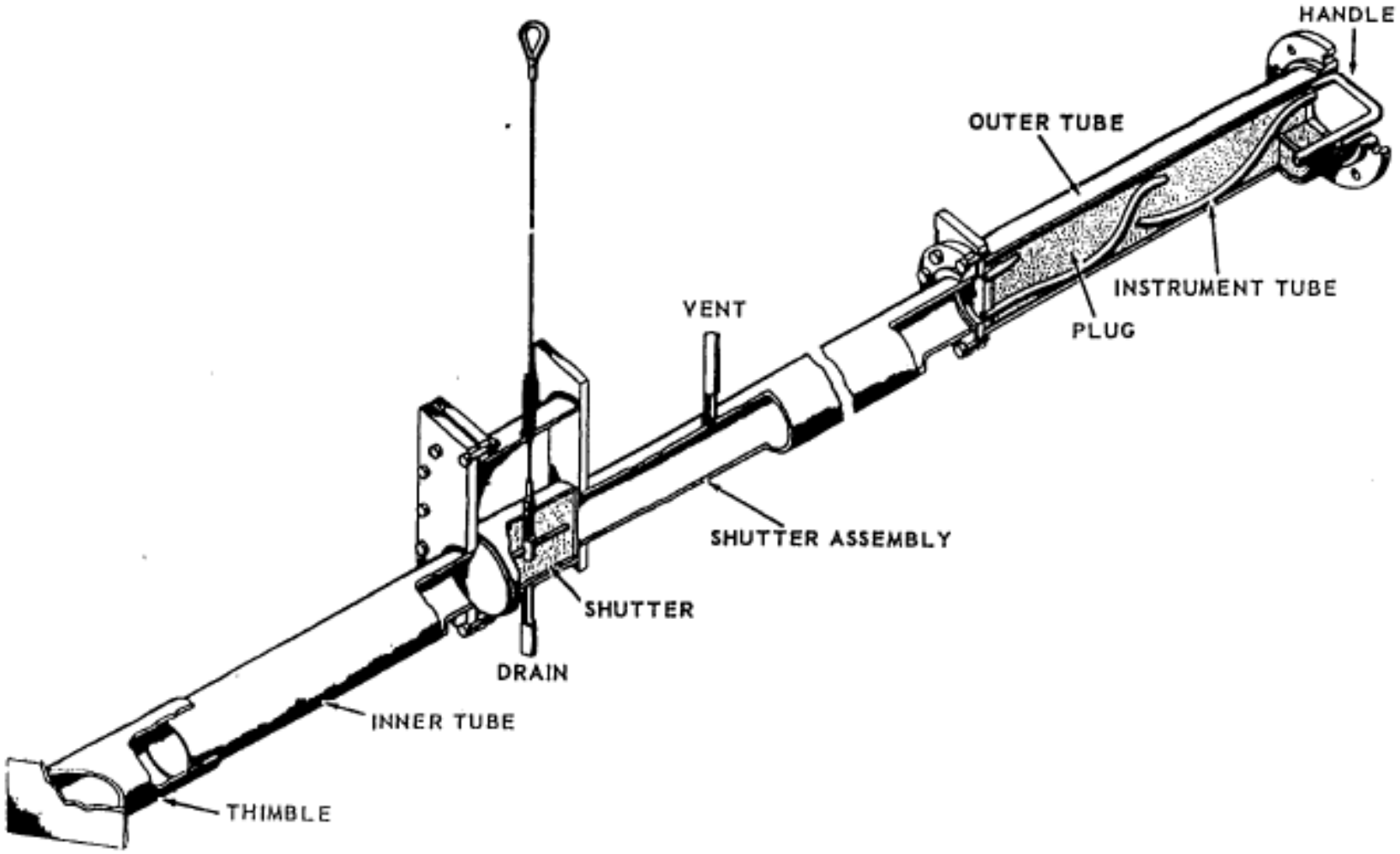

Figure 13.2.3-1 Typical Beam Port

reactor floor. Administrative controls are assumed to guarantee that the flow resistance path in each beam port is equal to, or more restrictive than, a round ½-inch diameter sharp-edged orifice at the exterior (beyond the reactor shielding) end of the beam port. The analytical model will be that of a large tank with six round ½-inch diameter holes around the tank at the same elevation. No credit will be taken for the flow resistance of the drain lines that enable the coolant to travel from the severed beam port to the other five beam ports that are intact.

The postulated accident sequence is the following:

1. A beam port is severed and enables the water to drain from the pool.
2. When the water level fall to 23.54 feet above the top of the fuel meat a reactor scram occurs.
3. The water level reaches the top of the core box.
4. The water continues to drain until the water level reaches the lowest point among the diameters of the six horizontal beam ports. (The lowest point in a 6-inch beam port is 3 inches below the horizontal centerline and 4 inches below in an 8-inch beam port.)
5. The water level continues to very slowly drop as water is boiled away by the decay heat.

After the scram the primary pump stays on and continues to run unless it is manually turned off. The heat rejection system that runs during normal operation also continues to operate. The core will remain submerged in water even after the pool water level has dropped and drained to the bottom of the beam ports if the primary pump continues to operate. The flow drawn out of the lower plenum of the core box by the operating primary pump goes, in order, through a 3000 gallon holdup (or delay) tank, the pump, a heat exchanger, a flow meter, and then is returned to the top of the core. General Electric drawings 198E299 (Reactor Assembly and Arrangement) and 197E651 (Assembly Frame and Header), which show the arrangement of the large rectangular ducts that lead the flow to the top of the core and draw flow from the lower plenum at the bottom of the core and up through the exit duct toward the pump, were carefully examined in order to better understand the behavior of the water level in the core box flow a LOCA. Figure 13.2.3-2, which was copied from Reference 1, shows the major structures depicted in General Electric drawing 198E299 and labels the vertical inlet and exit ducts as “flow channels”. Figure 13.2.3-3 shows a photograph of the core box region.

In the photograph in shown in Figure 13.2.3-3 all 14 fuel assemblies have been removed and the entire core structure, including the core box, which is suspended from overhead rails, has been move horizontally so that the inner ends of the six beam ports are visible from above. The red arrows were added to the photograph along the exterior of the inlet ducts in order to indicate the path of the inlet coolant flow inside the ducts. The vertical inlet duct in the photograph is the vertical flow channel that is toward the rear and mostly hidden Figure 13.2.3-2. The horizontal inlet duct immediately above the top of the core box and in the foreground in the photograph is the horizontal duct on the left in Figure 13.2.3-2. There is a rectangular opening in the vertical side of this duct that is closest to the core and not visible in the photograph, that provides the flow to the core inlet. The other horizontal duct in Figure 13.2.3-2 is part of the outlet flow path and is hidden behind the structure in the photograph.

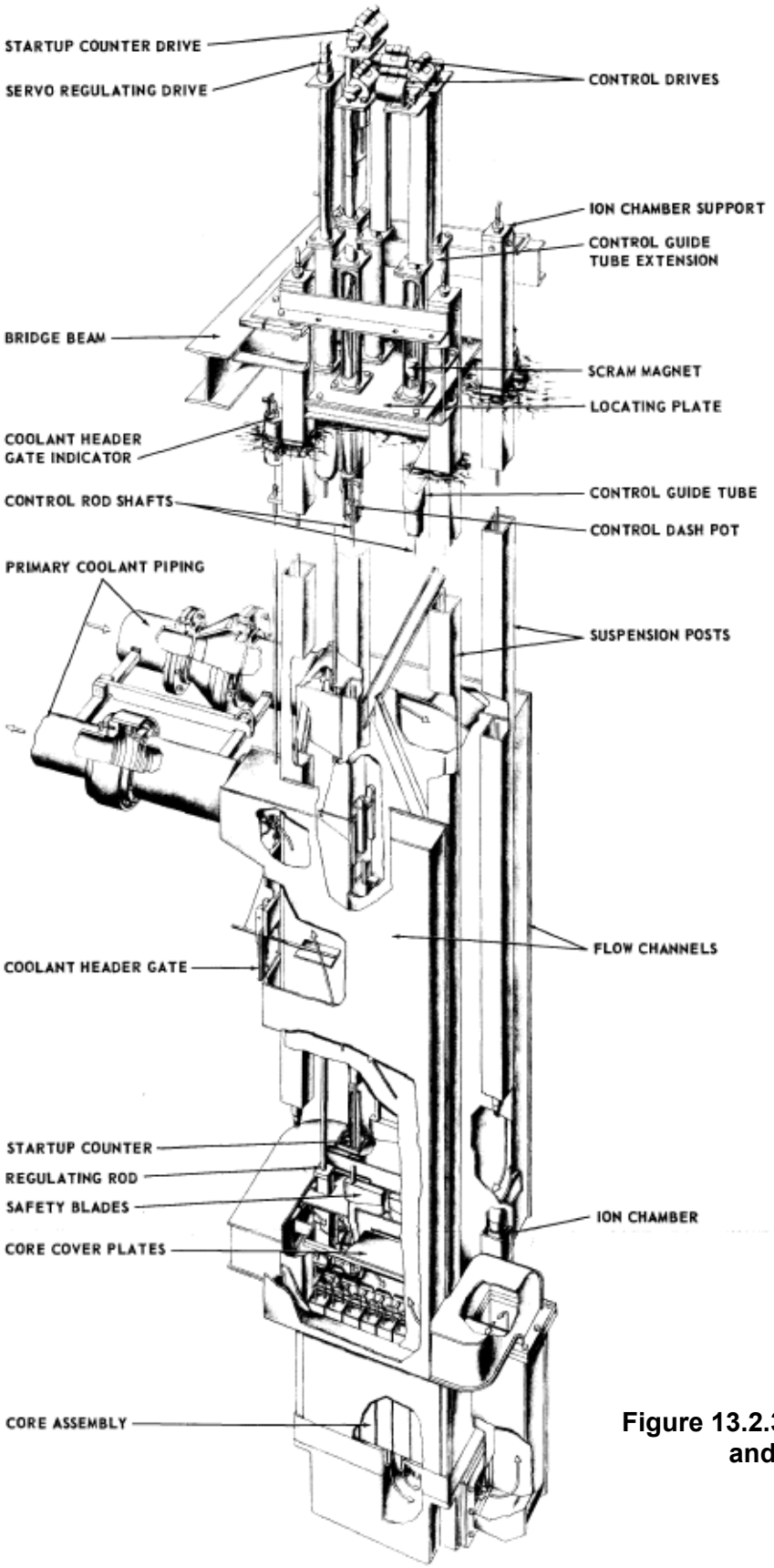

Figure 13.2.3-2 Reactor Assembly and Arrangement

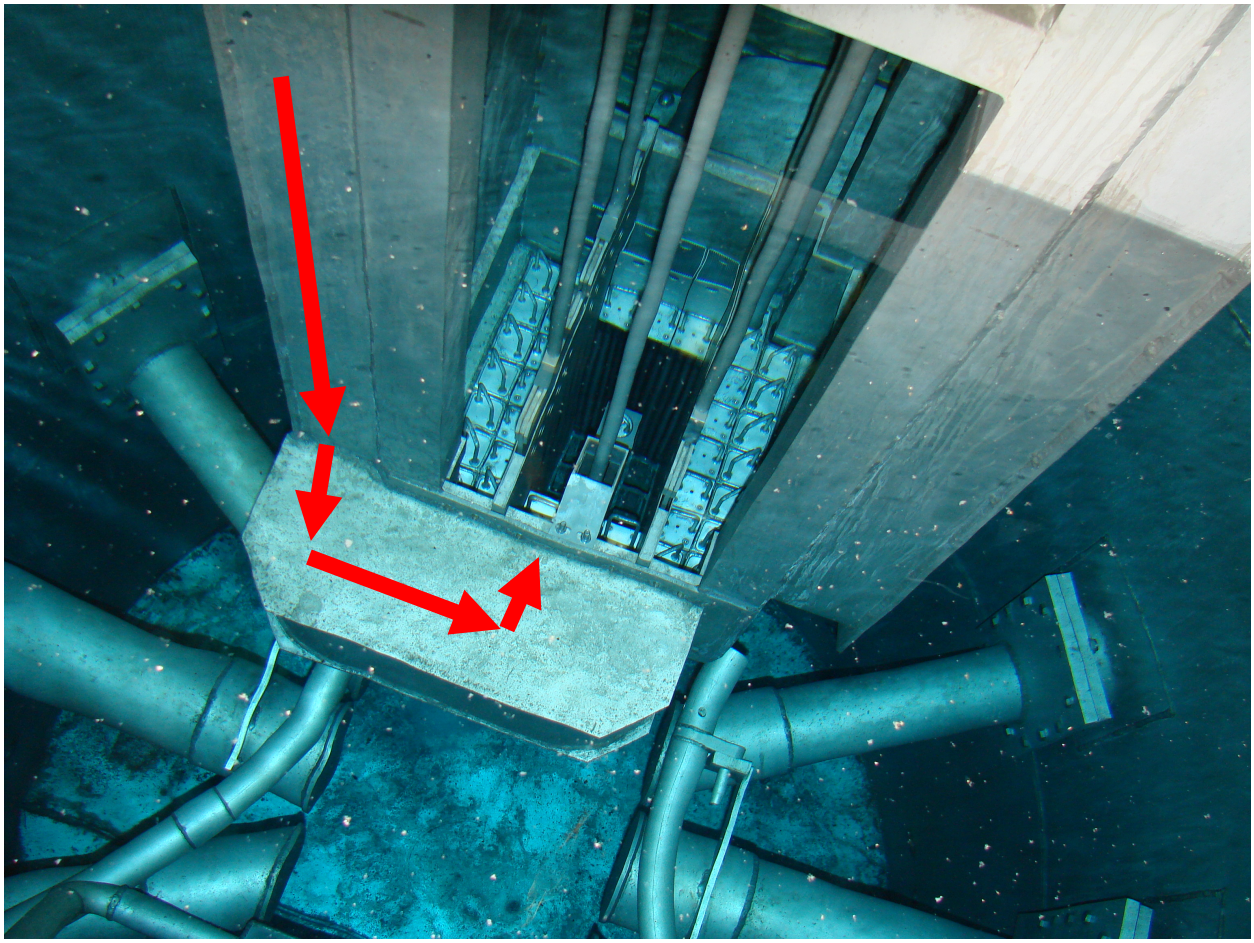

Figure 13.2.3-3 Photograph of Top of Core Box Region Taken during Maintenance

(The 14 fuel assemblies have been removed from the core box. The core structure, including the core box, which is suspended from overhead rails, has been moved horizontally so that the inner ends of the six beam ports are visible from above. The red arrows have been added to show the path of the inlet flow within the ducts.)

The two drawings, aided by the photograph, shows that there is vertical fence around the perimeter of the top of the core box that is no less than about a foot in height at its lowest point. Exterior sides of two vertical ducts form two sides of the fence. The horizontal inlet duct forms the third side of the fence. A vertical rectangular metal plate forms the fourth side of the fence and was attached to the structure before the horizontal outlet duct was attached.

While the pump is running, cooling water is continuously supplied to the top of the core and drawn off at the outlet plenum at the bottom. The water inlet, being located in the side of the fence, is always submerged. This minimizes the potential for water to splash over the top of the fence. The thimble that holds the regulating blade is immediately in the path of the inlet flow stream. However, a close examination of the photograph shows that the thimble has a horizontal bracket that is attached to the top of the fence by two rivets. This bracket would block flow that could splash upward off of the vertical side of the thimble. Thus, the water level will remain near

the top of the lowest point in the fence even if the water level in the remainder of the pool is at the drain point at the bottom of the beam ports.

Since there is a ½-inch diameter hole in the outlet plenum, the pump suction is constantly adding water to the flow circuit. This small amount of excess water should cause the inlet water to overflow the top of the fence. Hence, if the pump does not stop, water should be flowing through the core long after the pool level has reached the bottom of beam ports. Even if, by some unforeseen means water were to be lost from the circuit and the water level were to go below the top of the fuel meat, the core would still be cooled by the constant stream of flowing water. In the analysis no credit for the primary flow will be taken and it will be assumed that the operating primary pump has been stopped at the time of the scram.

When the pumps are stopped and the core flow rate drops below 1000 gpm, counterweights cause the coolant header gates, Figure 13.2.3.-2, to open. These gates, which are located about two feet below the two pipe stubs shown in the figure, were included in the reactor design to enable the core to be cooled by natural convection when neither of the two primary pumps is running. This natural circulation will stop when the water level drops below the level of the gates because water cannot enter the duct that connects to the lower plenum of the core. Then the fuel plates will be cooled by a combination of recirculation among the flow channels within the core box and local boiling. Recirculation will occur by water flowing up the hotter channels and down the colder channels. Local boiling will keep the fuel plate temperatures no higher than several degrees above the saturation temperature. While the pool water level is high enough to enter the top of the core box, warm water from the core box can enter the pool and be replaced by cold water from the pool. When the pool water level is too low to enter from the top of the core box, water can still enter the core box through a ½-inch diameter hole in the lower plenum. However, this flow should be relatively small.

We will calculate the time interval from the scram to when the water level reaches the top of the core box, which does not include the extra height due to fence formed mostly by the ducts that surround the core box on all four sides. Of course, additional time is required for the water level in the core box to reach the level of the bottom of the severed beam port. However, in order to keep the analysis simple, we will ignore this additional time and, in effect, assume that when the water level reaches the top of the core box, the fuel is exposed as if the water level had reached the lowest point in the horizontal beam ports. In succeeding sections, the decay heat at this time will be used to determine the maximum temperature of the hottest fuel plate.

13.2.3.2 Drain Time

The drain time is taken to be from the time of the scram until the water level reaches the top of the core box. For the calculation of the drain time, the elevations of the top of the core box and the water level at scram must be determined relative to the elevation of the leak. First, the distance from the bottom of the beam port to the top of the core box is calculated. Table 13.2.3-1, which provides a few key elevations relative to the elevation of the beam port leak, is based in part on the following. The centerlines of the beam ports and the core are at the same elevation. Based on the sketch at the top of Appendix C of Reference 2, the elevations of the core centerline and the top of the core box are 114.463 and 115.713 feet, respectively. The distance

between these two elevations is 115.713 − 114.463 = 1.25 feet, or 15 inches. The distance from the centerline to the bottom of the 8-inch beam ports is obviously 4 inches. Thus, the distance from the bottom of the beam port to the top of the core box is 4 + 15 inches, or 19 inches (1.58 feet).

Table 13.2.3-1
Elevations Relative to Drain Point

Location	Elevation
Scram Water Level	24.84 ft
Top of Core Box	19 in (1.58 ft)
Top of Fuel Meat	15.625 in
Core & Beam Port Centerlines	4 in
Drain Point (beam port bottom)	0 in

Next the distance from the bottoms of the 8-inch beam ports to the water level at scram is calculated. This distance is the distance from bottoms of the 8-inch beam ports to the top of the fuel plus the distance from the top of the fuel to the water level. The Safety Limit of the Technical Specifications provides that the true value of the water level above the active core shall be no less than 23.54 feet. Thus, the distance from the top of the fuel to the water level is taken to be 23.54 feet. The other required length is the distance from the bottoms of the 8-inch beam ports to the top of the core box, 19 inches, reduced by the few inches from the top of the core to the top of the core box. Since there are 15 inches from the fuel centerline to the top of the core box, as shown in the previous paragraph, and the fuel meat is 23.25 inches long, the required few inches is 15 − 23.25/2 inches = 3.375 inches. Thus, the distance from the bottoms of the 8-inch beam ports to the top of the fuel meat is 19 − 3.375 inches = 15.625 inches. Hence, the distance from the bottoms of the 8-inch beam ports to the water level at scram is 15.625 inches + 23.54 feet = 24.84 feet.

The model for the drain time is one of a large tank with vertical walls which at a particular elevation has six sharp-edged round ½-inch diameter orifices in its lateral wall. The initial water level in the tank is 24.84 feet above the elevation of the six orifices. We need to determine the time required for the water level to fall 23.26 feet so that the water level is 1.58 feet above the elevation where the orifices are located.

There is a small discrepancy between the core and beam port centerline elevations of Appendix C of Reference 2, quoted above, and those indicated in General Electric drawing “Pool Outline”, 198E273. This drawing indicates the approximate elevations of the centerlines of the 8-inch beam port, the core, and the 6-inch beam port are at 114 ft – 5-9/16 inches, 114 ft – 5 inches, and 114 ft – 4-7/16 inches, respectively. These are to be compared with the common centerline of 114.463 feet (114 ft – 5-9/16 inches) quoted above. The new values put the bottoms of the 8-inch beam port, the core, and the 6-inch beam port are at 114 ft – 1-9/16 inches, 113 ft – 5-3/8 inches, and 114 ft – 1-7/16 inches, respectively. A difference of a fraction of an inch will have a negligible effect on the drain time and on the resultant maximum decay power level that is used to determine the maximum fuel temperature. The placement of the bottom of the 6-inch beam port 1/8th inch below the bottom of the 8-inch one does not matter as long as the lower drain point is used in the analysis. However, what is important is the vertical distance from the lowest drain point to the bottom of the core. The new values show this to be (114 ft – 1-7/16 inches) − (113 ft – 5-3/8 inches), or 8-1/16 inches. The old values with coincident centerlines cause this length to be half of the fuel meat length minus 4 inches, or 11-5/8 inches − 4 inches = 7-5/8 inches. The smaller submerged length will produce greater peak fuel temperatures because it has

a larger exposed fuel plate length. Thus, for the analysis it will be assumed that Appendix C of Reference 2 is correct and the centerlines are coincident.

The analytical model for this situation with only one hole is derived in fluid mechanic textbooks. The jet of water issuing from the side of the tank reaches its minimum diameter, the "vena contracta" at a short distance outside of the tank wall. If A_1 and A_2 are the cross sectional areas of the tank and the jet's minimum diameter, respectively, V_1 is the velocity at which the fluid level is dropping, and V_2 is the velocity at A_2, then by the continuity equation:

$$V_1 = \frac{A_2}{A_1} V_2 \tag{1}$$

If h is taken to be the vertical distance in the upward direction from the orifice, then V_1 is $-dh/dt$, where t is time. The ratio of the minimum diameter ("vena contracta") area A_2 to the orifice hole area A, is given by the orifice coefficient C_d, which the published empirical data shows to be about 0.61 for water, i.e., $C_d = A_2/A = 0.61$. The Bernoulli equation is applied between the water surface and the minimum jet area A_2. Thus:

$$\frac{V_1^2}{2} + \frac{P_1}{\rho} + gZ_1 = \frac{V_2^2}{2} + \frac{P_2}{\rho} + gZ_2 \tag{2}$$

Where P_1 and P_2 are the pressures at A_1 and A_2, respectively, Z_1 and Z_2 are the elevations at A_1 and A_2, respectively, and g is the acceleration due to gravity. The two pressures are at atmospheric pressure and are equal. V_1 is negligibly small since A_1 is large compared to A_2. The difference $Z_1 - Z_2$ is the vertical height of the water level relative to the elevation of the orifice, which we will call h. Thus:

$$V_2 = \sqrt{2gh} \tag{3}$$

We now combine equations (1) and (3) and eliminate V_2, replace V_1 with $-dh/dt$, and replace A_2 with Cd × A, the resultant equation is:

$$\frac{dh}{dt} = -\frac{C_d A}{A_1}\sqrt{2gh} \tag{4}$$

Equation (4) can be integrated between the initial water level, h_1, and the final water level, h_f, over the time interval from t = 0 to $t = t_f$. The result is:

$$t_f = \frac{A_1}{C_d A}\sqrt{\frac{2h_1}{g}}\left[1 - \left(\frac{h_f}{h_1}\right)^{\frac{1}{2}}\right] \tag{5}$$

The above derivation would be unchanged if there were six orifices all at the same level and with the same area A, except that A would present the area of all six orifices combined. (An equivalent way to do the same thing is to assume the pool is divided into six segments of equal area, each containing one ½-inch sharp-edged orifice. The A_1 is divided by 6 and A represents the area of one ½-inch diameter orifice.) Appendix C of Reference 2 indicates that the total surface area of the pool surface is 150 ft^2. This can be verified from the dimensions given in General Electric drawing "Pool Outline", 198E273. The pool has three sections and a movable gate that can separate one end section from the other two sections. However, normal power operation is not allowed if the gate is in place. Therefore, in the analysis it is assumed that the movable gate is not in place and all three regions of the pool can drain simultaneously. The area of the orifice is taken to be six round ½-inch-diameter holes. The values for all of the quantities on the right side of equation (5) are summarized in Table 13.2.3-2. Substituting these values into equation (5), one obtains t_f is 2.792×10^4 seconds = 7.756 hours. This drain time will be used to determine the maximum decay power level, which, in turn, will be used to determine the maximum fuel plate temperature.

Table 13.2.3-2
Values of Equation (5)

Quantity	Value
C_d	0.61
A_1	150 ft^2
A	8.18×10^{-3} ft^2
g	32.2 ft/s^2
h_1	24.84ft
h_f	1.58 ft

13.2.3.3 Decay Power

Values of decay power as function of time after scram are provided by Stillman,[3] who considered infinite operation along with operation for about 40 years at 1) 40 hours per week, 2) 72 hours per week, 3) 120 hours per week, and 4) continuous operation of 168 hours per week. His data, for which 100% relative power corresponds to full reactor power, is plotted in Figure 13.2.3-4. For infinite operation at full power, the decay power fraction at 2.792×10^4 seconds (7.756 hours) after scram is 0.718%. The precise value is based on linear interpolation of the tabular data in the Stillman reference, which is included as Appendix B. Figure 13.2.3-4 also shows that if operation for about 40 years at 40 hours per week is assumed, which is a much more realistic assumption based on current operation, then the decay power fraction at 7.756 hours would be about half as much.

13.2.3.4 Development of Heat Transfer Model

Heat transfer analysis for the partially submerged core will focus on the highest powered fuel plate in the core. This fuel plate is the one in element D6 that is immediately adjacent to the central beryllium reflector. Since the centerline of the beam port is at the centerline of the core, half of the fuel meat length, 23.25/2 inches, is above the centerline and the other half is below it. The distance from the centerline of an 8-inch beam port to the bottom of the beam port is 4 inches. Thus, 23.25/2 − 4 inches, or 7.625 inches, of the fuel meat is submerged in water and the remaining 15.625 inches is exposed to the air.

Heat generated in the assembly above the waterline will be conducted down along the length of fuel element to the pool of water. This heat along with the heat generated in the submerged portion of the assembly will cause the water to boil and produce steam that rises up through the coolant channels. The rising steam in the coolant channels will remove heat by convection from

the exposed surfaces of the fuel plates. A coupled pair of ordinary differential equations will be derived – one to represent the axial distribution of the fuel plate temperature and one to represent the axial distribution of the steam temperature.

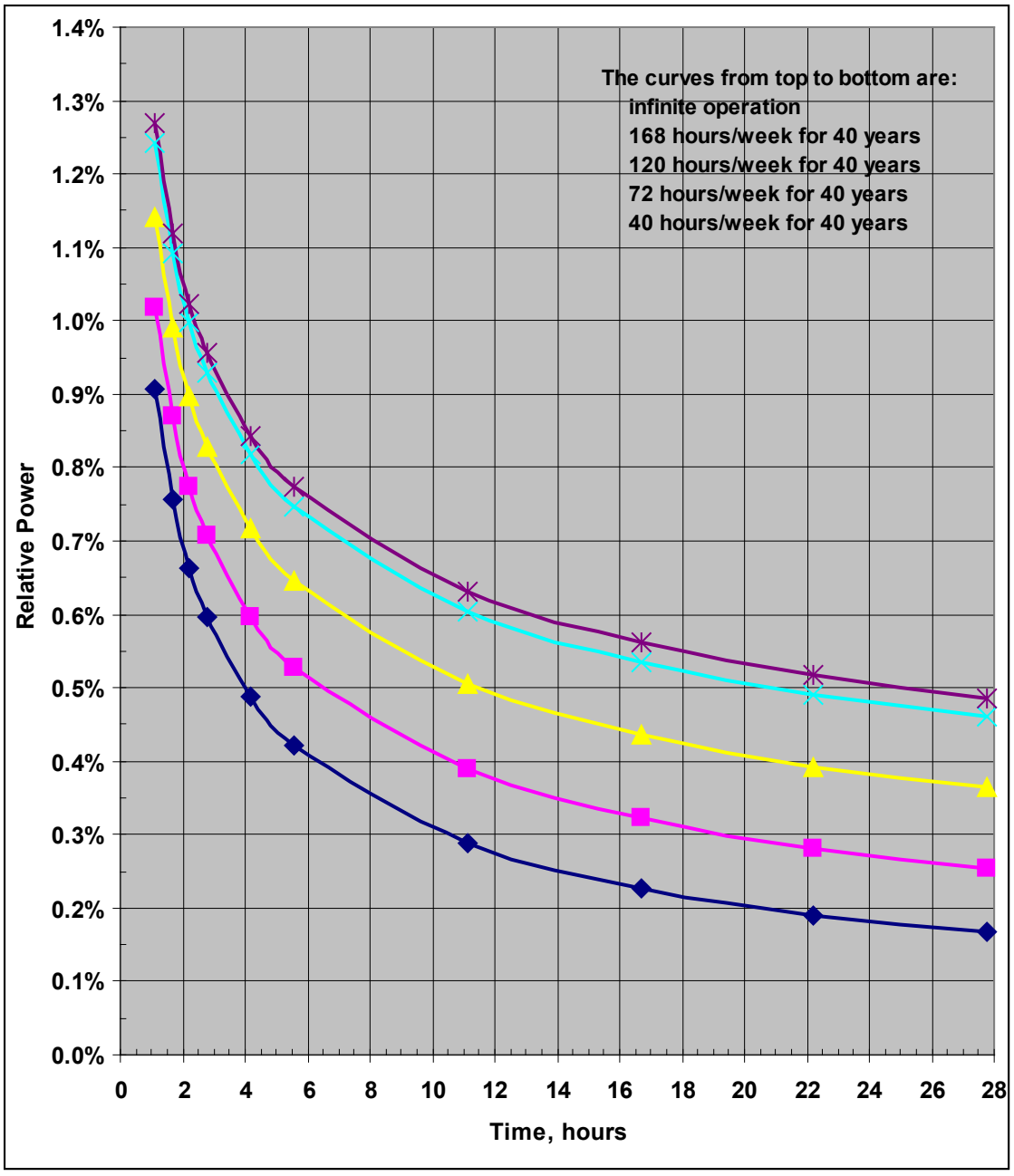

Figure 13.2.3-4 Decay Power

A steady-state model will be used. No credit is taken for the time required for the fuel plate to reach a steady-state condition. It is assumed that 7.756 hours after scram, the water level reaches the top of the core box and instantaneously drops to the bottom of the beam port and also achieves a steady-state temperature distribution in the 15.635-inch exposed length of the fuel plate.

In reality, during the time it takes for the water level to drop from the top of the core box to the bottom of the beam port and for the exposed portion of the fuel plate to achieve a steady-state condition, the decay power is decreasing. The heat-up of the fuel plate from the temperatures it had when it was fully submerged, which are essentially the pool water temperature, to the steady-state exposed condition could take many minutes. This is because the power generation rate in the fuel plate at decay power levels is relatively low and the heat capacity of the fuel plate is relatively high. Thus, a transient solution could produce a lower peak fuel temperature than will be predicted below. The transient effects are more important when the drain time is short because the decrease in decay power level is greatest immediately after the scram and slows down with increasing time. Long after the scram, the gradual decrease in power level is sufficiently small to enable steady-state solutions at an instantaneous power level to more closely predict the expected temperatures.

There are 22 fuel plates in each fuel assembly. We will consider a typical one and the associated portions of two side plates. Thus, a model will be developed of steady-state heat conduction along the length of a vertical beam that consists of the fueled portion of a fuel plate and 1/22 of two aluminum side plates, one on either end. Figure 13.2.3-5 shows the horizontal cross section of the model. The red-colored region is the fuel meat and the gray-colored regions are the aluminum clad and the associated portions of the two aluminum side plates. Because decay power is low relative to full reactor power and the thermal conductivities of aluminum and the fuel are high, it is reasonable to ignore temperature gradients within each horizontal cross section of this beam. Therefore, a one-dimensional steady-state model of heat transfer model of a beam of uniform cross section will be developed. The entire perimeter of the beam shown in Figure 13.2.3-5 will be assumed to be insulated except for the two fuel plate faces along the width of the flow channel that are not cover by the side plates. This width is 2.62 inches. The top surface of the beam is assumed to be insulated. In this model all of the decay power generated in the beam will be essentially conducted vertically down the length of the beam to the water or transferred by convection to the flowing steam in the two channels on either side. The model includes both the fuel plate and the coolant channels on either side. In order to avoid needless complexity, we will assume that the two coolant channels are identical. The solution will provide the axial temperature distributions for both the beam and the coolant. The maximum fuel temperature will be at the insulated top end of the beam. The top portion of the fuel plate that does not contain fuel is not included in the model.

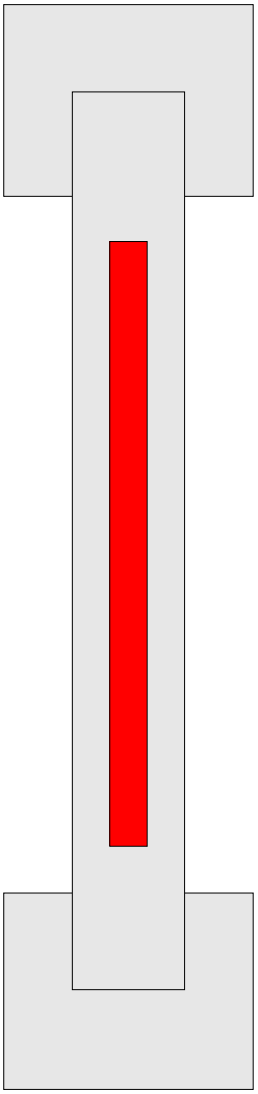

Figure 13.2.3-5 Horizontal Cross Section of the Fuel Plate in the LOCA Heat Removal Model (not to scale)

An issue is the axial distribution of the power along the length of

the fuel plate. Typically, the distribution will tend to be in the shape of a symmetric chopped cosine shape whose peak is near the center of the 23.25-inch fuel meat length. Since the center of the fuel meat length is 4 inches above the water level, within the exposed length of the fuel plate the power is skewed toward the bottom. The more that power is skewed toward the bottom, the lower the peak solid temperature will be. The reason for this is that heat generated lower in the exposed portion of the fuel plate length has a shorter conduction path to the surface of the water than does heat generated higher in the exposed portion. Moreover, as is obvious, lower fuel temperatures will also be produced if a greater portion of the heat produced over the entire fuel plate is generated below the surface of the water. Figure 4.6-5 (of the currently replaced section 4.6 of the RINSC reactor safety analysis report, "4.6 Steady-State Thermal-Hydraulic Analysis"), provides the axial power shape for the fuel meat length of the highest power plate, which is the one next to the beryllium reflector in assembly D6. In order to keep the model simple and avoid the issue of the precise axial power shape, we will use a bounding approach and assume that the heat generation rate in the fuel plate is uniformly distributed over the entire length of the fuel meat. The water level is at 0.672, i.e., 15.625 inches/23.25 inches, in the Figure 4.6-5. Numerical integration of the axial power in the figure shows that 56.6 % of the power is generated in the exposed portion of the fuel meat length and the remaining 43.4% is generated in the submerged portion. This is to be compared with the uniform distribution, in which 67.2% of the power is generated in the exposed part of the fuel meat length and the remaining 32.8% is generated in the submerged portion.

The next step is to use first principles to derive the governing differential equations. First, consider a horizontal slice of the beam of thickness, Δx. We will assume that x=0 at the waterline and x = L is at the insulated top surface of the beam where $dT_p/dx = 0$. Here, of course, $T_p(x)$ is the temperature of the beam. An energy balance of a typical Δx slice of the beam, as shown in Figure 13.2.3-6 can be stated as:

power into the beam at location x +
power generated in the slice of thickness Δx =
power out at location $x + \Delta x$ +
power transferred by convection from the beam to the two flowing steams between locations x and $x + \Delta x$ on either side of the fuel plate (6)

The power into the slice at x is:

$$-(k_{fuel} A_{fuel} + k_{al} A_{al}) \, dT_p/dx \text{ at } x \quad (7)$$

where k_{fuel} and k_{al} are the thermal conductivities of the fuel and the aluminum regions, respectively, and are taken to be know constant values and A_{fuel} and A_{al} are the cross sectional areas of the fuel and aluminum regions, respectively.

Similarly, the power out at $x + \Delta x$ is:

$$-(k_{fuel} A_{fuel} + k_{al} A_{al}) \, dT_p/dx \text{ at } x + \Delta x \quad (8)$$

These two power relationships are based on Fourier's law of heat conduction.

The power generated in the slice is:

$$q''' A_f \Delta x \quad (9)$$

where q''' is the volumetric heat generation rate of the fuel region.

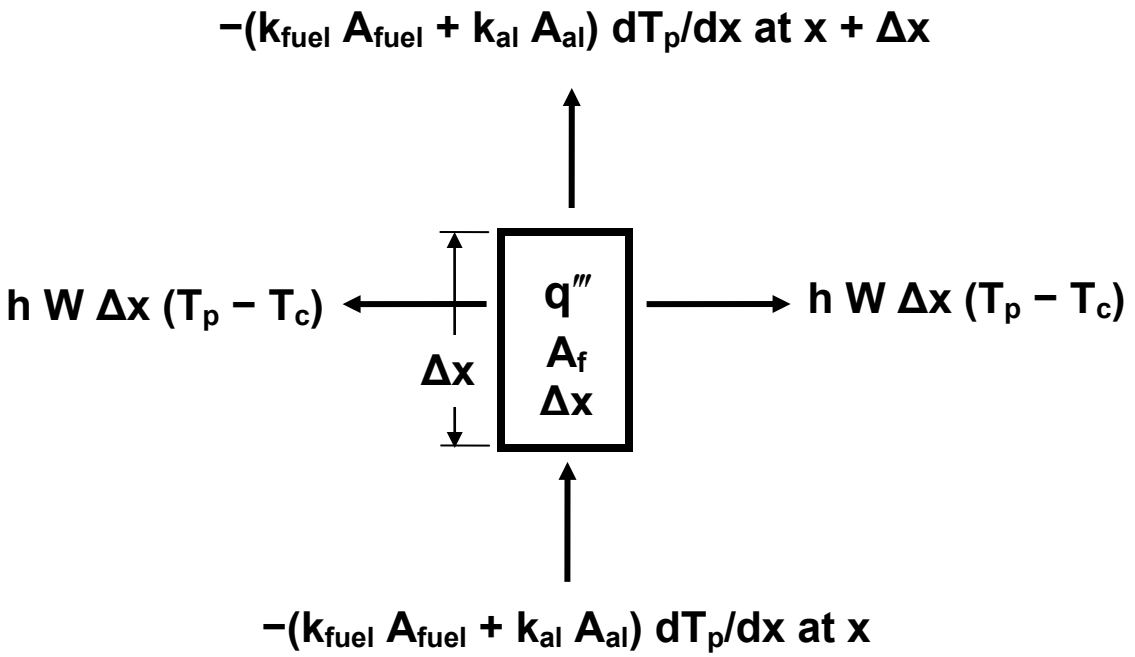

Figure 13.2.3-6 Heat Balance on Δx Length of Fuel

The power transferred by convection to the flowing steams between locations x and x +Δx is:

$$2 h W \Delta x (T_p - T_c) \quad (10)$$

where h is the film coefficient at the surface of the plate, W is the width of the plate (2.62 inches), and T_c is the coolant, i.e., steam, temperature.

Now, we substitute item (7) for the first term of equation (6), item (9) for the second term, item (8) for the third term of equation (6), and item (10) for the last term. Then we divide all terms by Δx and take the limit as Δx goes to zero. The resultant equation is simplified to produce the following:

$$\frac{d^2 T_P}{dx^2} = \alpha \left(T_p - T_c\right) - \beta \quad (11)$$

where:

$$\alpha = \frac{2 h W}{k_f A_f + k_{al} A_{al}} \quad (12)$$

and

$$\beta = \frac{A_f \; q'''}{k_f A_f + k_{al} A_{al}} \tag{13}$$

Next we consider one of the two coolant channels on either side of the fuel plate, which are assumed to be identical. If the fuel plate is not the end fuel plate in the assembly, then there is an identical coolant channels on either side of the fuel plate. In this case there is a vertical plane of symmetry in the middle of each of the two coolant channels. Then the fuel plate and its two immediately adjacent half channels are modeled. The two half channels are assumed to received all of the power transferred by convection from the fuel plate. Since the highest power fuel plate in the core is next to the central beryllium reflector, its two flow channels are not identical and one channel is heated from two sides and the other is heated from only one side. However, in the model it will be assumed that both channels, whether they are half or whole channels, are identical. Therefore, the analysis will consider two cases. In case 1 the fuel plate has a half channel on either side. In case 2 the fuel plate has two whole channels on either side, but each whole channel is heated from only one side. The coolant channel model derivation is the same for both cases. Both cases will be considered and whichever of the two produces the highest fuel plate temperature will bound the asymmetric case that needs to be considered.

An energy balance of a typical Δx slice of one of the two half channels (for case 1) or two whole channels (for case 2), as shown in Figure 13.2.3-7, can be stated as:

power flowing with the coolant into the slice at x +
power transferred by convection into the channel from the surface
of the plate between x and x + Δx =
power flowing with the coolant out of the slice at x + Δ x (14)

The power flowing with the coolant into the slice at x is:

$$\frac{\dot{m}}{2} C_p \, T_c(x) \tag{15}$$

where $\dot{m}$ is the combined flow rate of the two half channels of case 1 (or the two whole channels of case 2), and C_p is the specific heat capacity of the steam.

Similarly, the power flowing with the coolant out of the slice at x + Δx is:

$$\frac{\dot{m}}{2} C_p \, T_c(x + \Delta x). \tag{16}$$

The power transferred by convection into the half channel (or whole channel for case 2) from the one fuel plate surface is half of what is given by item (10), above, or:

$$h \, W \, \Delta x \, (T_p - T_c) \tag{17}$$

Now, we substitute item (15) for the first term in equation (14), item (17) for the second term, and item (16) for the third and last term. Then we divide all terms by Δx and take the limit as Δx goes to zero. The resultant equation is simplified to produce the following:

$$\frac{dT_c}{dx} = \gamma \left(T_p - T_c \right) \tag{18}$$

where:

$$\gamma = \frac{2\ h\ W}{\dot{m}\ C_p} \tag{19}$$

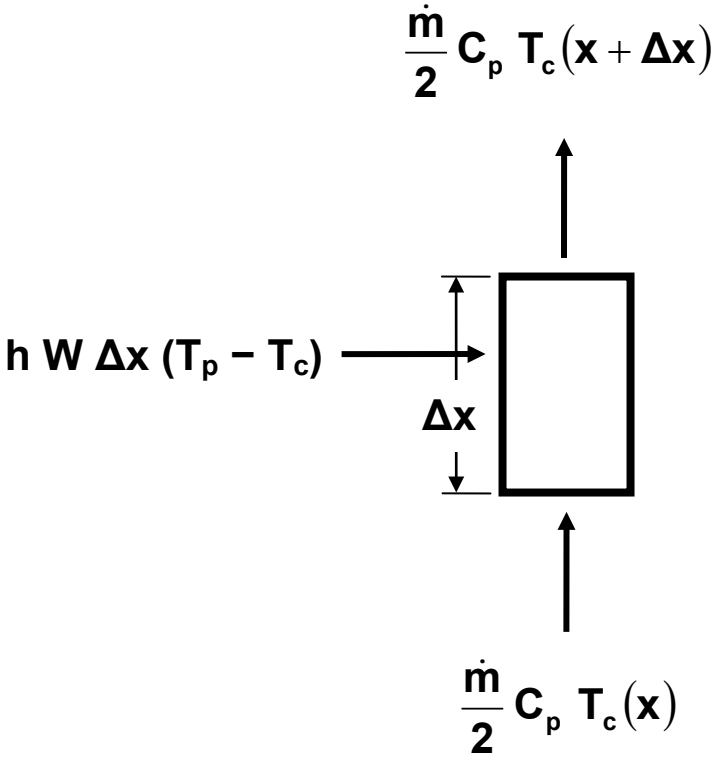

Figure 13.2.3-7 Heat Balance on Δx Length of One of Two Identical Half Coolant Channels

The two boundary conditions for equation (11) are:

$$T_p(0) = T_{p0} \tag{20}$$

and

$$\frac{dT_p}{dx} = 0 \quad \text{at } x = L \tag{21}$$

where T_{p0} is slightly more than the boiling point of water at 1 bar and is as determined below, L is the exposed length of the beam, which is 15.625 inches, or 0.3969 m.

The boundary condition for equation (18) is:

$$T_c(0) = T_{c0} \quad (22)$$

where T_{c0} is the boiling point of water at 1 bar, 212° F, or 100° C.

13.2.3.5 Steam Flow Rate, $\dot{m}$

The flow rate, $\dot{m}$, is the amount of steam that is produced by the power that is transferred from the submerged end of the plate to the water. Because of buoyancy, the water in the submerged portion of each channel will stratify, with the hottest water closest to the surface. Water enters the bottom of the assembly at the pool temperature, which is taken to be 40° C, 104° F, and leaves at the surface of the water as saturated steam. The specific enthalpies for liquid at 40° C and 1 bar and saturated vapor at 1 bar are 167.6 and 2675 kJ/kg, respectively, based on the 1996 NIST/ASME Steam Tables, which are used to obtain all of the steam properties used in the analysis. Thus, the increase in coolant specific enthalpy from 40° C liquid to saturated steam at 1 bar, Δi, is 2675 − 167.6 kJ/kg, or 2507 kJ/kg. This implies that for every 2507 kJ of energy transferred from the submerged portion of the fuel plate, half of a kg of saturated steam travels up each side of the fuel plate in each of its two half (or whole) channels.

If a higher value of pool water temperature is used, less energy is needed to produce a kg of steam. For example, if the water temperature were 45° C, its specific enthalpy would be 188.5 instead of 167.6 kJ/kg and Δi would be 21 kJ/kg less. Hence, lower water temperature values in the model are more limiting than higher ones because lower ones produce less saturated steam to cool the fuel plate.

The power transferred from the submerged portion of the fuel plate, p, has two components – 1) p_1, the power produced in the submerged portion and 2) p_2, the power transferred from the exposed portion to the submerged portion (at x = 0). Because the power is assumed to be uniformly distributed along the axial length of the fuel meat, the first component is the total decay power produced in the fuel meat times the ratio of submerged fuel meat length to the total fuel meat length. This ratio is 7.625 inches / 23.25 inches. The second component is analogous to items (7) and (8), above, but is evaluated at x = 0 and the negative sign is removed because the heat flow in the negative-x direction instead of the positive one is needed. Thus, the second component is:

$$p_2 = (k_{fuel} A_{fuel} + k_{al} A_{al}) \, dT_p/dx \text{ at } x=0 \quad (23)$$

Thus, $p = p_1 + p_2 = \dot{m} \, \Delta i$, or:

$$\dot{m} = p / \Delta i \quad (24)$$

13.2.3.6 Fuel Plate Temperature at the Surface of the Water, T_{p0}

The temperature of the fuel plate at the surface of the water is slightly higher than the saturation temperature because vapor bubbles do not form on the submerged surface of the fuel plate until the temperature exceeds the saturation temperature by a small amount. For this example of pool boiling, the value is a function of the surface material and roughness and the fluid. A relationship that predicts this slight excess temperature[4] is:

$$\frac{c_l(T_w - T_{sat})}{i_{lg}} = C_{sf}\left\{\frac{q''}{\mu_l i_{lg}}\left[\frac{g_c\sigma}{g(\rho_l - \rho_g)}\right]^{1/2}\right\}^r \left(\frac{c_l\mu_l}{k_l}\right)^s \quad (25)$$

where T_w and T_{sat} are the surface temperature and the coolant saturation temperature, respectively, c_l, μ_l, k_l, and ρ_l are the specific heat at constant pressure, the viscosity, thermal conductivity, and density of the saturated liquid, respectively, q'' is the heat flux, i_{lg} is the heat of vaporization of the fluid, σ is the surface tension of the liquid, ρ_g is the density of the saturated vapor, g_c is the proportionality constant in Newton's second law of motion [32.174 lb-ft/(lb_f-s^2) or 1 in SI units], g is gravitational acceleration, and s, r, C_{sf} are parameters that depend on the surface and the fluid. The reference recommends r = 0.33, s = 1.0 for water (1.7 for all other fluids), and provides a range of 0.003 to 0.015 for $C_{sf.}$ The left side of the equation and the quantity in the curly brackets on the right side are dimensionless quantities. The quantity in the parentheses on the right side is the Prandtl number for the saturated liquid, which is also a dimensionless quantity. The quantity $T_w - T_{sat}$ is the required temperature difference. It is largest when C_{sf} is the largest. Therefore, 0.015 will be assumed for $C_{sf.}$ Values for key parameters needed to evaluate equation (25) are provided in Table 13.2.3-3. The heat flux, q'', is obtained by divided the highest plate power at decay power by the heated surface area of the plate, which is 2 × channel width × the plate heat length. All of the quantities needed to determine q'' are included in Table 13.2.3-4. Thus, q'' = 69.309 W / (2 × 0.066548 m × 0.59055 m) = 881.8 W/m^2 = 0.8818 kW/m^2. When equation (25) is solved for $T_w - T_{sat}$ a value of 2.2° C is obtained. In the analysis this value will be rounded up to 5° C and T_{p0} of equation (20) will be assumed to be 105° C.

13.2.3.7 Film Coefficient, h

The film coefficient, h, in equation (19) is a function of Reynolds number for turbulent flow and is independent of Reynolds number for laminar flow. The Reynolds number is the product of the steam density, steam velocity, and the channel hydraulic diameter divided by the steam viscosity. A mathematically equivalent definition of Reynolds number is that it is 4 times the channel flow rate divided by the product of the viscosity and the channel wetted perimeter. The highest channel flow rate possible is one in which all of the power generated over the entire fuel meat length is used in steam production. For this case, p in equation (24) is 69.309 W. Since Δi is 2507 kJ/kW, $\dot{m}$ for this extreme case is 69.309 W / 2507 kJ/kW = 2.765 × 10^{-5} kg/s. The fuel plate under consideration is the one in assembly D6 that is next to the central beryllium reflector. As shown in Table 4.6-5, the channel that is next to the beryllium reflector is 0.0645 inches thick and has a wetted perimeter of 0.1367 m and the channel on the other side of the fuel plate and formed between two fuel plates, is 0.088 inches thick and has a 0.1376 m wetted perimeter. The viscosity of steam at 1 bar has a range of 1.22 × 10^{-5} to 2.86 × 10^{-5} Pa-s between 100 and 500° C. Even if the smaller of these two values is used along with the smaller wetted perimeter, the Reynolds number is only 4 × 2.765 × 10^{-5} kg/s /(1.22 × 10^{-5} Pa-s × 0.1367 m) = 66.3. Thus, the flow is clearly laminar for all conceivable cases.

Table 13.2.3-3 Key Pool Boiling Parameters for Determination of $T_w - T_{sat}$

Parameter	Symbol	Value
pressure, bar		1.00
g, m/s^2	g	9.80665
g_c (SI units)	g_c	1
density liquid, kg/m^3	ρ_l	958.6
density vapor, kg/m^3	ρ_g	0.5903
viscosity liquid, Pa s	μ_l	0.0002828
enthalpy liquid, kJ/kg		417.5
enthalpy vapor, kJ/kg		2675
enthalpy vapor - enthalpy liquid, kJ/kg	i_{lg}	2257.5
Specific heat of liquid at constant pressure, kJ/kg-K	c_l	4.215
conductivity of liquid, W/m-K	k_l	0.679
surface tension, N/m	σ	0.05899
C_{sf} (Surface-Fluid Combination)	C_{sf}	0.015
r	r	0.33
s	s	1.0
heat flux, kW/m^2	q''	0.8818
Prandtl number		1.756
$T_w - T_{sat}$, C	$T_w - T_{sat}$	2.17

In Section 13.2.3.10, below, the effect on film coefficient on maximum fuel temperature is studied and a sound basis for using a value of 100 W/m^2-K is given. There it is shown that the peak fuel plate temperature varies within a range of about 10° C for values of h above 20 W/m^2-K. Thus, in the interim, it will be shown that h is at least 20 W/m^2-K for both the channel that is bounded by two fuel plates and the one that is next to the central beryllium reflector.

The film coefficient can be estimated from published values of Nusselt number, Nu. $Nu = h \times D_h / k$, where D_h is the hydraulic diameter of the duct and k if the thermal conductivity of the coolant. Values of Nusselt number for rectangular channels of various aspect ratios with constant heat flux or constant temperature boundary conditions can be found in Table 8-2 of reference 5. The table also includes values for parallel plates that are heated from only one side instead of two. The aspect ratio for the 0.088-inch thick internal channel is about 30 and about 40 for the 0.0645-inch thick channel next to the beryllium reflector. Pertinent values of Nusselt numbers for Table 8-2 of reference 5 are listed in Table 13.2.3-5. Since the channels are heated by fuel plates, the constant heat flux boundary condition is more appropriate than the constant temperature one in Table 13.2.3-5.

From Table 4.6-5 (of the currently replaced section 4.6 of the RINSC reactor safety analysis report, "4.6 Steady-State Thermal-Hydraulic Analysis"), the hydraulic diameter for the channel next to the reflector is 3.936×10^{-3} m and 4.325×10^{-3} m for the other channel. The thermal conductivity of steam at 1 bar ranges are 0.02508 W/m-K at 100° C, 0.04342 W/m-K at 300° C and 0.06698 W/m-K at 500° C. In the estimation of the film coefficient, the thermal

conductivity of steam at 300° C and the Nusselts for parallel plates (i.e., infinite aspect ratio) with constant heat flux boundary conditions will be used. Thus, for the internal 0.088-inch thick channel, the film coefficient is 8.235 × 0.04342 W/m-K / 4.325× 10^{-3} m = 82.7 W/m^2-K and for the channel next to the beryllium reflector the film coefficient is 5.385 × 0.04342 W/m-K / 3.936 × 10^{-3} m = 59.4 W/m^2-K. Except for the difference in film coefficient, the model is the same whether the fuel plate is assume to be cooled by 1) two internal 0.088-inch thick channels that are each heated from both sides or 2) two 0.0645-inch thick channels that are each heated by only the fuel plate itself. In reality, the beryllium reflector would server as a heat sink rather than as an insulated boundary. Heat would be transferred from the fuel plate to the reflector where it would be conducted down the length of the reflector to the pool of water. However, this beneficial heat transfer is not included in the analytical model.

Table 13.2.3-4 Key Parameters for Thermal Analysis

Parameter	Symbol	Value
Fuel meat, m (in)		
Length		0.59055 (23.25)
Width		0.060833 (2.395)
Thickness		5.0800 (0.020)
Volume of fuel meat, m^3		1.8250×10^{-5}
Width of channel, m (in)	W	0.066548 (2.62)
Conductivity of Fuel, W/m-K	k_f	88
Area of Fuel, m^2	k_{al}	180
Conductivity of aluminum, W/m-K	A_f	3.090×10^{-5}
Area of aluminum, m^2	A_{al}	8.548×10^{-5}
Highest plate power for 2-MW operation, kW		9.653
Decay power fraction		0.718 %
Highest plate power at decay power, W		69.309
Fuel volumetric decay power generation, W/m^3	q'''	3.7978×10^6
Exposed plate length, m (in)	L	0.39688 (15.625)
Power generated in submerged fuel length, W	p_1	22.730
Heat capacity of steam at constant pressure, kJ/kg-K	C_p	2.0
Parameter defined by equation (13), C/m^2	β	6481
Enthalpy to convert 40° C liquid to sat. steam, kJ/kg	Δi	2507
Steam inlet temperature, C	T_{c0}	100
Fuel plate temperature at x=0, C	T_{p0}	105

13.2.3.8 Values of Other Model Parameters

Key parameters for the thermal analysis are summarized in Table 13.2.3-4. For the calculated 7.756-hour drain time, the relative decay power, assuming infinite operation, is 0.718%. The fuel plate powers and heat fluxes in the table are based on this fraction. The fuel meat

Table 13.2.3-5 Nusselt Numbers for Laminar Flow in Rectangular Ducts

Duct Aspect Ratio	Sides Heated	Nusselt Number	
		Constant Heat Flux	Constant Temperature
8.0		6.60	5.95
infinite	2	8.235	7.54
infinite	1	5.385	4.86

dimensions for the plate are included in the table because they are needed to determine the fuel meat volume and volumetric heat generation rate. As provided in section 4.6.8, the power of the highest power plate during full power reactor operation at 2.0 MW is 9.653 kW.

The thermal conductivity of the fuel, k_f, is 88 W/m-K, as provided in Appendix A. The thermal conductivity of aluminum, k_{al}, is that of aluminum 6061, which is 180 W/m-K. The area of the fuel meat, A_f, is the width of the fuel meat times the thickness of the fuel meat, or 2.395 inches times 0.020 inches. These values are based on Drawing 422873, "Rhode Island Nuclear Science Center, Test Reactor Training Reactor 5 Fuel Plate", released 7-22-92, where the meat width is given as between 2.32 and 2.47 inch. Thus, $A_f = 0.0479\ in^2 = 3.090 \times 10^{-5}\ m^2$.

The area of the aluminum portion of the cross section, A_{al}, is the cross sectional area of the fuel plate cladding plus the associated cross sectional areas of the two side plates. Drawing 422873 shows the fuel plate width to be between 2.780 and 2.800 inches and the plate thickness to be between 0.048 and 0.052 inches. The average dimensions of 2.790 and 0.050 inches will be used here. Thus, the cross sectional area of the fuel plate excluding the fuel meat cross sectional area is: $(2.790 \times 0.050 - 2.395 \times 0.020)\ in^2 = 0.0916\ in^2$. Each side plate, as given in Drawing 38004, "Rhode Island Side Plate Left Hand & Right Hand Plates", March 1993, is 0.187 inches thick and 3.045 inches long. Each has 22 groves that are 0.058 inches wide and 0.094 inches deep. Thus, the cross sectional area of each side plate is: $(0.187 \times 3.045 - 22 \times 0.058 \times 0.094)\ in^2 = 0.4495\ in^2$. This value is doubled, since there are two side plates, and then divided by the 22 fuel plates per fuel element. Thus, the side plate cross sectional area per fuel plate is $2 \times 0.4495 / 22\ in^2 = 0.0409\ in^2$. Thus, $A_{al} = 0.0916 + 0.0409\ in^2 = 0.1325\ in^2 = 8.548 \times 10^{-5}\ m^2$.

The variation in the values of specific heat, at constant pressure between 100 and 500° C is not monotonic. The values in this temperature range are close to 2.0 kJ/kg-K. A good method of estimating average specific heat between two temperatures is to divide the specific enthalpy change between the two temperatures by the temperature difference. Thus, between 100 and 500° C, the average specific heat at constant pressure is 2.03 kJ/kg-K. Therefore, 2.0 W/m-K was used in the analysis.

13.2.3.9 Solution Method

The model is the coupled pair of ordinary differential equations (11) and (18), subject to the boundary conditions (20), (21), and (22). The parameter γ in equation (18), as shown in equation (19), is a function of $\dot{m}$, which is a function of the amount of power conducted from the exposed part of the fuel plate to the submerged part at x = 0. This power, p_2, is defined by equation (23), which requires the value of dT_p/dx at x=0. Thus, the solution is an iterative one. The initial guessed value of dT_p/dx at x=0 is $\beta \times$ the exposed length, L. This corresponds to solution to equation (11) when h is 0, which implies that α is 0. The solution is solved several times until the magnitude of the change in dT_p/dx at x=0 is less than one part in a million. The number of iterations increases with h. No more than 11 iterations were needed per solution.

The solution of the couple pair of ordinary differential equations is accomplished with the aid of the Matlab software package[6]. As is commonly done, a second order differential equation is replaced with two first order ones. Thus, in the solution, equation (11), which is a second order

differential equation, is replaced with two first order differential equations. This is accomplished by defining a new variable, y(2) to be dT_p/dx. In the Matlab solution, y(1) is T_p, y(2) is dT_p/dx, and y(3) is T_c, where y(1), y(2), and y(3) are vectors. Essentially all of the Matlab statements needed to solve the problem for a film coefficient of 20 W/m^2-K are provided in Figures 13.2.3-8 and 13.2.3-9. The later is in two parts, which should be combines into one ".m" file that is named "exec_loca.m". Figure 13.2.3-8 lists three ".m" functions, which should each be stored in three separate files, as indicated. The first defines the right-hand side of each equation of the set of three coupled ordinary differential equations. The second provides the boundary conditions, and the third provides initial guessed values for the solution. In the Matlab interface it is necessary to use the "addpath" command to define the path(s) where all four files can be found. The commented out second line was included in the Figure 13.2.3-9 to provide an example of the command. Then the command "exec_loca" (without the quotes) is entered from the Matlab interface. The results, including a plot of the axial distributions of the two temperatures should appear. Results for other cases can be obtained by appropriately modifying values in the "exec_loca.m" file and following the same procedure. The computing time for each solution consisting of multiple iterations was short enough to be considered to be instantaneous.

Figure 13.2.3-8 Matlab Equation Definition, Boundary Condition, and Initial GuessFunctions for Solution of Couple Set of Differential Equations

(They were saved as "LOCA_Plate_ODE_function.m", "LOCA_Plate_Bound_Cond_function.m", and "LOCA_Plate_Initial_Cond_function", respectively.)

```
function dydx = LOCA_Plate_ODE_function(x,y, alpha1, beta1, gamma1)
% x is the distance along the length of the plate or the coolant channel
% y(1) is the plate temperature
% y(2) it the derivative of the plate temperature
% y(3) is the coolant temperature
dydx = [  y(2)
          alpha1*(y(1) - y(3)) - beta1
          gamma1*(y(1) - y(3)) ];

function res = LOCA_Plate_Bound_Cond_function(ya,yb, alpha1, beta1, gamma1)
Tplate_0 = 105.;
Tcoolant_0 = 100.;
res = [ ya(1)-Tplate_0
        ya(3)-Tcoolant_0
        yb(2) ];

function yinit = LOCA_Plate_Initial_Cond_function(x)
Tplate_0 = 105.;
Tcoolant_0 = 100.;
yinit = [ Tplate_0
          0
          Tcoolant_0 ];
```

Figure 13.2.3-9 Matlab Statements to Obtain a Solution for Film Coefficient of 20 W/m^2-K

(This was stored in "exec_loca.m" file. The three functions listed in the previous figure are also needed. To obtain the solution for this case, open Matlab, use the "addpath" command to add the directory where the files are store to the path [See the second and third lines, which should be one line when properly recombined.], and enter "exec_loca", and press "enter".)

```
clear all
% addpath 'C:\Documents and Settings\feldman\My Documents\MATLAB_Files\Rhode_Island_Aug10'
k_fuel = 88.0;  % fuel meat, W/m-K
A_fuel = 3.090e-5; % fuel meat cross section, m^2
k_alum = 180.; % aluminum, W/m-K
A_alum = 8.548e-5; % aluminum cross section, m^2
C1 = k_fuel*A_fuel + k_alum*A_alum; % W-m/K
hfilm = 20.; % film coefficient, W/m^2-K
width = 0.066548; % (=2.62 inches) width of channel, m
rel_pow = 0.00718; % decay power fraction
pow_plate_2MW = 9653; % plate power for 2-MW operation, W
tot_decay_pow_W = rel_pow*pow_plate_2MW;  % W
L_plate = 23.25; % fuel meat length, inches
L_exposed = 15.625; % fuel meat length out of water (= L_plate/2 + 4), inches
V_plate = 1.113675; %volume of fuel meat in 1 plate (= 23.25 * 2.395* 0.020) inches^3
qppp = tot_decay_pow_W/(V_plate*0.0254^3); % volumetric heat generation rate of fuel meat, W/m^3
pow_sub = tot_decay_pow_W *(L_plate - L_exposed)/L_plate;
                                % power generated in submerged part of plate, W
Cp = 2.000; % specific heat capacity of superheated steam, kJ/kg-K
alpha1 = 2*hfilm*width/C1; % alpha, 1/m^2
beta1 = A_fuel*qppp/C1; % beta, C/m^2
length = 0.396875;
dy1dx = beta1*length; % initial guess of plate temperature derivative at water surface, C/m
delta_enth = 2507; % specific enthalpy from 40 C to saturated vapor at 1 bar, KJ/kg
format short e
n_segs = 50; % number of equal segments that exposed length is divided
for count = 1:20
   dy1dx_old = dy1dx;
   pow_trans = C1 * dy1dx;
            % power transferred from exposed portion of plate to submerged portion, W
   pow_steam = pow_sub + pow_trans;  % total power that goes to produce steam, W
   m_dot = pow_steam /(1000*delta_enth); % steam flow rate, kg/s
   gamma1 = 2*hfilm*width/(m_dot*Cp*1000.); % gamma, 1/m
   solinit = bvpinit(linspace(0, length, n_segs), LOCA_Plate_Initial_Cond_function);
   sol = bvp4c(@LOCA_Plate_ODE_function,@LOCA_Plate_Bound_Cond_function,solinit, ...
                                        [],alpha1, beta1, gamma1);
   xint = linspace(0, length, n_segs);
   Sxint = deval(sol,xint);
   dy1dx = Sxint(2,1);  % plate temperature derivative at water surface, C/m
   error = (dy1dx - dy1dx_old)/dy1dx;  % error in dTp/dx at x=0 relative to previous iteration
   if abs(error) < 1e-6
      break
   end
end
```

Continued Below

Figure 13.2.3-9 Matlab Statement for Film Coefficient of 20 W/m^2-K (Continued)

```
pow_frac_st = pow_steam / tot_decay_pow_W; % fraction of power to steam production
Tmax_est = 100. + (1 - pow_frac_st) / pow_frac_st * delta_enth / Cp; % Estimate of Max Steam
Temperature, C
plot( xint, Sxint(1,:), xint, Sxint(3,:) )
xlabel('x (distance above water surface), meters')
ylabel('Temperature, C')
legend('Plate','Coolant','Location','NorthWest')
char '       x       Tplate     dTplate/dx    Tcoolant   Tplate - Tcool'
[xint', Sxint(1,:)', Sxint(2,:)', Sxint(3,:)', [Sxint(1,:) - Sxint(3,:)]']
store(1) = hfilm;
store_name(1,:) = ': hfilm      ';
store(2) = tot_decay_pow_W;
store_name(2,:) = ': tot_decay_W';
store(3) = pow_sub;
store_name(3,:) = ': pow_sub    ';
store(4) = alpha1;
store_name(4,:) = ': alpha1     ';
store(5) = beta1;
store_name(5,:) = ': beta1      ';
store(6) = count;
store_name(6,:) = ': count      ';
store(7) = n_segs;
store_name(7,:) = ': n_segs     ';
store(8) = error;
store_name(8,:) = ': error      ';
store(9) = pow_trans;
store_name(9,:) = ': pow_trans  ';
store(10) = pow_steam;
store_name(10,:) = ': pow_steam  ';
store(11) = pow_frac_st;
store_name(11,:) = ': pow_frac_st';
store(12) = Tmax_est;
store_name(12,:) = ': Tmax_est   ';
store(13) = m_dot;
store_name(13,:) = ': m_dot      ';
store(14) = dy1dx;
store_name(14,:) = ': dy1dx      ';
[num2str(store'), store_name]  % output these values in a column to copy to Excel
```

13.2.3.10 Effect of Film Coefficient on Results

Intuitively, one would expect that as the film coefficient is increased, more heat is removed from the plate by convection and therefore the maximum plate temperature, which is at the exit, would decrease monotonically with increasing film coefficient. As Table 13.2.3-6 shows, sometimes intuition is wrong. As the film coefficient is increased from 0 to 4 W/m^2-K the maximum plate temperature decreases from 615.5 to 461.9° C and then gradually increases to 486.4° C at a film coefficient of 100 W/m^2-K. From there to a virtually infinite value of film coefficient, the maximum temperature rises by only a few degrees to an asymptotic value of 488.6° C. The

initial decrease in plate exit temperature is due to increased convective heat transfer to the fluid, as one would expect. This leads to an increase in coolant exit temperature. Also, as more power is removed by convection (to superheat the steam), less is left to go into the pool to produce steam, as the third column in Table 13.2.3-6 shows. Therefore, the amount of steam being produced goes down as the film coefficient is increased. The steam temperature rise is directly proportional to the power removed by convection and inversely proportional to the steam flow. Thus, both of these effects cause the steam temperature to rise as the film coefficient is increased. As the steam exit temperature is increased, the plate exit temperature, which must always be the larger than the coolant exit temperature, must increase, too.

Table 13.2.3-6 Effect of Film Coefficient on Maximum Plate Temperature

Film Coefficient W/m^2-K	Maximum Plate Temperature, C	Fraction of Power Used for Steam Production	Temperature Difference at Exit, C
0	615.5	1.000	515.5
1	494.5	0.862	193.8
2	467.9	0.819	91.6
3	462.0	0.801	50.7
4	461.9	0.791	31.5
5	463.4	0.785	21.2
6	465.3	0.782	15.2
7	467.1	0.779	11.4
10	471.5	0.774	5.84
20	478.8	0.769	1.54
50	484.3	0.765	0.255
100	486.4	0.764	0.0644
1,000	488.4	0.763	0.000651
10,000	488.6	0.763	6.52e-8

Film coefficients of 82.7 and 59.4 W/m^2-K were calculated above for the 0.088-inch internal channel and the channel next to the beryllium reflector, respectively. As Table 13.2.3-6 shows, the peak for fuel plate temperatures for film coefficients 20, 50, 100, and 10,000 W/m^2-K, are 478.8, 484.3, 486.4, and 488.6° C, respectively. Therefore, 100 W/m^2-K is assumed for all future cases.

13.2.3.11 Verification of Results

A closed-form solution to the model exists for the special case where h in equation (10) is zero, For this special case α and γ are zero. This implies that none of the power produced in the plate is transferred to the flowing steam. Thus, the solution for the steam is that its temperature is 100° C over the entire length. Then equation (11) may be solved, subject to its two boundary conditions, equations (20) and (21), to obtain:

$$T(x) = T(0) + \beta\left(Lx - \frac{x^2}{2}\right) \tag{26}$$

This equation is to be compared to the equation for one-dimensional steady-state heat transfer in a beam of uniform heat generation rate, q'''_{beam} and uniform conductivity, k_{beam}. The model derivation and solution, which can be found in heat transfer textbooks, is analogous to that used to obtain equation (11), but the convection term omitted. The solution is equation (26), but with $\beta = q'''_{beam} / k_{beam}$. In order to compare the single material solution to the one above with fuel and alumimum, the following is proposed: 1) $A_{beam} = (A_f + A_{al})$, 2) $A_{beam}\ q'''_{beam} = A_f q'''$, 3) $k_{beam}\ A_{beam} = (k_f A_f + A_{al} k_{al})$. Item 1) preserves the beam cross sectional area. Item 2) preserves the power generated per unit length, since q''' is the fuel meat volumetric heat generation rate. The power conducted along the length of the beam is the heat flux time, which is proportional to the conductivity times the cross sectional area. In there are two materials, such as fuel and aluminum, the heat flow through each material must be considered. Item 3 preserves the power conducted along the length of the beam. Another way to view item 3) is that the thermal conductivity of the beam for the fuel plate is to use the relative-area-weighted average of the two thermal conductivities to obtain the equivalent thermal conductivity, or $k_{beam} = (k_f A_f + A_{al} k_{al}) /(A_f + A_{al})$. When items 2) and 3) are substituted into equation (13), $\beta = q'''_{beam} / k_{beam}$ is obtained. Thus, equation (26) with β as given in equation (13) is consistent with the model for one-dimensional steady-state heat transfer in a beam of uniform heat generation rate and uniform conductivity.

Equation (26) with β as given in equation (13) can be compared with the Matlab solution for h = 0. As Figure 13.2.3-10 shows, the Matlab solution and the hand calculation solutions coincide. The Matlab solution for the coolant is a constant value of 100° C as it should be.

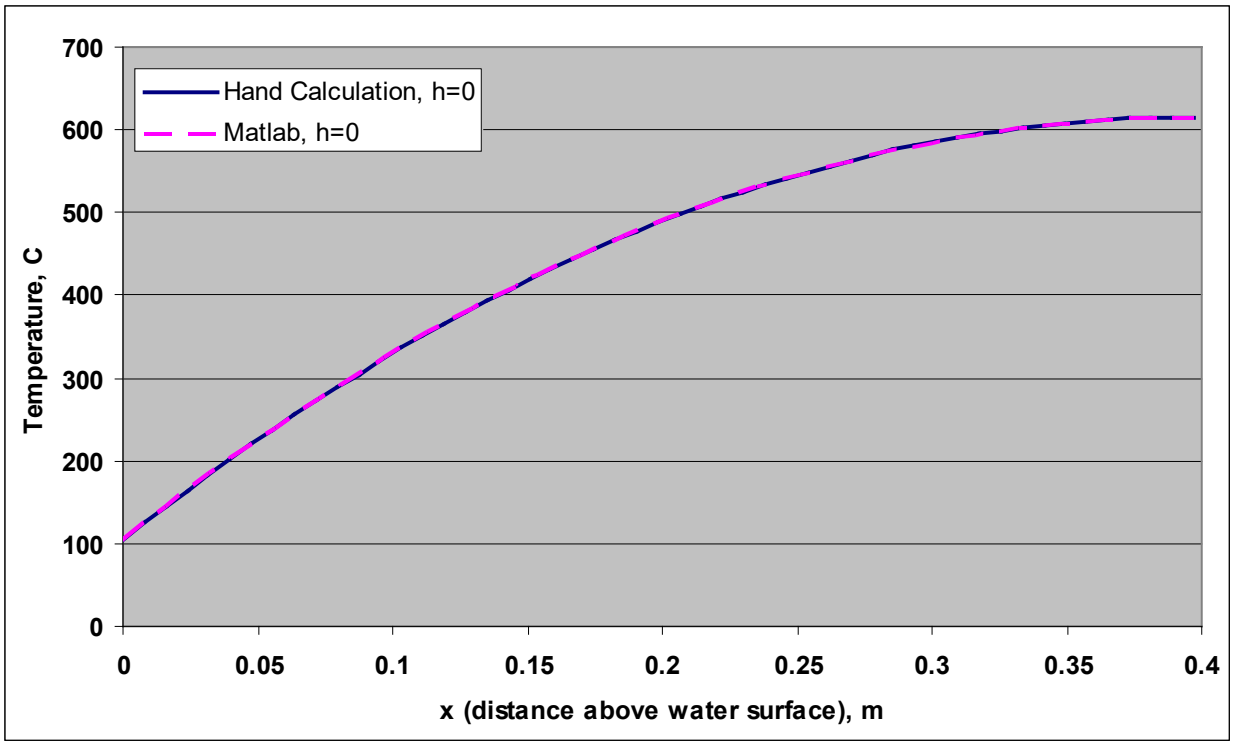

Figure 13.2.3-10 Comparison of Matlab Solution with Hand Calculation for h = 0

Another useful test, is to show that energy is balanced in the Matlab solution for a case where h is not 0. The h = 100 W/m^2-K solution was analyzed. There are 69.31 W generated in the fuel plate. Since 15.625 inches of the fuel meat length are above the waterline and 7.625 inches are below, 46.58 W are generated above and 22.73 W, a Matlab input, are generated below. Of the 46.58 W generated above the waterline, 30.25 W, a Matlab output, are conducted down the length of the plate to the submerged portion. The remaining 16.33 W is transferred to the flowing steam by convection from the two exposed faces of the fuel plate. This remaining value can also be obtained from the integral of $2 \times h \times W \times (T_p - T_c) \times dx$ over the exposed length of the plate. (See item (17).) The integrated average of $(T_p - T_c)$ over the exposed length of the plate was obtained by trapezoidal integration of the numerical values of $T_p - T_c$ obtained from the Matlab solution and is 3.090° C. The power value obtained from this method is 16.32 W.

Since 69.31 W are produced in the plate and 16.33 W go to superheat the steam, then the remaining 52.98 W must go to make the steam. This 52.98 W can also be obtained by adding the power transferred from the exposed portion of the plate to the submerged portion, 30.25 W to the power produced in the submerged portion, 22.73 W. 52.98 W go into converting 40° C water in the liquid phase to saturated steam. Therefore, the steam flow rate is 52.98 W divided by the specific enthalpy increase from 40° C to saturated steam, 2507 kJ/kg, or 0.02113 kg/s. This flow rate agrees with the Matlab output. The 30.25 W conducted from the exposed part of the plate to the submerged part, p_2, can be determined from equation (23), where the plate temperature derivative value of 1670.5 C/m is obtained from the Matlab solution. Thus, both Matlab and equation (23) each predict 30.25 W for the value of p_2. A final check is an overall energy balance. 69.31 W raises 2.113×10^{-5} kg/s of subcooled water at 40° C to superheated steam at 486.36° C. The specific enthalpy of water at 40° C and 1 bar is 167.6 kJ/kg. The specific enthalpy of superheat steam at 486.36° C and 1 bar is 3460 kJ/kg. The flow rate times the specific enthalpy increase is 2.113×10^{-5} kg/s × (3460 -167.6) kJ/kg = 69.57 W. which is 0.1% greater than 69.31 W.

13.2.3.12 Effect of Decreasing Water Level Due to Boil-Off of Water

A minor consideration is that if there is no intervention and no make-up water is added to the pool, the water will steadily boil away, gradually exposing more length of fuel plate. The rate at which the water level drops can be estimated from an energy balance. In an interval of time, Δt, the water level will decrease by an amount, Δz meters. The water surface area is 150 ft^2. Since the density of water at 40° C is 992.2 kg/m^3, the mass of water boiled away is $992.2 \text{ kg/m}^3 \times 150 \text{ ft}^2 \times (12 \text{ in/ft} \times 0.0254 \text{ m/in})^2 \times \Delta z = 1.383 \times 10^4 \Delta z$ kg. Since 2507 kJ/kg are required to convert 40° C water to saturated steam, the amount of energy consumed is $1.383 \times 10^4 \times 2507 \times \Delta z$ kJ = $3.466 \times 10^7 \Delta z$ kJ. Although the decay power level decreases with time, it will be assumed to be constant at 0.718% of 2.0 MW, which will slightly exaggerate the rate of decrease in water level. The decay power added to the water by the reactor in Δt seconds is 0.718% × 2.0 MW × Δ t. Hence: $3.466 \times 10^7 \Delta z$ kJ = 0.718% × 2.0 MW × Δ t. The rate of decrease in the water level is $\Delta z/\Delta t = 4.143 \times 10^{-7}$ m/s = 1.491 mm/hr.

The increase in the exposed length of the fuel as the water boils away causes the peak fuel temperature to increase while the decrease in decay power over time causes the peak fuel temperature to decrease. Thus, the two effects must be considered together. The water level

reached the bottom of the 8-inch beam ports 7.756 hours after scram and cause 15.625 inches of the fuel length to be exposed. As shown above, this resulted in a peak fuel temperature of 486.42°C. The data in Reference 3 shows that for the infinite power history decay curve, between 20,000 s (5.5556 hr) and 40,000 s (11.111 hr) the power fraction decreases from 0.775% to 0.631%, which corresponds to a rate of 7.2×10^{-6} %/s. The decay power at 7.756 hours is 0.718%. Thus, one hour (3600 s) later, at 8.756 hours after scram, the decay power for the infinite decay curve is 0.02592% lower, or 0.692%. The water level at 8.756 hours is 1.491 mm or 0.0587 inches lower. Therefore, Matlab is used to obtain a solution with h = 100 W/m^2/K for a power fraction of 0.692% and with the exposed length increased by 0.0587 inches and the submerged length decreased by the same amount. The resultant peak fuel temperature is 475.89° C, which is 10.53° C less than was predicted for 7.756 hours after scram. For comparative purposes the solution was repeated with the decrease in power level, but with the original 15.625-inch exposed fuel length. The peak fuel plate temperature for this case is 475.62° C, which is only 0.27° C less than was obtained with the lower water level. Hence, the drop in power level more than compensates for the slight increase in exposed fuel plate length. Thus, the decrease in water level has a relatively small effect on the maximum fuel plate temperature and it can be concluded that the peak fuel plate temperature occurs with the water level at the bottom of the 8-inch beam port, and not at a lower water level.

A related concern is the potential for a lower water level in the core box than in the remainder of the pool. In theory, this could occur because as water boils away from the core, water must enter the core box through the ½-inch diameter hole in the lower plenum. The flow into the core box through this hole is a result of the pressure difference across the hole caused by differences in buoyancy between the core box water and the pool water. This pressure difference may require a slightly lower water level in the core box than in the rest of the pool. The flow rate through the hole is equal to the rate at which is boiled from the core. Thus, analogous to a similar calculation above, the flow rate is power divided by the specific enthalpy change, or 0.00718 × 2 MW / 2507 kJ/kg = 5.728×10^{-3} kg/s. The volumetric flow rate is this value divided by the density of 40° water, 992.2 kg/m^3, or 5.773×10^{-6} m^3/s. The velocity of the coolant going through the ½-inch hole is the volumetric flow rate divided by the hole area, $\pi/4 \times (0.5 \times 0.0254)^2$ m^2 = 1.267×10^{-4} m^2. Thus, the velocity is 0.04557 m/s. A high value for the hydraulic resistance of the hole corresponds to a form-loss, or K-loss value of 2. The friction pressure drop through the hole is the K-loss time the water density times the velocity squared, or 2 × ½ × 992.2 kg/m^3 × (0.04557 m/s)^2 = 2.060 Pa. This pressure difference must be produce by the differences in buoyancy pressure between the core box and the rest of the pool. A bounding approach is to ignore the beneficial effect of the liquid water near the surface of the fuel in the core box being hotter and, therefore, less dense than the water outside of the core box. Instead, it will be assumed that the buoyancy difference is due only to the water level in the core box being lower than that in the rest of the pool by an amount ΔZ. Thus, the required buoyancy pressure difference is the water density times the acceleration due to gravity, 9.80665 m/s^2, times ΔZ. Thus, 992.2 kg/m^3 × 9.80665 m/s^2 × ΔZ = 2.060 Pa, or ΔZ = 0.2112 mm. Thus, this shows that the drop in core box water level relative to the rest of the pool water level is negligible. Moreover, if the lower density of the heated water in the core box were taken into account this value would be even smaller. Conceivably, the core box level could be slightly higher than that of the rest of the pool.

13.2.3.13 Results

The axial distribution of the fuel plate and of the coolant temperature for the reference case, of a 7.756 hour drain time, infinite power history yielding a power fraction of 0.718%, and h = 100 W/m^2-K, are shown in Figure 13.2.3- 11. The maximum fuel and coolant temperatures for this case are 486.42 and 486.36° C, respectively.

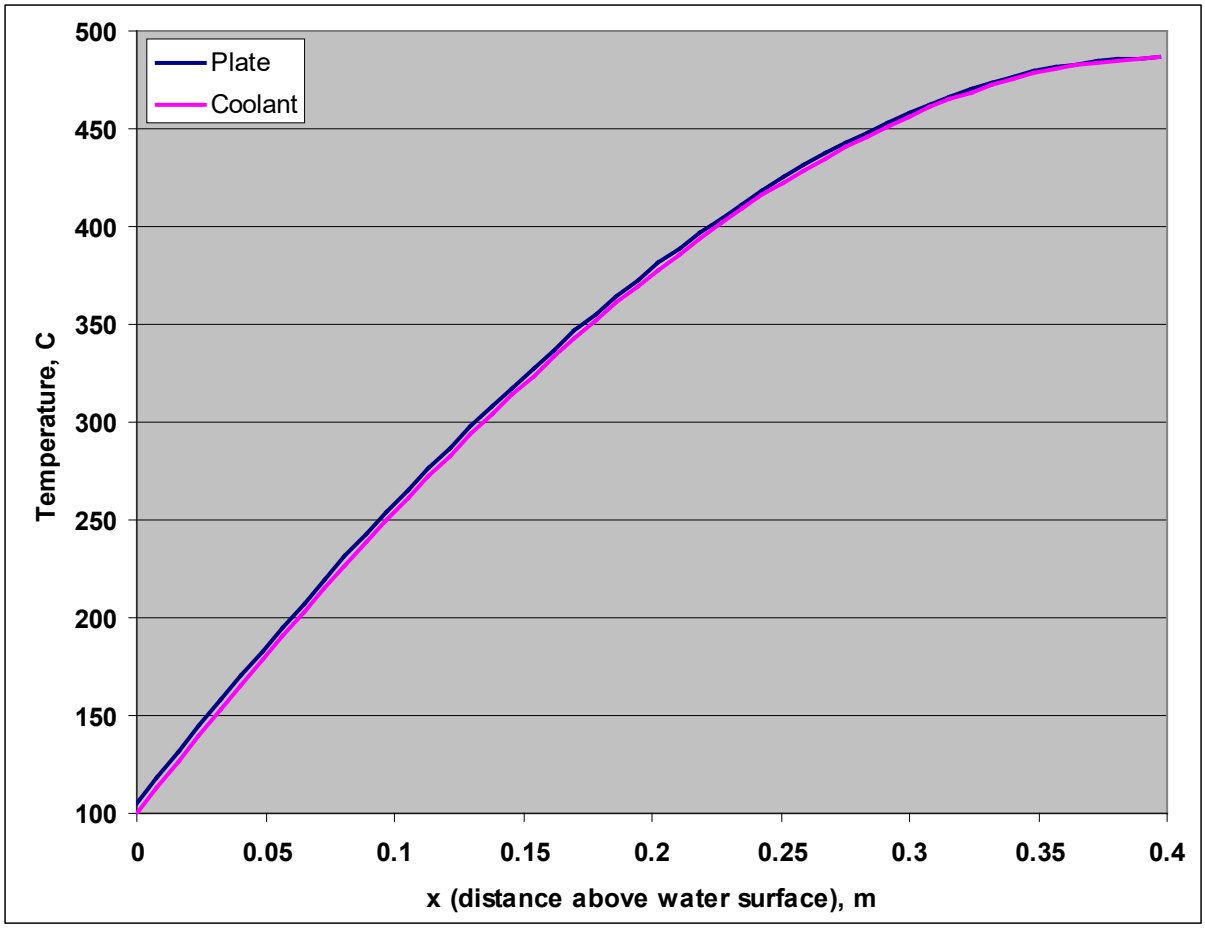

Figure 13.2.3-11 Axial Distributions of Fuel Plate and Coolant Temperatures (Reference Case, 0.718% Power, h = 100 W/m^2-K)

13.2.3.14 Effect of Decay Power for the Reference Water Level

All of the analysis assumes an infinite power history and a specific drain time. Changes in these assumptions will alter the decay power fraction. Therefore, with the aid of Matlab, solutions were obtained for a range of power fractions for the reference water level and h = 100 W/m^2-K. The peak fuel plate temperature obtained from these solutions as shown in Figure 13.2.3-12 and Table 13.2.3-7. An acceptable fuel and cladding temperature limit not to be exceeded under any conditions of operation is 530° C.[7] As the table shows, several extra Matlab runs were made to find the decay power fraction that corresponds to 530° C. This decay power fraction, 0.827% occurs at 4.51 hours after scram if an infinite power history is assumed. The pair of results

shown in red in the table corresponds to conditions predicted for the RINSC reactor and the 530° C limiting case.

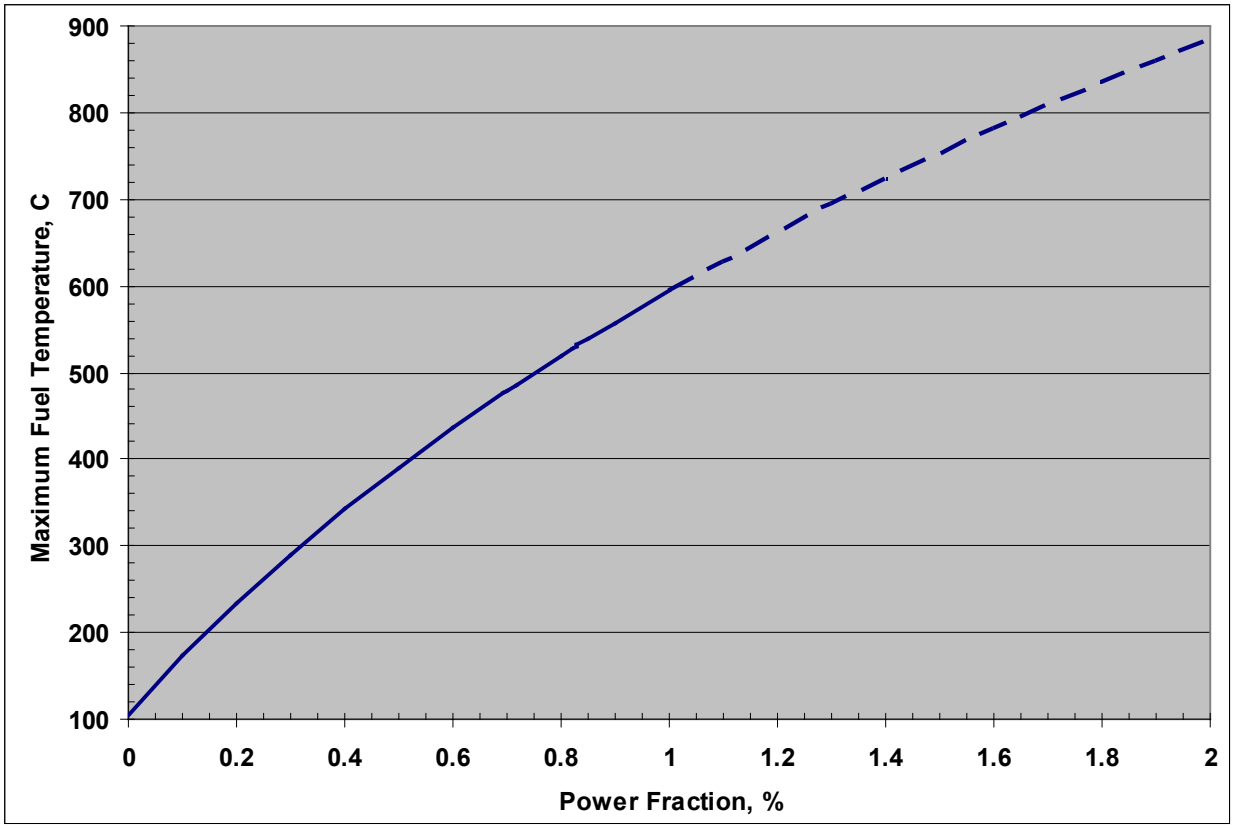

Figure 13.2.3-12 Effect of Power Fraction on Maximum Fuel Plate Temperature

As Figure 13.2.3-4 shows, higher values of decay power occur closer to the time of the scram where the decay power is decreasing rapidly. In this region the heat capacity of the fuel is extremely important in determining the maximum fuel temperature achieved during a LOCA. Inclusion of the heat capacity would require a transient analysis which could result in much lower maximum temperature in this region. To emphasize this point, the curve in Figure 13.2.3-12 for values of decay power above 1% is shown as a dashed line. The precise cutoff is arbitrarily. The 1% value was chosen by examination of Figure 13.2.3-4. Similarly, the portion of Table 13.2.3-7 for values above 1% is segregated from the rest of the table.

13.2.3.15 Discussion and Conclusions

The loss-of-coolant accident that results from a failure of a beam port was analyzed. In this accident the water drains down to the level of the leak, which is assumed to be the lowest point among the six horizontal 6-inch and 8-inch beam ports. The dropping water level is assumed to produces a scram when the water level is 23.54 feet above the top of the fuel meat. This is the smallest value permitted by the Safety Limits of the Technical Specifications. Each beam port is assumed to have a ½-inch diameter hole in the outer cover of the beam port. All other hydraulic resistances in the beam ports are ignored. Since all six beam ports are connected by common

interconnected drain lines, it is assumed that water drains from all six ½-inch diameter holes simultaneously. The drain time is taken to be the time after scram that the water level reaches the top of the core box. This time is shorter than the time required for the water level to drop to the beam port level.

A model of water draining from a tank that has six ½-inch sharp-edged orifices is developed. A detailed derivation is provided. The model is evaluated. The drain time is found to be 7.756 hours. The decay power fraction at 7.756 hour after scram for an infinite power history is 0.718%. The highest power plate in the reactor during normal operation is the one in assembly D6 that is immediately adjacent to the central beryllium reflector. During 2-MW reactor operation, this plate produce 9.653 kW. Thus, the corresponding decay power for this plate 7.756 hours after scram is 69.31 W.

An analytical model of the thermal behavior of the limiting fuel plate, based on a series of conservative assumptions – including infinitely-long full power operation prior to the LOCA, no automatic addition of water to the pool via make-up systems, no operator action to add water to the pool, no credit for heat capacitance in the fuel plate, and near worst-case film coefficient on the fuel surface – was developed from engineering fundamental. When the water level reaches the bottom of the beam ports, 7.625 inches of the 23.25-inch core length is submerged in the pool of water and the remaining 15.625 inches in exposed to the air. Heat is removed from the exposed portion by conduction down the length of the plate to the pool of water and by convection to the flow of steam that is produced as water is boiled off at the surface the pool. A detailed model derivation is provided. The model was solved with the aid of the Matlab software package. The solution was tested with a known solution for the special case of no convection from the exposed fuel plate surfaces. Energy balances were checked to demonstrate that the solution for the reference case is internally consistent.

The results show that the peak fuel plate temperature is 486° C, which is 44° C below the 530° C limit that is accepted by the US Nuclear Regulatory Commission.

Figure 13.2.3-7 Effect of Power Fraction on Maximum Fuel Plate Temperature

Power Fraction, %	Maximum Fuel Plate Temperature, C
0	105
0.1	172.44
0.2	233.67
0.3	289.90
0.4	341.98
0.5	390.55
0.6	436.09
0.692	475.62
0.7	478.96
0.718	486.42
0.8	519.48
0.82	527.32
0.827	530.05
0.83	531.22
0.85	538.94
0.9	557.89
1.0	594.40
1.1	629.17
1.2	662.37
1.3	694.11
1.4	724.51
1.5	753.67
1.6	781.67
1.7	808.60
1.8	834.51
1.9	859.48
2.0	883.56

References:

1. Operation and Maintenance Manual, One-Megawatt Open Pool Reactor for Rhode Island Atomic Energy Commission, Providence, RI, GEI-77793, General Electric, San Jose, California, October 1962.

2. *Safety Analysis Report for the Low Enriched Fuel Conversion of the Rhode Island Nuclear Science Center Research Reactor*, Revision 1, December, 1992.

3. Argonne Intra-Laboratory Memo, John Stillman to Jim Matos, "Decay Heat Anaysis for Spent Reactor Fuel in Cyclic and Continuous Operations," May 5, 2010. (See Appendix B.)

4. Warren M. Rohsenow, James P. Hartnett, Ejup N. Ganić (Editors), *Handbook of Heat Transfer Fundamentals*, Second Edition, McGraw-Hill Book Company, New York, 1985, p. 12-31.

5. W. M. Kays, *Convective Heat and Mass Transfer*, McGraw-Hill Book Company, New York, 1966, p. 117.

6. "MATLAB®, The Language of Technical Computing," Version 7.0.4.365 (R14) Service Pack 2, January 29, 2005, The MathWorks, Inc., Copyright 1984-2005.

7. *Guidelines for Preparing and Reviewing Applications for the Licensing of Non-Power Reactors*, NUREG-1537, Part 1, Format and Content, Appendix 14.1, Section 2.1, Page 3, US Nuclear Regulatory Commission, February 1996.

Appendix A

(Copied from *Safety Analysis Report for the Low Enriched Fuel Conversion of the Rhode Island Nuclear Science Center Research Reactor*, Revision 1, December, 1992.)

LEU THERMAL CONDUCTIVITY CALCULATION

Density of U_3Si_2

The densities of the dispersants are taken form reference (1) with the volume fraction related to the uranium density, Pu, in the fuel by:

$$Pu = 1.28Vf$$

where Vf is the volume fraction of the dispersant

for the purposes fuel loading of 12.5 $\frac{g/cc}{plate}$ (22 plate element, 275 g U-235)

the density is 3.4682 per reference (2)

the volume fraction of U_3Si_2 in fuel meat is

$$Vf^{U_3Si_2} = \frac{3.4682}{11.28} = .3068 \text{ or } 30.68\%$$

From reference (3), page 11

$$Vp = .072\ Vf - .275\ Vf^2 + 1.32\ Vf^3$$

therefore $Vp = .072\ (.3068) - .275\ (.3068)^2 + 1.32\ (.3068)^3 = .0343$

where Vp and Vf are volume fractions or porosity and fuel in the meat, respectively.

Thermal Conductivity of U_3Si_2

Volume fraction of fuel plus voids = .3068 + .0343 = .3411
the thermal conductivity is obtained from Figure 6, page 16 of reference (3)

$$K = 88\ W/m.k$$

REFERENCES

(1) R.F. Domagala, T.D. Wiencek, and H.R. Tresh, "Some Properties of U-Si Alloys in the Composite Range U_3Si to U_3Si_2," CONF-8410173, ANL, RERTR/TM-6, 47, July 1985.

(2) Memo from W. Woodruff (B17681 at ANLOS) to Eugene Spring (RMA101 at URI MUS), Sept 5, 1989.

(3) J.L. Snelgrove, R.F. Domagala, G.L. Hofman, T.C. Wiencek, G.L. Copeland, R.W. Hobbs, and R.L. Senn, "The Use of U_3Si_2 Dispersed in Aluminum in Plate-type Fuel Elements for Research Reactors," Argonne National Laboratory (ANL/RERTR/TM-11), October 1987.

Appendix B

Argonne National Laboratory

May 5, 2010 Intra-Laboratory Memo from John Stillman to Jim Matos

Decay Heat Analysis for Spent Reactor Fuel in Cyclic and Continuous Operations

May 5, 2010

TO: Jim Matos NE

FROM: John Stillman NE

SUBJECT: Decay Heat Anaysis for Spent Reactor Fuel in Cyclic and Continuous Operations

Decay heat data for spent research reactor fuel were calculated using the ANSI/ANS-5.1-2005 Decay Heat Standard[1], assuming a cyclic operation of a facility fueled with U-235 as the primary fissile isotope. The reactor was assumed to operate for a maximum of 40, 72, 120, and 168 hours/week, followed by a shutdown for the remainder of the week. In the final case (168 hours/week), the reactor is operated continuously without shutdown. The illustration below illustrates the cyclic operations of the facility.

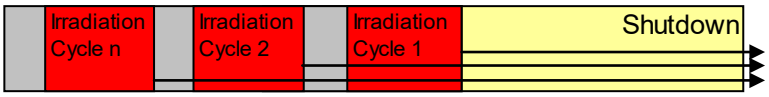

The decay heat was calculated using correlation parameters for U-235 thermal fission for a finite reactor operation time (T), followed by shutdown for t seconds using parameters from Table 9 in Ref. 1. The decay heat/fission is calculated as

$$F(t,T) = \sum_{i=1}^{i=23} \frac{\alpha_i}{\lambda_i} e^{-\lambda_i t}(1 - e^{-\lambda_i T})\ MeV / Fission. \qquad \text{(Eq. 1)}$$

The bulk of the decay heat following reactor shutdown comes from the last cycle complete ("Cycle 1" in the above illustration). However, each previous cycle also contributes to the decay heat in the shutdown interval. To calculate the decay heat from cycle n, the shutdown time used was

t + (n-1)*7*24*3600 seconds,

accounting for 7 days/week, 24 hours/day, and 3600 seconds/hour. Up to 1000 years of continuous operations were evaluated in the analysis in order to compare the results calculated from Equation 1 with the tabulated data for an "infinite" irradiation in Table 5 of Ref. 1.

With increasing numbers of cycles, the decay heat contribution from the n^{th} cycle to the total decay heat diminishes to very small amounts. Figure 1 plots the decay heat following shutdown for a cyclic operation of 72 hours/week (3 days/week) as a function of the number of weeks of operation modeled. One week of operations is not sufficient to properly account for the decay heat in a fuel element which is involved in weekly operations. However, after several hundred weeks (see the curves for 15.4 and 38.5 years), the decay heat following shutdown is seen to reach an equilibrium.

[1] *Decay Heat Power in Light Water Reactors*, American Nuclear Society, ANSI/ANS-5.1-2005, April 2005.

Figure 2 plots the decay heat as a function of time after shutdown of the last cycle for reactor operations of 72, 120, and 168 hours/week. A total of 38.5 years (2001 weeks) were simulated in calculating these data. The 168 hours/week case represents continuous operation of the facility. Also included on the plot is the 2005 Decay Heat Standard results for infinite (10^{13} seconds) operation.

Table 1 summarizes the decay heat results for the cases considered. It can be seen that for the continuous operation case (168 hours/week), modeling 40 years of continuous operation yields nearly the same results as the data tabulated in Ref. 1 for infinite operations (10^{13} seconds), and increasing the years of operation in the model to 1000 years ($3x10^{10}$ seconds) yields decay heat values within 1% of the values tabulated for infinite operation.

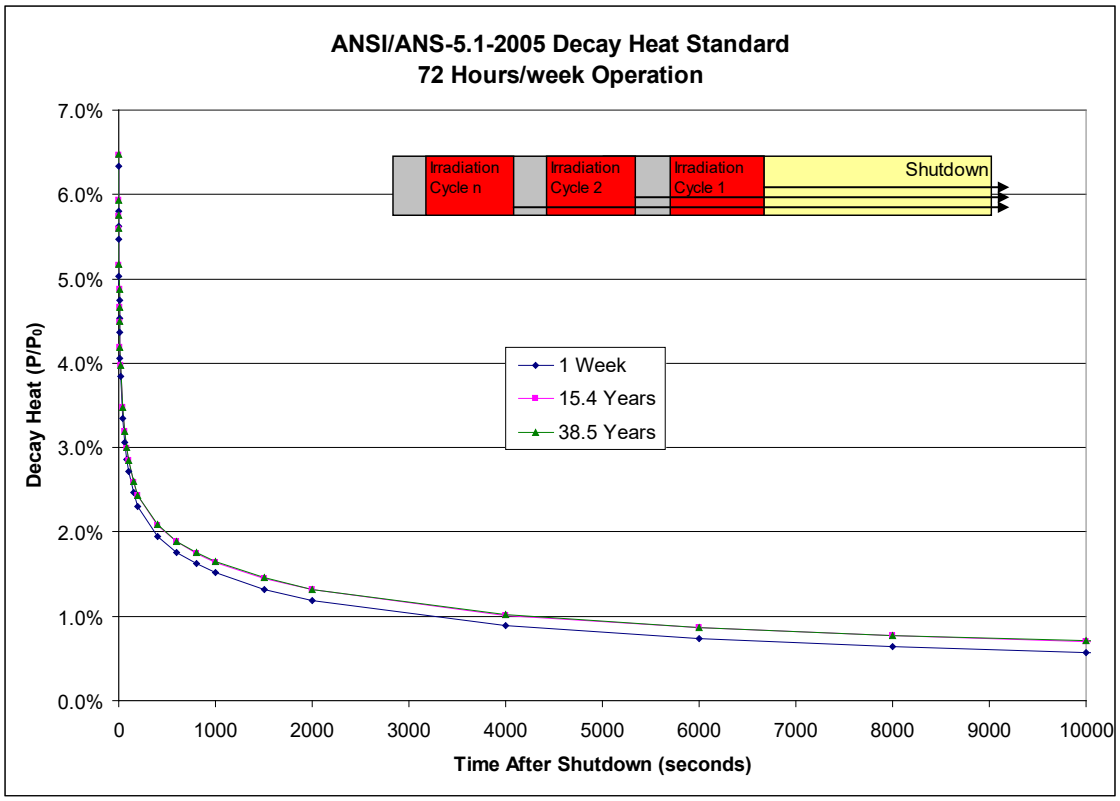

Figure 1.

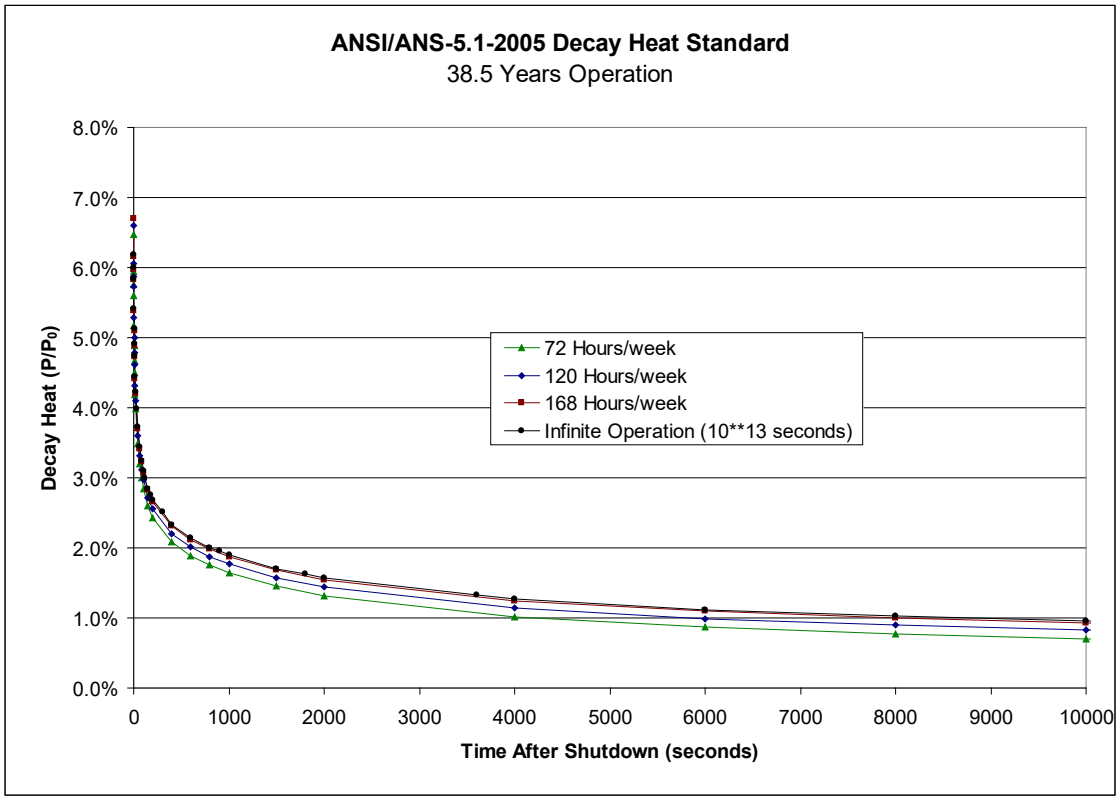

Figure 2.

Table 1. Decay Heat (Fraction of Steady State Power) as Function of Reactor Operation Scenario, ANSI/ANS-5.1-2005 Decay Heat Standard.

Shutdown time (sec)	*Cyclic Operations*							Infinite Operation (10^{13} seconds)
	40 hrs/wk for ~40 years	72 hrs/wk for ~40 years	120 hrs/wk for ~40 years	168 hrs/wk for ~20 years	168 hrs/wk for ~40 years	168 hrs/wk for 100 years	168 hrs/wk for 1000 years	
0	6.358%	6.473%	6.595%	6.586%	6.698%			
1	5.823%	5.937%	6.060%	6.051%	6.163%	6.181%	6.186%	6.190%
1.5	5.638%	5.752%	5.875%	5.866%	5.978%	5.996%	6.001%	6.005%
2	5.485%	5.600%	5.723%	5.713%	5.825%	5.843%	5.848%	5.850%
4	5.053%	5.167%	5.290%	5.281%	5.393%	5.411%	5.416%	5.420%
6	4.765%	4.880%	5.002%	4.993%	5.105%	5.123%	5.128%	5.130%
8	4.551%	4.665%	4.788%	4.778%	4.891%	4.909%	4.914%	4.917%
10	4.382%	4.497%	4.620%	4.610%	4.722%	4.740%	4.745%	4.749%
15	4.077%	4.192%	4.314%	4.305%	4.417%	4.435%	4.440%	4.443%
20	3.864%	3.979%	4.101%	4.092%	4.204%	4.222%	4.227%	4.230%
40	3.365%	3.480%	3.603%	3.593%	3.705%	3.723%	3.729%	3.732%
60	3.080%	3.195%	3.317%	3.308%	3.420%	3.438%	3.443%	3.446%
80	2.883%	2.997%	3.120%	3.110%	3.222%	3.240%	3.246%	3.249%
100	2.735%	2.850%	2.972%	2.963%	3.075%	3.093%	3.098%	3.101%
150	2.484%	2.599%	2.721%	2.712%	2.824%	2.842%	2.847%	2.850%
200	2.321%	2.435%	2.558%	2.548%	2.660%	2.678%	2.684%	2.687%
400	1.970%	2.084%	2.207%	2.197%	2.310%	2.328%	2.333%	2.336%
600	1.778%	1.892%	2.015%	2.005%	2.117%	2.135%	2.141%	2.144%
800	1.641%	1.755%	1.878%	1.868%	1.980%	1.998%	2.004%	2.007%
1000	1.535%	1.649%	1.771%	1.761%	1.874%	1.892%	1.897%	1.900%
1500	1.341%	1.455%	1.577%	1.567%	1.680%	1.698%	1.703%	1.706%
2000	1.206%	1.319%	1.442%	1.432%	1.544%	1.562%	1.568%	1.570%
4000	0.906%	1.019%	1.141%	1.131%	1.243%	1.261%	1.267%	1.269%
6000	0.757%	0.869%	0.991%	0.981%	1.093%	1.111%	1.117%	1.119%
8000	0.664%	0.775%	0.896%	0.886%	0.998%	1.016%	1.022%	1.024%
10000	0.597%	0.707%	0.828%	0.818%	0.930%	0.948%	0.953%	0.956%
15000	0.488%	0.596%	0.717%	0.707%	0.818%	0.836%	0.842%	0.844%
20000	0.421%	0.528%	0.647%	0.637%	0.748%	0.766%	0.772%	0.775%
40000	0.289%	0.389%	0.505%	0.495%	0.605%	0.623%	0.628%	0.631%
60000	0.227%	0.322%	0.436%	0.426%	0.534%	0.552%	0.558%	0.561%
80000	0.191%	0.282%	0.393%	0.384%	0.490%	0.508%	0.514%	0.517%
100000	0.168%	0.255%	0.364%	0.355%	0.460%	0.478%	0.484%	0.486%
150000	0.134%	0.215%	0.319%	0.310%	0.412%	0.430%	0.436%	0.439%
200000	0.117%	0.192%	0.293%	0.283%	0.383%	0.401%	0.407%	0.410%
400000	0.089%	0.153%	0.242%	0.233%	0.324%	0.342%	0.348%	0.351%
600000	0.077%	0.135%	0.216%	0.207%	0.292%	0.310%	0.316%	0.318%
800000	0.070%	0.123%	0.198%	0.188%	0.269%	0.287%	0.293%	0.295%